KARADENIZ TECHNICAL UNIVERSITY
THE GRADUATE SCHOOL OF NATURAL AND APPLIED SCIENCES

GEOMATICS ENGINEERING GRADUATE PROGRAM

ESTIMATING BASIC FOREST STAND PARAMETERS FROM UAS IMAGES

Ph.D. THESIS

Volkan YILMAZ, M.Sc.

DECEMBER 2017
TRABZON

KARADENİZ TECHNICAL UNIVERSITY
THE GRADUATE SCHOOL OF NATURAL AND APPLIED SCIENCES

GEOMATICS ENGINEERING GRADUATE PROGRAM

ESTIMATING BASIC FOREST STAND PARAMETERS FROM UAS IMAGES

Volkan YILMAZ, M.Sc.

This thesis is accepted to give the degree of
DOCTOR OF PHILOSOPHY
By
The Graduate School of Natural and Applied Sciences at
Karadeniz Technical University

The Date of Submission : 22 / 11 /2017
The Date of Examination : 22 / 12 /2017

Thesis Supervisor : Prof. Dr. Oğuz GÜNGÖR

Trabzon 2017

KARADENİZ TECHNICAL UNIVERSITY
THE GRADUATE SCHOOL OF NATURAL AND APPLIED SCIENCES

GEOMATICS ENGINEERING GRADUATE PROGRAM
Volkan YILMAZ

ESTIMATING BASIC FOREST STAND PARAMETERS FROM UAS IMAGES

Has been accepted as a thesis of

DOCTOR OF PHILOSOPHY

after the Examination by the Jury Assigned by the Administrative Board of the Graduate School of Natural and Applied Sciences with the Decision Number 1729 dated 28 / 11 / 2017

Approved By

Chairman	: Prof. Dr. Fevzi KARSLI	.....
Member	: Prof. Dr. Oğuz GÜNGÖR	.....
Member	: Prof. Dr. Bülent BAYRAM	.....
Member	: Assoc. Prof. Dr. Halil AKINCI	.....
Member	: Assoc. Prof. Dr. Ali İhsan KADIOĞULLARI	.....

Prof. Dr. Sadettin KORKMAZ
Director of Graduate School

FOREWORD

This PhD thesis entitled “Estimating Basic Forest Stand Parameters from UAS Images” has been submitted to the Karadeniz Technical University, The Graduate School of Natural and Applied Sciences, Geomatics Engineering Graduate Program.

I would like to express my sincere gratitude to my supervisor Prof. Dr. Oğuz GÜNGÖR for his guidance throughout my PhD studies. I am grateful to him for his invaluable opinions and recommendations about my thesis. I will always remain in intellectual debt to him not only for his guidance, but also for his brotherlike attitude to me. I would also like to give my special thanks to Assoc. Prof. Dr. Ali İhsan KADIOĞULLARI, who played an important role in the specification of my PhD topic. His innovative and informing opinions encouraged me to dive into forestry, which I have never thought to work before. I am also deeply grateful to my PhD thesis committee member Prof. Dr. Fevzi KARSLI for his encouragement and expertise not only for my PhD thesis, but also for other academic and non-academic support. My very special thanks also go to the other members of my PhD thesis committee, Prof. Dr. Bülent BAYRAM and Assoc. Prof. Dr. Halil AKINCI for their constructive comments and opinions on my thesis. I also thank Fırat University for letting me use their DJI Phantom 3 Unmanned Aerial System data in my thesis.

I would also like to extent my gratitude to my colleagues Res. Asst. Berkant KONAKOĞLU, Res. Asst. Fatih KADI, Res. Asst. Ziya USTA and Res. Asst. Sultan Sevinç KURT KONAKOĞLU for their all-time support and friendship. My sincerest thanks also go to Sadık KARAKOÇ and Muhammet GÜMRÜKÇÜOĞLU for their support.

I am also thankful to all my family members for their constant support and help. They always make me feel that they are there for me.

Finally, I would like to thank my wife Res. Asst. Çiğdem ŞERİFOĞLU YILMAZ for her endless love, support and patience throughout my PhD studies. She has always been there by my side through good times and bad. Without her support and encouragement, I could not have achieved this thesis.

Volkan YILMAZ

Trabzon 2017

STATEMENT OF ETHICS

I declare that, this PhD thesis, I have submitted with the title "Estimating Basic Forest Stand Parameters from UAS Images" has been completed under the guidance of my supervisor Prof. Dr. Oğuz GÜNGÖR. All the data used in this thesis are obtained by simulation and experimental works done as parts of this work in our research labs. All referred information used in this thesis has been indicated in the text and cited in reference list. I have obeyed all research and ethical rules during my research and I accept all responsibility if proven otherwise. 22/12/2017.

Volkan YILMAZ

TABLE OF CONTENTS

Page No.

PhD. Thesis

SUMMARY

ESTIMATING BASIC FOREST STAND PARAMETERS FROM UAS IMAGES

Volkan YILMAZ

Karadeniz Technical University
The Graduate School of Natural and Applied Sciences
Geomatics Engineering Graduate Program
Supervisor: Prof. Dr. Oğuz GÜNGÖR
2017, 96 Pages

Owing to their numerous benefits to humanity and other species, forests are considered the lungs of our planet. Unplanned use of forests causes the humanity face with a wide variety of critical issues such as climate destabilisation, air pollution, temperature instability, landslides, etc. This, of course, attaches importance to the sustainability of forests. Managing forests in conjunction with technological developments play a significant role in the continuity of the service provided by forests. A high-quality forest management depends heavily on the proper specification of forest characteristics, i.e. stand parameters. These parameters are used to produce forest management plans. In Turkey, stand parameters are generally obtained with terrestrial measurements. However, field measurements are neither cost- nor time-efficient in most cases, especially in large-scaled forests. The aim of this thesis is to estimate critical stand parameters (location, number, height, crown closure and crown diameter of trees) with point clouds extracted from Unmanned Aerial Systems (UAS). A novel polynomial fitting-based (PFB) approach was also proposed to estimate crown diameters of trees. The results of the proposed methodology were compared to the reference data and to the results of widely used segmentation-based approaches. All stand parameters were estimated in MATLAB environment. The results showed that the developed MATLAB script managed to estimate the stand parameters with a high accuracy and that the PFB methodology outperformed the other segmentation-based approaches in crown diameter estimation. The main conclusion drawn from this thesis is that using UASs enables the accurate estimation of stand parameters.

Key Words: Forest stand parameters, Unmanned aerial systems, Forestry, Aerial photogrammetry, MATLAB

Doktora Tezi

ÖZET

TEMEL ORMAN MEŞCERE PARAMETRELERİNİN İHA GÖRÜNTÜLERİNDEN TAHMİNİ

Volkan YILMAZ

Karadeniz Teknik Üniversitesi
Fen Bilimleri Enstitüsü
Harita Mühendisliği Anabilim Dalı
Danışman: Prof. Dr. Oğuz GÜNGÖR
2017, 96 Sayfa

İnsanlığa ve diğer canlı türlerine olan sayısız faydalarından dolayı ormanlar gezegenimizin akciğerleri olarak kabul edilmektedirler. Ormanların plansız kullanımı insanlığın iklimlerdeki dengenin bozulması, hava kirliliği, sıcaklıklarda istikrarsızlık ve toprak kaymaları gibi birçok olumsuzlukla yüzleşmesine neden olmaktadır. Bu durum ormanların sürdürülebilirliğinin önemini arttırmaktadır. Ormanların yönetiminin teknolojik gelişmelere paralel olarak gerçekleştirilmesi ormanlardan sürekli bir şekilde faydalanmada oldukça önemli bir rol oynamaktadır. Başarılı bir orman yönetimi ormanların fiziksel özelliklerinin (meşcere parametrelerinin) hassas bir şekilde belirlenmesine dayanmaktadır. Meşcere parametreleri orman amenajman planlarının üretiminde büyük pay sahibidir. Ülkemizde meşcere parametreleri genellikle yersel ölçümlerle belirlenmektedir. Ancak, özellikle geniş alanlara yayılan ormanlarda, meşcere parametrelerinin yersel ölçümlerle belirlenmesi oldukça uzun zaman alan ve maliyeti yüksek bir işlemdir. Günümüzün gelişmiş uydu ve fotogrametri sistemleri yeryüzü üzerindeki nesneler hakkında oldukça hassas ve detaylı bilgilerin oldukça kısa zamanda ve çok daha az maliyetlerle elde edilmesine olanak tanıdıklarından dolayı, bu sistemler yersel ölçüm tekniklerine alternatif olarak kullanılabilirler. Bu tezin amacı bazı önemli meşcere parametrelerinin (ağaçların konumu, sayısı, yükseklikleri, kapalılık oranları ve tepe çapları) İnsansız Hava Araçlarından (İHA) elde edilen nokta bulutları ile kestirilmesidir. Tez kapsamında ağaçların tepe çaplarının kestirimi için eğri uydurma tabanlı yeni bir yöntem geliştirilmiştir. Önerilen yöntemin sonuçları referans verilerle ve ayrıca sıklıkla kullanılan görüntü bölütleme tabanlı yaklaşımların sonuçları ile karşılaştırılmıştır. Tez kapsamında bütün meşcere parametreleri MATLAB programlama dilinde geliştirilen yazılım ile kestirilmiştir. Sonuçlar yazılan MATLAB kodu ile meşcere parametrelerinin yüksek hassasiyetle belirlenebildiğini ve önerilen yöntemin tepe çapı kestiriminde diğer görüntü bölütleme tabanlı yaklaşımları geride bıraktığını göstermektedir. Önerilen yöntemin ağaçların tepe çaplarını 1 m' den daha iyi Karesel Ortalama Hata (KOH) değerleri ile kestirebildiği gözlemlenmiştir. Tepe çaplarının hassas bir şekilde elde edilmesiyle ağaçların tür ayrımı daha başarılı bir şekilde yapılabilecektir. Elde edilen sonuçlara göre İHA' ların kullanımının orman meşcere

parametrelerinin belirlenmesinde oldukça etkin bir rol oynayabildiği görülmektedir. İHA' ların kullanımı meşcere parametrelerinin kısa zamanda ve daha az bir maliyetle belirlenmesini sağlayabilmektedir.

Anahtar Kelimeler: Orman meşcere parametreleri, İnsansız hava araçları, Ormancılık, Fotogrametri, MATLAB

LIST OF FIGURES

Page No.

LIST OF TABLES

Page No.

LIST OF ABBREVIATIONS

AFI	Area Fit Index
AIC	Akaike's Information Criterion
ALS	Airborne Laser Scanning
ANOVA	Analysis of Variance
APP	Agisoft Photoscan Professional
ATIN	Adaptive TIN
AVHRR	Advanced Very High-Resolution Radiometer
BioSTRUCT	Biomass Estimation from Stand STRUCTure
CHM	Canopy Height Model
DBH	Diameter at Breast Height
DCM	Digital Canopy Model
DMP	Derivative of the Morphological Profile
DOQ	Digital Orthophoto Quadrangle
DSM	Digital Surface Model
DTM	Digital Terrain Model
ETM	Enhanced Thematic Mapper
FN	False Negative
FP	False Positive
GCP	Ground Control Point
GLCM	Grey Level Co-occurrence Matrix
GPS	Global Positioning System
HRV	High Resolution Visible
IR	Infra-Red
İHA	İnsansız Hava Aracı
k-MSN	k-Most Similar Neighbours
KOH	Karesel Ortalama Hata
LAI	Leaf Area Index
LiDAR	Light Detection and Ranging
LKF	Linear Kernel Function
MAE	Mean Absolute Error

MD	Minimum Distance
ML	Maximum Likelihood
MLS	Mobile Laser Scanning
MODIS	Moderate Resolution Imaging Spectroradiometer
MPBS	Morphological Profiles Based Segmentation
MRS	Multiresolution Segmentation
MRT	Multivariate Regression Technique
MSS	Mean Shift Segmentation
NDVI	Normalized Difference Vegetation Index
NPP	Net Primary Productivity
O-A-A	One-Against-All
O-A-O	One-Against-One
OS	Over-Segmentation
OTB	Orfeo ToolBox
PCA	Principal Component Analysis
PDE	Parzen Density Estimate
PFB	Polynomial Fitting-Based
PP	Parallel-Piped
QR	Quality Rate
RANSAC	Random Sample Consensus
RBF	Radial Basis Function
RF	Random Forest
RMSE	Root Mean Square Error
RS	Remote Sensing
RSP	Reference Sample Plot
RSS	Residual Sum of Squares
RTK	Real Time Kinematic
SAGA	System for Automated Geoscientific Analyses
SDD	Standard Deviation of Differences
SF	Sigmoid Function
SfM	Structure from Motion
SPOT	Satellite Pour l'Observation de la Terre
SRGS	Seeded Region Growing Segmentation

SVM	Support Vector Machines
T1E	Type I Error
T2E	Type II Error
TCM	Tree Canopy Model
TCT	Tasselled Cap Transformation
TE	Total Error
TIN	Triangulated Irregular Network
TLS	Terrestrial Laser Scanning
TM	Thematic Mapper
TP	True Positive
UAS	Unmanned Aerial Systems
US	Under-Segmentation
WS	Watershed Segmentation
WT	Watershed Transformation

1. GENERAL INFORMATION

1.1. Introduction

Forests play a significant role in the economy of a country as well as in the protection of soil and water resources. In parallel to the increase in human population, improper use of forests causes losses in the quantity and quality of forests. This, of course, causes critical environmental issues such as landslides, decrease in biodiversity, destabilization of ecosystem etc [1,2]. Some of the benefits of forests can be listed as [3-5];

- Climate stabilisation
- Soil enrichment
- Water circle regulation
- Providing most of the living species a home
- Ensuring biodiversity
- Purification of air
- Providing material for a wide variety of medicine
- Providing psychological relaxation
- Controlling temperature

The statistics published by the General Directorate of Forestry indicated that forests cover an area of 22,000,000 ha (28% of the whole country) in Turkey by the year 2015 [6,7] and that the majority of the forests are managed by the General Directorate of Forestry under the supervision of the state. On the other hand, the forests subject to private property cover a smaller amount of area (18,000 ha). In Turkey, sustainability of forests is maintained by means of forest management plans, which are produced for 10- or 20-year periods [6,8,9]. Up-to-date and robust information about forest characteristics is needed to ensure an efficient forest management plan [9,10-13].

Inventory collection is the most vital step when producing a forest management plan. The aim of the inventory collection is to extract numerical or attribute information about forest characteristics, i.e., stand parameters. Owing to their advantages to provide accurate

and detailed information about the features on the ground, field measurements are generally conducted to determine stand parameters [7]. However, conducting terrestrial measurements is neither cost- nor time-efficient [7,14-18] in most cases. It is also labour-intensive, especially in large-scaled areas. Forest characteristics should be monitored periodically to observe the actual status of forests. However, it may not always be possible to renew terrestrial measurements since it requires a considerable amount of time, cost and labour force [7]. In such cases, remote sensing (RS) techniques can be utilized to determine stand parameters [7,16,19-21]. On the other hand, today's remote sensing technologies are able to offer 3D position accuracy comparable to terrestrial measurements.

1.2. History of the Use of RS Data in Estimating Forest Characteristics

Estimating stand parameters using remote sensing technologies has been studied for a couple of decades. The very early attempts for stand parameter estimation were carried out with optical imageries. de Wulf et al [22] used SPOT (Satellite Pour l'Observation de la Terre)-1 panchromatic and multispectral imageries to extract stand parameters stand density, average tree diameter, average canopy height, stand age, stand basal area and stand volume. They concluded that the arithmetic mean of sample window radiance was the only efficient estimator and that the red and green SPOT-1 wavebands were useless for stand parameter estimation. They also found that the SPOT-1 data was useful to estimate average canopy height and stand density. Cohen and Spies [23] investigated the relationship between forests' spectral and texture characteristics, which were extracted from 30-m Landsat TM (Thematic Mapper) multispectral, 10-m SPOT HRV (High Resolution Visible) panchromatic and 16 forest structural features. Most of the stand features were found to be related with the texture features of the HRV data, whereas the TM data was found to have a weak relationship with all features. The wetness, a feature of the TCT (Tasselled Cap Transformation), was also found to be highly correlated with stand features. The authors indicated that satellite data was useful to estimate the stand age, standard deviation of tree sizes; and mean size and density of trees. Tokola et al [24] used several satellite materials to estimate the stem volumes by means of the RSP (Reference Sample Plot) method, which is a distance-weighted *k*-nearest neighbour estimation technique. The nearest field plots were weighted with two methods, namely the inverse distance and covariance weighting. The authors concluded that both methods yielded similar results on more than 15 plots. The differences

in standard errors were found to be minimum when using SPOT multispectral, SPOT panchromatic and Landsat TM imageries. Holmgren et al [25] used the combination of satellite imagery and terrestrial data to estimate the basal area and stem volume in forest compartments by means of the weighted *k*-nearest neighbour method. The authors estimated the stem volumes with a standard error of 36% when they used only spectral data. They got a standard error of 17% when they took into account the age of the trees, average tree height and site index. Astola et al [26] developed the Forestime software that estimates forest variables through the calculation of feature vectors obtained from satellite images. The software also incorporates the combination of the terrestrial reference data and stand clusters obtained via unsupervised clustering. As a result, the average stem diameter, total stem volume and stem number were found with the RMSEs (Root Mean Square Error) of 23.4%, 37.4% and 87%, respectively. Sivanpillai et al [27] used Landsat ETM+ (Enhanced Thematic Mapper+) data to predict the age and density of loblolly pine stands with the Multivariate Regression Techniques (MRT). The authors found out that a linear combination of ETM4/ETM3, NDVI (Normalized Difference Vegetation Index) and Tasselled cap wetness index was very efficient to estimate the stand age. The PCA (Principal Component Analysis) technique was found to be informative about the relationship between the stand features and Landsat ETM+ reflectance values. The authors also indicated that ETM+ data is very useful to extract structural information from forest stands. Hall et al [28] modelled the aboveground biomass and stand volume by means of Landsat ETM+ data. They introduced the BioSTRUCT (*Bio*mass estimation from stand *STRUCT*ure) technique to build a relationship between the remotely sensed data and forest characteristics. The authors used Landsat ETM+ and field plot data to modelling the height and crown closure attributes. These attributes were then used to modelling the aboveground biomass and stand volume. ETM+ bands 3, 4 and 5 managed to modelling the tree heights with an adjusted R^2 of 0.65, whereas ETM+ bands 3, 4 and 7 modelled the crown closure with an adjusted R^2 of 0.57. The stand volume was estimated as 4 m^3/ha, whereas the aboveground biomass as 4 tonnes/ha. Kayitakire et al [29] estimated the age, circumference, top height, basal area and density of spruce stands by means of IKONOS imagery. These forest attributes were estimated from the texture features extracted from the GLCM (Grey-Level Co-occurrence Matrix). The age, stand density, top height and circumference attributes were modelled with R^2 values ranging from 0.76 to 0.82. The basal area was found to have a weak relationship with texture features (R^2=0.35). Peuhkurinen et al [30] estimated the stand parameters by using the *k*-MSN (*k*-Most Similar

Neighbours) method on IKONOS data. The authors achieved the best results by using the spectral characteristics derived from the multispectral imageries. The mean total stem volume, mean height and basal area were estimated with RMSEs of 52.2 m^3/ha, 3.1 m, and 5.6 m^2/ha, respectively. Ozdemir and Karnieli [31] used a WorldView-2 multispectral imagery to estimate the forest variables in a dryland forest. The authors investigated the relationship between the image texture characteristics and structural variables basal area, number of trees, Clark-Evans index, contagion index, gini coefficient, diameter differentiation index, standard deviation of diameters at breast height and stem volume. They concluded that there was a significant correlation between the texture features and forest structural variables. Kilkki and Päivinen [32], Hagner [33], Reese et al [34], Couteron et al [35], Wolter et al [36], Günlü et al [37] and Günlü et al [38] are some of the other researchers who utilized optical imageries to estimate stand parameters.

The advent of LiDAR (Light Detection and Ranging) technologies has attracted the analysts' attention. The main reason for this is that LiDAR point clouds offer multiple returns, which is very efficient when extracting forest structural characteristics. Hence, various studies reported in the literature used LiDAR data to estimate forest characteristics. Kwak et al [39] used LiDAR data to detect individual trees and estimate their heights. First, they classified raw LiDAR points into four groups as ground, low vegetation, medium vegetation and high vegetation. Then, they calculated the DCM (Digital Canopy Model) by subtracting the DTM (Digital Terrain Model) from DSM (Digital Surface Model). They applied the extended maxima transformation of morphological image analysis methods on the calculated DCM to detect the tree tops. The WS (Watershed Segmentation) was then implemented to delineate each individual tree. Finally, they estimated the tree heights by finding the maximum elevation value of each crown segment. Estimated tree characteristics were then compared against field measurements. The results showed that the *Pinus koraiensis*, *Larix leptolepis* and *Quercus spp*. were detected with accuracies of 68.1%, 86.7% and 67.4%, respectively. Rahman and Gorte [40] presented a method to delineate individual tree crowns by using high resolution airborne LiDAR data. The method was based on the fact that the laser pulses are denser at the centre of a tree crown and that density decreases towards the edges of the crown. The tree crowns were delineated using the inverse WT (Watershed Transformation) algorithm. The results were compared with those of the CHM (Canopy Height Model)-based tree detection approach. The authors concluded that the performance of the presented method was higher than the CHM-based approach. It was also

concluded that the CHM-based approach delineated the coniferous tree crowns better than the proposed methodology. Suárez et al [41] used airborne LiDAR data together with aerial photography to identify each individual tree and find their heights. The reason for using these two data was to get benefit from the spectral characteristics of the aerial photography and height information of the LiDAR data. In the study, they performed image segmentation to the aerial photography in order to identify each individual tree crown. Afterwards, they applied an object-based classification to the TCM (Tree Canopy Model) produced by the subtraction of the DTM from DSM. The authors compared their results against the field measurements. They concluded that their approach detected most of the tree tops and that the tree heights were found with an accuracy greater than 70% [41]. Li et al [42] proposed an algorithm for segmentation of individual trees using a LiDAR point cloud. The algorithm was based on relative spacing between trees. Once a tree top point is obtained, other points belong to the same tree are included with respect to a predefined threshold. The algorithm identifies trees from the tallest to the shortest. A shape index was also used to avoid incorrect segmentation. The results showed that 86% of the trees were detected. In addition, 94% of the segmented trees were found to be correct. They also indicated that the proposed algorithm managed to delineate individual trees in mixed conifer stands. Liu et al [43] proposed a method in which tree crowns were extracted with LiDAR data. In this method, a slope-based filtering methodology was applied to the raw LiDAR data in order to classify the points as ground and non-ground. Retrieved non-ground points were then segmented. The obtained segments were classified based on their size and multiple echoes. Finally, the points of each individual tree were grouped and each tree crown was delineated by using the spoke wheel algorithm. The authors found out that more than 85% of the trees were extracted with an accuracy greater than 95%. Morsdorf et al [44] and Gupta et al [45] used the *k*-means clustering algorithm to delineate the trees. In their approach, they determined the local maxima of the smoothed CHM. Calculated maxima were then used as seeds and the *k*-means clustering algorithm was applied to delineate the trees. They indicated that their approach has a huge potential in tree crown delineation. Further information about the use of the *k*-means clustering algorithm in tree crown delineation can be found in [44] and [45]. Lee et al [46] introduced an adaptive tree clustering method for airborne LiDAR data. They determined the boundary of each tree crown by using the ground points obtained through the classification of LiDAR data. A minimum radius value was used to estimate the seed points i.e. tree tops. Region growing was then applied to each seed point. Finally, the clusters of

each individual tree were merged hierarchically by applying agglomerative clustering technique. Tree detection accuracy was found 95.1% with no significant bias [46]. Pascual et al [47] proposed an approach for the characterization of the *Pinus sylvestris* stands using LiDAR data. They used the eCognition software to delineate each tree on the CHM of the study area. The *k*-means algorithm was used to cluster the segments into five structure types ranging from high dense canopy to sparse coverage. The median and standard deviation statistics were found to be the best features that managed to characterize the *Pinus sylvestris* stands [47]. Reitberger et al [48] delineated the trees and found the stem positions with a dense airborne LiDAR data. The tree segments were produced by employing the watershed algorithm on the CHM. The stem positions were then determined using the local maxima of the segments. A three-step procedure was conducted to determine the stem positions accurately. In the first step, the points between the ground and crown base were discriminated. Second, candidate stem positions were determined by using a hierarchical clustering technique. Third, each tree stem was found by a RANSAC (Random Sample Consensus)-based adjustment of the stem points. They applied the proposed methodology on a full waveform LiDAR data and detected the deciduous and coniferous trees with accuracies of 44% and 61%, respectively. They concluded that the pulse width and intensity facilitated to discriminate the ground, crown and stem points. In addition, the mean intensity of the stem points was found to be the most significant feature for the discrimination of trees [48].

Despite its advantages, LiDAR technology has some disadvantages, too. LiDAR systems may have difficulties to produce dense point clouds, which are very important for the 3D reconstruction of tree crowns. Besides, the acquisition and processing of LiDAR data is still not cost-efficient [49]. In addition, quality of signals sent by LiDAR sensors deteriorates as the acquisition range increases [50], which is likely to lead to a point cloud of low quality. On the other hand, using UAS (Unmanned Aerial System)-based aerial photos enables the generation of dense point clouds owing to low-altitude flights. Hence, using point clouds produced with aerial photos taken from UASs would be a reasonable approach to estimate stand parameters. Díaz-Varela et al [49] used high-resolution UAS data to estimate the crown parameters (crown diameter and tree height) of olive trees. They found the local maxima (i.e. possible tree tops) by employing a square search window on the DSM. The ground heights were then found by using the DSM. An object-based classification was applied on the segmented data, which was generated by means of the MRS (Multiresolution

Segmentation) algorithm implemented in the eCognition software. In the classification stage, the infrared and three visible layers of the UAS photogrammetry-derived orthophoto image were used together with the DSM and NDVI images. They found the heights and crown diameters of the trees with an RMSE less than 0.45 m [49]. Kattenborn et al [51] detected the individual palm trees by using the pouring algorithm, which is similar to the WS. As a first step, the DTM and DSM of the study area were produced by using the point cloud extracted from UAS images. Afterwards, a normalized DSM was obtained from the DTM and DSM. Tree crowns were delineated using the pouring algorithm, which computed the local maxima of the normalized DSM. The mapping accuracy was found 86.1% [51]. In a similar study, Sperlich et al [52] utilized the pouring algorithm to detect each single tree in coniferous and deciduous sites. 87.68% of the coniferous trees were detected with 1 m search radius, whereas 90.41% of the coniferous trees were detected with 2 m search radius. Only 13.33% of the deciduous trees were detected with 1 m search radius, while 30% of them were detected with 2 m search radius. According to the authors, these low tree detection accuracies were due to the highly diverse forest structure.

1.3. Stand Parameters

Determination of stand parameters is of huge importance in the forest management. The more accurate estimation of stand parameters, the more efficient forest management plan. Following are a few of the most important stand parameters.

1.3.1. Number of Trees

This parameter is one of the most significant stand parameters and is usually given as trees/ha. It is very efficient in investigating regeneration and can be used to determine if a stand is under- or over-stocked by comparing with a management ideal. It is also an efficient parameter if trees are of similar size and age [53]. In the literature, many remote sensing-based approaches have been conducted to estimate this parameter, as an alternative to terrestrial measurements. McCombs et al [54] combined small-footprint LiDAR data with high-resolution multispectral image to estimate tree density. The tree identification accuracy was found 64.7% and 87.3% in the test sites with LiDAR data, whereas it was found 78.6%

and 92.4% with multispectral data. The results showed that the combined dataset significantly improved the tree identification accuracy over single-dataset methods with 83.5% and 94.8% in the test sites. Sivanpillai et al [27] used the MRT to estimate stand density. The regression model formed with Landsat ETM+ bands 1, 4 and 7 was found to be effective in predicting the stand density with an R^2 value of 60%. Yılmaz et al [55] used a Hough transformation-based methodology to count the trees in the test area. They managed to detect more than 90% of the trees. Yilmaz et al [7] determined the number of trees by employing a sliding window on a CHM, which was extracted from UAS-based aerial photos. The authors' methodology managed to detect 72.3% of the trees.

1.3.2. Height of Trees

Height of a tree is simply the vertical distance between its top and bottom points. Mean tree height of a stand is often used as a measure of stand height. Since this parameter has a strong relationship with some other important stand parameters such as volume and biomass, it should be determined accurately. In fact, measuring the heights of trees in a small area is not a big deal. All measurements are added together and divided by the total number of trees to obtain the mean height. Sample-based measurement is another alternative to determine the mean stand height. In this measurement type, mean tree height is calculated from randomly selected trees [56]. Height of a tree is illustrated in Figure 1.

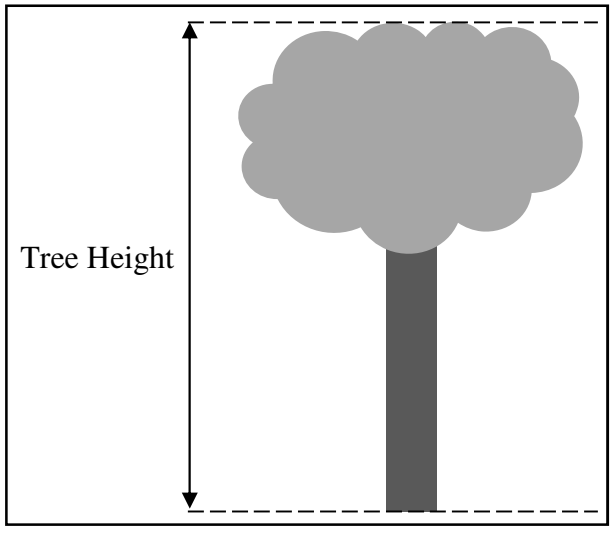

Figure 1. Height of a tree

Nilsson [57] estimated the heights of the trees in a Scots pine stand with airborne LiDAR data. The mean tree height was found to be underestimated by 2.1-3.7 m. Later in 1997, Næsset [58] used LiDAR data to determine the mean tree height of 36 stands including Norway spruce and Scotch pine. The author computed the mean height as the arithmetic mean of the LiDAR-based canopy heights. A weighted mean of the LiDAR-derived canopy heights resulted in an underestimation of ground truth mean height by 2.1-3.6 m. The Standard Deviation of Differences (SDD) between the ground truth and LiDAR-derived mean height was found 1.1-1.6 m. Næsset and Økland [59] estimated the mean tree height by means of ALS (Airborne Laser Scanning) data. Ground truth height values were regressed against laser-based canopy heights. Cross-validation of regressions indicated that the SDD between the ground truth heights and estimated tree heights was 3.15 m (17.6%). The cross-validation resulted in a precision of 1.49 m (7.6%). The authors concluded that making use of laser data was more efficient in determining tree heights than the other techniques. Holmgren [60] developed estimation models using ALS data to estimate tree heights and some other stand parameters. As a result, the author estimated the tree heights with an RMSE of 0.59 m (3%) at stand level. Olofsson and Holmgren [61] proposed a stand delineation method that uses the local maxima of CHMs and region merging of corresponding Voronoi cells. Tree heights were determined from the segmented CHM. The coefficient of determination (R^2) and average coefficient of variation for the tree heights were found 0.68-0.88 and 0.07-0.19, respectively.

1.3.3. Crown Closure

Crown closure, which is the proportion of the ground area covered by the vertical projection of tree crowns [62], is used as a measure of tree density. Crown closure ratio increases in areas consisting of interlocking trees. In Turkey, a closure ratio between 11% and 40% refers to a sparse density, whereas a closure ratio between 41% and 70% refers to a moderate density. A crown closure ratio greater than 71% indicates a high density [63,64]. Crown closure is one of the most important stand variables and can be determined either by terrestrial measurements or by remote sensing technologies. In ground measurements, canopy closure is determined manually by using auxiliary devices. Estimating the canopy closure with ground measurements suffers from some limitations. Estimation result may be affected by various factors such as the landform, perspective of the surveyor etc. If the

application area is relatively smaller, then ground measurements won't be a big deal [65]. However, field measurements may not always be efficient in large-scaled areas, since it requires a huge amount of labour force and time. Aerial and satellite imageries can be used to eliminate the limitations of ground measurements [65-67]. In the literature, various studies utilized remote sensing technologies to produce crown closure maps. Huang et al [68] estimated the canopy closure by using a Landsat ETM+ data and a high-resolution (1-m) DOQ (Digital Orthophoto Quadrangle) data. Their methodology included the establishment of a relationship between the Landsat ETM+ data and tree canopy density by means of regression tree and linear regression techniques. The regression tree approach was found to be more successful than the linear regression technique. The authors recommended their strategy for large-scaled areas. Hansen et al [69] used a MODIS (Moderate Resolution Imaging Spectroradiometer) data to estimate the crown closure ratio. The training data used by the authors was derived from over 250 classified Landsat images. The closure map was produced with a supervised regression tree algorithm. The results indicated that the MODIS data yielded greater spatial detail in the characterization of canopy closure compared to the AVHRR (Advanced Very High-Resolution Radiometer) data [69]. Hansen and DeFries [70] investigated the changes in global forest cover between the years 1982 and 1999 by using regression tree on AVHRR data. They derived the training data from high-resolution imagery. The authors concluded that Latin America and tropical Asia were the most deforested regions in the world. Hansen et al [71] used a MODIS data to produce a closure map. To do so, they tested 40-day composites, single-date images and annual MODIS metrics. It was found that the composites outperformed the metrics at local scale, whereas the metrics surpassed the composites at global scale. A comparison between the test area and produced closure map revealed that the canopy closure was estimated successfully. Further information about this study can be found in [71]. Rokhmatuloh et al [72] estimated the crown closure ratio of Africa by using a coarse-resolution MODIS imagery. They used 11 scenes of QuickBird images as training data. In a similar study, Rokhmatuloh et al [73] used a MODIS data to estimate the crown closure ratio of Asia. They used 22 scenes of QuickBird images as training data. Tunay and Ateşoğlu [74] used a Landsat TM imagery to map the canopy closure. They found out that, out of a few band ratios, only the ratio image obtained by dividing the band 5 to band 4 (TM 5/4) was statistically significant in terms of the ANOVA (Analysis of Variance) test. Hence, this ratio image was classified with the ML (Maximum Likelihood) algorithm by using a training data collected for sparsely (11% -

40%), moderately (41% - 70%) and highly (71% - 100%) dense areas. As a result, the closure map of the test area was produced with an overall classification accuracy of 83.3% [74]. Meydan and Berberoğlu [75] used a Landsat ETM+ (30 m) imagery to produce a closure map that was then used as an input to estimate the NPP (Net Primary Productivity), which refers to the net amount of carbon provided for biomass. Günlü et al [76] produced a canopy closure map by classifying a Landsat ETM+ data. They classified the imagery with an overall classification accuracy of 85% and a Kappa of 0.94. In a similar study, Günlü [18] classified a Landsat TM data to produce a closure map. The overall classification accuracy and Kappa were found 90.4% and 0.88, respectively.

1.3.4. Crown Diameter

Crown diameter, which is another significant forest structural characteristic, is defined as the maximum width of the vertical projection of a tree crown. It can also be defined as the diameter of the circle enclosing the vertical projection of a tree crown. In field, crown diameter of a tree is measured with a calliper in two perpendicular directions, one being the diameter passing through the centre of the crown in north-south direction and the other one being perpendicular to the first. The crown diameter is obtained with the arithmetic mean of the two measured diameters. The crown diameter is one of the most commonly estimated dendrometric parameters, which are used to derive the diameter at breast height (DBH), tree volume, and biomass with allometric equations. Figure 2 illustrates the crown diameter of a single tree.

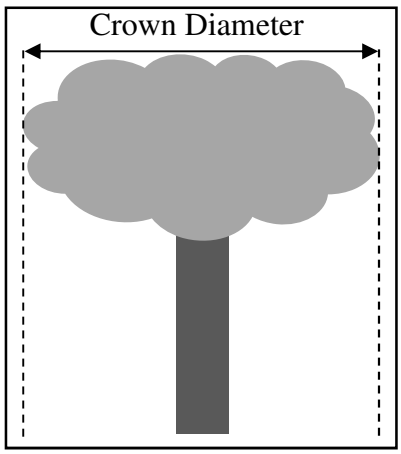

Figure 2. Crown diameter of a tree

In the literature, a wide variety of approaches has been introduced to estimate crown diameters. Popescu et al [77] estimated the crown diameters from small-footprint LiDAR data. In order to calculate the crown diameters, they fitted a 4^{th}-degree polynomial for each tree on two perpendicular profiles, centred on the top of the tree. The critical points of the fitted polynomials were then determined. Crown diameter was computed as the average of the two values measured along two perpendicular directions from the tree top. As a result, crown diameters were estimated with RMSEs ranging from 1.36 m to 1.41 m. Falkowski et al [78] estimated the crown diameters by conducting spatial wavelet analysis to a LiDAR data. They convolved a LiDAR-derived CHM with 2D Mexican hat wavelets. The local maxima of the wavelet transformation-derived image were used to determine the heights and crown diameters of trees. The results showed that the estimated tree crown diameters were well correlated (r=0.97) with terrestrial measurements. Later in 2008, Popescu and Zhao [79] used LiDAR data to estimate the crown diameters by means of a method based on the analysis of two perpendicular profiles of the CHM. The estimated crown diameters were evaluated with terrestrial measurements. They estimated the pines, deciduous trees and all trees with RMSEs of 1.68 m, 2.08 m and 1.84 m, respectively. Ke and Quackenbush [80] estimated the crown diameters with an approach based on the spectral and shape characteristics of tree crowns. In the first step, they used a region-based active contour model to generate the crown area. A spectral-shape-based approach was used to detect the tree tops, which were then used within a new hill-climbing algorithm to delineate crown pixels. Calculated crown diameters were compared against field measurements. Crown diameter estimation errors were found to be less than 0.5 m. Wu et al [81] identified the trees by using a voxel-based marked neighbourhood searching method on MLS (Mobile Laser Scanning) data. They concluded that the estimated crown diameters corresponded well with field-measured crown diameters. The crown diameters were estimated with R^2 values greater than 0.9. Díaz-Varela et al [49] delineated the tree crowns by applying the MRS algorithm to a multilayer image containing the DSM, NDVI, DifMin (calculated for each pixel by the difference between its DSM value and the minimum elevation value within a given neighbourhood) and three visible and IR (Infra-Red) layers. Comparison with the field measurements indicated that the used methodology estimated the crown diameters with R^2 values of 0.58 and 0.22 for the test sites 1 and 2, respectively; and with R^2 values of 0.66 and 0.53 for the test sites 1 and 2 at genotype level, respectively. Panagiotidis et al [82] used UAS-based aerial photos to extract the CHMs of test sites. After smoothing the produced

CHMs with a morphological filter, they determined the local maxima of the CHMs to detect the tops and heights of the trees. The tree crowns were delineated with the inverse WS algorithm. The crown diameters were computed from the delineated segments. They compared the crown diameter estimates against ground measurements and concluded that their methodology estimated the crown diameters with RMSEs ranging from 14.29% to 18.56%.

1.4. Motivation

Since forests play a significant role in the ecosystem, their sustainability should be maintained so that they constitute a natural resource utilized by people and other life forms [83]. Unsystematic management of the forests causes decrease in biodiversity, erosions, environmental pollution, forest destructions and failure in achieving sustainability [84]. Forest management plans are produced to preserve the forests and maintain their sustainability. In Turkey, forest management plans are produced for 10- or 20-year periods. Inventory collection, the fundamental step to produce a forest management plan, is made periodically to monitor the actual status of forests [2]. In Turkey, field measurements are generally used to collect forest inventory data. However, terrestrial measurements are costly and labour-intensive, especially for large-extent areas. In recent years, remote sensing technologies draw attentions owing to their advantages to provide robust information about forest inventory. Using remote sensing technologies in forestry applications reduces the amount of the time and labour force needed. In the literature, a wide variety of studies uses satellite data to collect inventory data. Since point clouds offer a very good representation of the surface of the earth, they have been used in a large number of forestry studies as an alternative to satellite imageries. Since LiDAR point clouds result in multiple returns, they are very efficient for the collection of forest inventory. However, the acquisition and processing of LiDAR data is still not cost-efficient, which constitutes an impediment to the use of them. The use of point clouds extracted from stereo aerial photos taken from UASs may be considered a reasonable alternative for LiDAR point clouds in cases where there are no LiDAR data. The aim of this thesis is to investigate the feasibility of UAS-based point clouds in the estimation of stand parameters such as the location, number, height, crown closure and crown diameter of trees.

1.5. Thesis Outline

In the context of this thesis, Section 1 presents information about the stand parameters and how they have been estimated in the literature. This section also gives theoretical background for the used image classification, ground filtering and image segmentation algorithms. Section 2 provides information about the followed methodology to estimate stand parameters. The theory of the proposed polynomial fitting-based (PFB) crown diameter estimation methodology was also given in this section. Section 3 shares the estimation results of the stand parameters. Estimation results were also evaluated in this section. Section 4 presents the conclusions drawn from this thesis.

1.6. Ground Filtering

CHMs have been used in many forestry applications to reconstruct tree stands in 3D, owing to their advantages to offer a good representation of the physical characteristics of tree stands [85-89]. Since a CHM is computed by subtracting a DTM from a DSM, the very first step of the CHM generation is the extraction of a DTM. A DTM represents the topography of the bare earth surface. Hence, the point cloud to be used to generate a DTM should be filtered to remove the points of the above-ground objects, which is called 'ground filtering'. As topography gets more abrupt, ground filtering process becomes more challenging [90,91]. Once the point cloud is filtered, a DTM is generated through the interpolation of retrieved ground points.

A wide variety of ground filtering algorithms have been introduced in the literature. These algorithms can be classified as morphology-based [92-98], segmentation-based [99], slope-based [100] and interpolation-based [101-103]. The morphology-based algorithms utilize the erosion, dilation, opening and closing morphological operations to remove the non-ground points within user-defined windows. Many morphology-based approaches use a fixed-sized processing window, which makes it challenging to remove objects with varying sizes. The segmentation-based approaches use segmentation and clustering techniques to remove the points belong to the above-ground objects. The slope-based approaches remove the non-ground points by using the slope between a candidate point and its neighbours. The slope-based approaches generally use a fixed slope threshold to reduce computational load, which can be a huge drawback to remove above-ground objects on a sloping terrain. The

interpolation-based methods compare the elevation values of the points with their estimated values through various interpolation algorithms. The Adaptive TIN (ATIN), which is an interpolation-based ground filtering algorithm implemented in the Agisoft Photoscan Professional (APP) software, was used in this thesis to filter the point clouds. Further information about the ATIN algorithm is given in the following subsection.

1.6.1. ATIN Filtering Algorithm

The ATIN algorithm, developed by Axelsson [104], removes non-ground points by using the distances between each point and TIN (Triangulated Irregular Network) surface. This algorithm first divides the data into square grids. Afterwards, a reference TIN is generated from the seed points, which are the points with minimum elevation values within each grid [105-106]. Each unclassified candidate point is then added to each triangle in TIN. Points are classified with respect to their distances to triangular surface and to the angle with the nodes of the triangles. An unclassified point is labelled as ground if computed distance and angle are smaller than a threshold. Otherwise, it is said to be a non-ground point. In the next iteration, TIN is densified by adding new ground points to it. This process continues until there is no point to classify [98,104-106]. Figure 3 illustrates the theory of the ATIN algorithm.

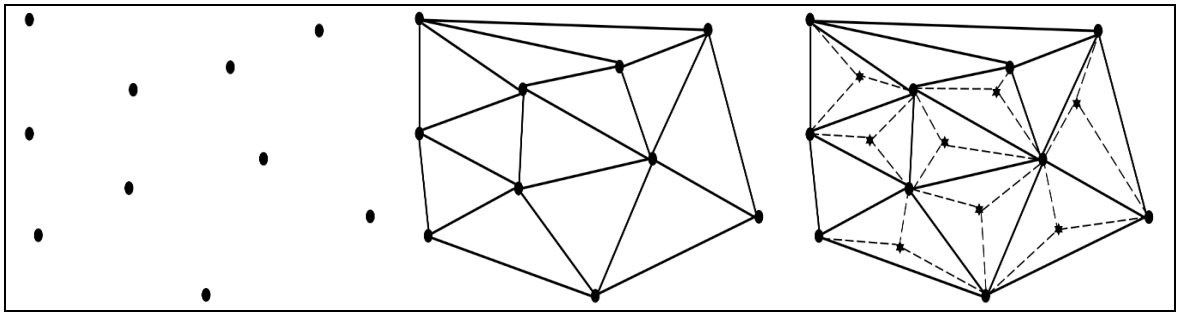

Figure 3. Filtering principle of the ATIN algorithm. Initial seed (ground) points (left), TIN generation from seed points (middle), densification of the TIN by adding new ground points (right)

1.6.2. Accuracy Assessment of Ground Filtering

Performance of the used ground filtering algorithm plays a vital role in 3D accuracy of the produced DTM, which attaches importance to the evaluation of ground filtering result [91]. Sithole and Vosselman [107] stated that ground filtering process introduces two types of errors, the omission and commission error. The former is related to the misclassification of ground points, whereas the latter is the classification of non-ground points as ground [91,106].

In most cases, it is not practical to investigate the performance of a ground filtering algorithm through the examination of all points in the point cloud. Zhang et al [96] and Zhang and Whitman [108] stated that it is reasonable to use randomly selected test points to evaluate the ground filtering result quantitatively. The Type I Error (T1E), Type II Error (T2E) and Total Error (TE), which were proposed by Sithole and Vosselman [107,109,110], have been used in many studies to investigate the performance of filtering algorithms. These error metrics were given by Montealegre et al [111] as;

$$T1E = \frac{o}{GP}$$
$$T2E = \frac{c}{NGP} \tag{1.1}$$
$$TE = \frac{o + c}{GP + NGP}$$

where, o defines the omission error and c stands for the commission error. GP and NGP stand for the total number of ground and non-ground points, respectively [111,112].

1.7. Tree Crown Segmentation

Segmentation is partitioning of any given image into non-overlapping homogenous segments to make the image more meaningful for further analysis. In other words, image segmentation is a pixel labelling process in which the pixels with similar spectral structure are assigned to the same label [113]. Image segmentation algorithms generally consider two significant criteria: the homogeneity of each segment and continuity of each segment's border. Most of the segmentation techniques perform by using some parameters need to be

fine-tuned by the user, which makes segmentation process a highly subjective task [114-117]. In this thesis, the MSS (Mean Shift Segmentation), MPBS (Morphological Profiles Based Segmentation), MRS, SRGS (Seeded Region Growing Segmentation) and WS techniques were used to delineate the tree crowns and estimate their diameters on CHMs.

1.7.1. MSS

The mean shift, pioneered by Fukunaga and Hostetler [118] and generalized by Cheng [119], is an iterative procedure in which each data point is shifted to the average of the neighbouring data points [120]. The modes in a probability density function based on the PDE (Parzen Density Estimate) [118] are detected in the MSS algorithm. Zheng et al [120] stated that the MSS algorithm is a straightforward extension of the discontinuity preserving smoothing algorithm. Comaniciu and Meer [121] defined the mean shift $m(x)$ as;

$$m_{h,G}(x) = \frac{\sum_{i=1}^{n} x_i g\left(\left\|\frac{x - x_i}{h}\right\|^2\right)}{\sum_{i=1}^{n} g\left(\left\|\frac{x - x_i}{h}\right\|^2\right)} - x \tag{1.2}$$

where, x_i is a data set in a d-dimensional Euclidean space ($x = \{x_1, x_2, \dots, x_n\}$), G is the kernel for weights and x is the centre of the window. The mean shift vector always points to the direction of the maximum increase in the density. The mean shift procedure is applied successively by calculating the mean shift vector and translate the kernel $K(x)$ by the mean shift vector. The algorithm converges at a point where estimate has zero gradients [120,121]. The mean shift algorithm iteratively updates y_j, which is defined as [120];

$$y_{j+1} = \frac{\sum_{i=1}^{n} x_i K_W(y_j - x_i)}{\sum_{i=1}^{n} K_W(y_j - x_i)} \tag{1.3}$$

where, $K_W(x) = |X|^{-1/2} K\left(W^{-1/2}x\right)$, W is a symmetric positive definite $d \times d$ bandwidth matrix and d is the dimension of feature space. $K(x)$ is a d-variate radically symmetric kernel [120]. Comaniciu and Meer [121] used a four-step procedure to conduct the MSS algorithm;

- Run the mean shift algorithm for the data. All information relating to the d-dimensional convergence points in z_i (z_i is the filtered image pixels in the joint spatial-range domain) are stored.
- Delineate the clusters by grouping together all z_is, which are closer than spectral bandwidth h_r (spectral difference between classes in the spectral domain) and spatial bandwidth h_s (spatial difference between classes in the spatial domain).
- Assign a label for each point.
- Remove regions having less than M pixels (optional). Further information about the MSS algorithm can be found in [120-125].

The Orfeo ToolBox (OTB) software uses three parameters to perform the MSS algorithm; the spatial radius, range radius and mode convergence threshold. The spatial radius parameter specifies the spatial radius of the neighbourhood and the range radius parameter defines the radius in the image (in elevation unit in our case). Iterative scheme stops if the mean shift vector is below the mode convergence threshold parameter.

1.7.2. MPBS

The MPBS algorithm, developed by Pesaresi and Benediktsson [126], is based on the morphological characteristics of connected components in images. The opening and closing operations are the most commonly-used ones in mathematical morphology. These operations examine the geometrical interactions of an image with a structuring element [127], which is basically a set of known shapes such as disk, square, line etc. The opening operation is the conduction of dilation to an eroded image to reconstruct as much as possible of the eroded image. Conversely, the closing operation is the conduction of erosion to a dilated image to reconstruct the initial shape of dilated image structures [128]. In other words, the opening and closing operations isolate bright and dark objects in images, where bright means brighter than the surrounding structures and dark means darker than the surrounding structures [126]. Pesaresi and Benediktsson [126] defined each image object as a connected component of pixels with the same morphological features. The MPBS algorithm applies the opening and closing by reconstruction operations with increasing-sized structuring elements to form multiscale characteristics called ‘morphological profiles’ [129]. Pesaresi and Benediktsson

[126] defined the DMP (Derivative of the Morphological Profile) as a vector where the slope of the opening-closing profile is recorded for every step of an increasing structuring element series. The MPBS algorithm assigns a segment label to each pixel with respect to the scale that corresponds to the greatest derivative of its profiles [126,129,130].

The MPBS algorithm, which was implemented in the OTB software, utilizes four parameters to perform; the profile size, initial radius, radius step and decision threshold. The profile size parameter specifies the size of the profiles, the initial radius parameter defines the initial radius of the structuring element (in pixel) used to perform morphological operations and the radius step parameter specifies the radius step along the profile (in pixel). The MPBS algorithm ignores the profiles whose values are below the decision threshold parameter.

1.7.3. MRS

The MRS, a bottom-up region merging method [131], starts with one-pixel objects and merges them with neighbouring pixels by considering a relative homogeneity criterion, which is a combination of the colour and shape criteria. The homogeneousness or heterogeneousness of objects are measured with this homogeneity criterion [132]. The MRS algorithm uses three parameters as the scale, shape and compactness. The scale parameter, which is a threshold value used as a stopping criterion for optimization process, is used to determine the average size of the segments [133]. Smaller scale parameters result in smaller image objects, whereas greater values yield larger ones [131,132]. Lowe and Guo [134], Li and Shao [135] and Kavzoglu and Yildiz [133] indicated that the scale parameter is the most effective parameter of this segmentation process. Benz et al [131] and Elmqvist et al [136] stated that over-segmentation effect can be reduced by increasing the scale parameter. The colour and shape parameters are weighted between 0 and 1 to calculate the heterogeneity within an object [137]. Since spectral information is essential for segmentation, colour parameter cannot be less than 0.1 [136]. The sum of standard deviations of each band identifies the spectral heterogeneity (colour) [137]. Baatz et al [138] stated that minimizing only spectral heterogeneity results in spectrally similar objects or objects with fractally shaped borders. Hence, incorporating the shape information to the segmentation process helps reconstruct the objects. The shape heterogeneity is defined by the terms compactness and smoothness [134,137]. The compactness is the ratio between the perimeter of an object

and square root of the number of pixels in the object. The smoothness is calculated by the ratio between the perimeter of an object and perimeter of its bounding box [134-136]. Platt and Rapoza [137] stated that the optimum smoothness and compactness parameters are dependent on the type and size of the objects to be classified. If the objects are homogenous, then the optimum smoothness and compactness parameters would be high. Otherwise, they would be low.

The MRS algorithm is generally conducted with the eCognition software. The software defines the heterogeneity criterion f as [131];

$$\begin{aligned} f &= w_{colour} \cdot \Delta h_{colour} + w_{shape} \cdot \Delta h_{shape} \\ w_{colour} &+ w_{shape} = 1 \end{aligned} \tag{1.4}$$

where, w_{colour} ($w_{colour} \in [0,1]$) and w_{shape} ($w_{shape} \in [0,1]$) are the weights for the colour and shape, respectively. f criterion should be less than a threshold. The MRS algorithm adds a weight w_c to each band of the image to enable multi-variant segmentation. Difference in spectral heterogeneity Δh_{colour} is defined as [131];

$$\Delta h_{colour} = \sum_c w_c \left(n_{merge} \cdot \sigma_{c,merge} - \left(n_{obj1} \cdot \sigma_{c,obj1} + n_{obj2} \cdot \sigma_{c,obj2} \right) \right) \tag{1.5}$$

where, n_{merge} is the total number of pixels in merged object. σ_c is the standard deviation within object of band c. n_{obj1} and n_{obj2} are the number of pixels in the objects 1 and 2, respectively. The shape heterogeneity is defined as [131];

$$\begin{aligned} \Delta h_{shape} &= w_{compct} \cdot \Delta h_{compct} + w_{smooth} \cdot \Delta h_{smooth} \\ \Delta h_{smooth} &= n_{merge} \cdot \frac{l_{merge}}{b_{merge}} - \left(n_{obj1} \cdot \frac{l_{obj1}}{b_{obj1}} + n_{obj2} \cdot \frac{l_{obj2}}{b_{obj2}} \right) \\ \Delta h_{compct} &= n_{merge} \cdot \frac{l_{merge}}{\sqrt{n_{merge}}} - \left(n_{obj1} \cdot \frac{l_{obj1}}{\sqrt{n_{obj1}}} + n_{obj2} \cdot \frac{l_{obj2}}{\sqrt{n_{obj2}}} \right) \end{aligned} \tag{1.6}$$

where, l and b are the perimeters of the object and object's bounding box, respectively. Benz et al [131] and Platt and Rapoza [137] pointed out that there is no such thing as optimal

parameters in image segmentation process. Hence, analysts usually use trial-and-error strategy to define suitable parameters to initiate segmentation process [133,134,139].

1.7.4. SRGS

The SRGS algorithm, proposed by Adams and Bischof [140], requires some known (seed) points from which the algorithm starts to grow regions. Image regions continue to grow with respect to predefined similarity rules until the algorithm reaches some stopping criteria, which are used to define the final borders among image regions [141]. Two problems must be solved before the implementation of the region growing segmentation [142]. The first one is related to the determination of the seed points. Local maxima filtering approaches have been widely used in the literature to retrieve the seed points [143,144]. Local maxima filtering is the identification of the point that has greater magnitude compared to its neighbours within a window [144,145]. An appropriate window size should be selected to identify each tree. Hirschmugl et al [141] stated that one or more seed points can be defined for each tree. In order to avoid too many tree crowns, the algorithm removes all seed points except the one that is the actual tree top. Misdetection of seed points results in unnatural image segments. The second problem that should be solved before the segmentation is the definition of similarity rules. The algorithm recursively compares the value of a seed pixel with those of its neighbours. If any neighbouring pixel is within a predefined similarity threshold, then this point is said to be belong to the same region as the seed point [146] and added to the seed point's region. Region growing continues until all pixels are assigned to a region. Small regions are merged into the neighbouring ones that are within a certain spectral distance threshold. This segmentation technique is famous for its speed and simplicity. In addition, spatially/spectrally homogenous regions are guaranteed in this segmentation technique. This technique also enables the production of regions at multi scales [147]. On the other hand, it does not have any certain limitations [148], which is the biggest disadvantage of this technique. The SRGS approach works well if only one seed is identified for each tree crown and if the seed is located in the centre of the tree crown [141]. It should be noted that the location of each seed point directly affects the segmentation result, which attaches importance to accurate determination of seed points.

The SAGA (System for Automated Geoscientific Analyses) software is generally used to perform the SRGS. In this software, seed points can be defined manually or can be

determined automatically by the representativeness analysis [149], which is based on the fact that spectral characteristics of neighbouring pixels will more likely have similar values than those of further pixels. The representativeness r_c of a pixel's feature in band c is computed as [150];

$$g_v = \frac{\sum_{i=1}^{m} \frac{v_i}{d_i d_i^p}}{\sum_{i=1}^{m} \frac{1}{d_i^p}} \qquad (1.7)$$

$$r_c = \frac{0.5 v_m}{g_v}$$

where, v_m is the global image variance. The algorithm computes an average semi-variance gradient as the inverse distance weighted mean of all semi-variance gradients within the distances d_1 to d_m with the weights $1 / d_1$ to $1 / d_m$. Each of these weights is powered by p. The performance of this approach is improved by using an increasing radius d_i to decrease the image resolution around targeted pixel.

The SAGA software offers two alternate region growing algorithms. The conventional region growing algorithm is implemented with the following steps [150];

- An array is initialized with the seed locations and their property space.
- The border pixels are listed for each seed. A border point can fall in multiple clusters.
- For any border point, the maximum Euclidean distance to its seed is computed and stored in the property space.
- For every cluster, the n-dimensional border of the property space is computed and stored. Then repeat the following while the list of border points is not empty;
- For each cluster, the border point and cluster with the minimum maximal Euclidean distance in the property space are found. - This border point is added to the cluster and the border of this cluster is updated. - This border point is removed from the border point list and the new border points of the merged cluster are added. - The membership, attribute distance to the seed and spatial position are determined for each cluster [150].

The second alternative, the fast region merging, is generally implemented on the representativeness component. If the representativeness of a pixel is the local maximum of all other neighbouring pixels, then the pixel is merged with an image object.

1.7.5. WS

The WS algorithm, which was introduced in image analysis by Beucher and Lantuéjoul [151], is known to be a powerful mathematical morphology algorithm [152,153] based on region growing [154]. It considers grey-scale images as topographic relief [154-156]. In other words, each intensity value is considered an elevation value. Minima of this relief are found and 'pierced'. The entire relief is then immersed into the water. As the relief goes deeper, flooded areas start to merge. To avoid this, some infinitely tall dams are raised along watershed lines. The network of all these dams specifies the watershed of the image [157]. Each minimum is associated with a basin [155]. Figure 4 illustrates the principle of the WS.

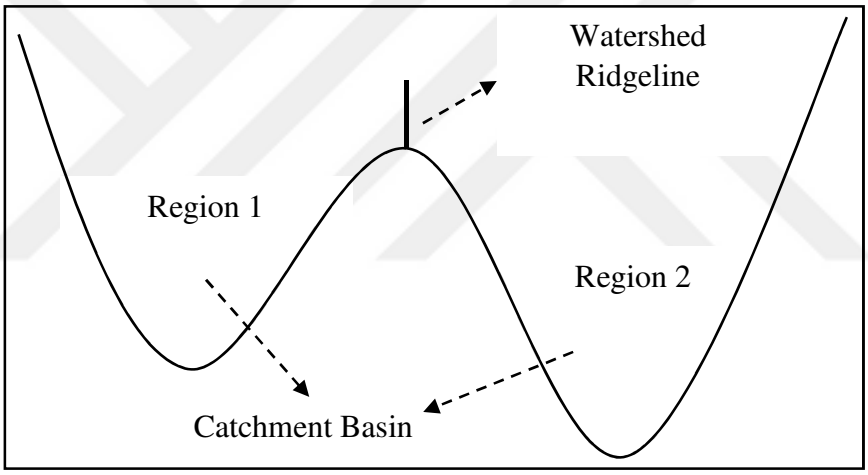

Figure 4. WS principle

The WS is usually applied to image gradient [153,158] so that the drainage directions are identified for each pixel. Most steeply uphill and downhill directions are specified by means of eight neighbours of each point. The WS algorithm starts to generate the segments (regions) by marking the locations of intensity minima points with unique segment identifiers. The gradient information of other points is used to follow the image downhill to some intensity minimum. The algorithm then records the identifier of this extremum in the output pixel that corresponds to this point. Segmentation process continues until all pixels are associated with their corresponding minimum. Boundaries of the segments are found by detecting the changes in region numbers [159].

The WS algorithm tends to produce over-segmented regions due to a high number of local minima, which is the biggest disadvantage of this algorithm. The number of local minima can be decreased by filtering the image with a smoothing filter prior to the segmentation [160]. Some post-processing procedures can also be used to reduce the over-segmentation effect. Over-segmented regions can be merged after segmentation. The difficulty of this approach lies in finding an appropriate merging criterion.

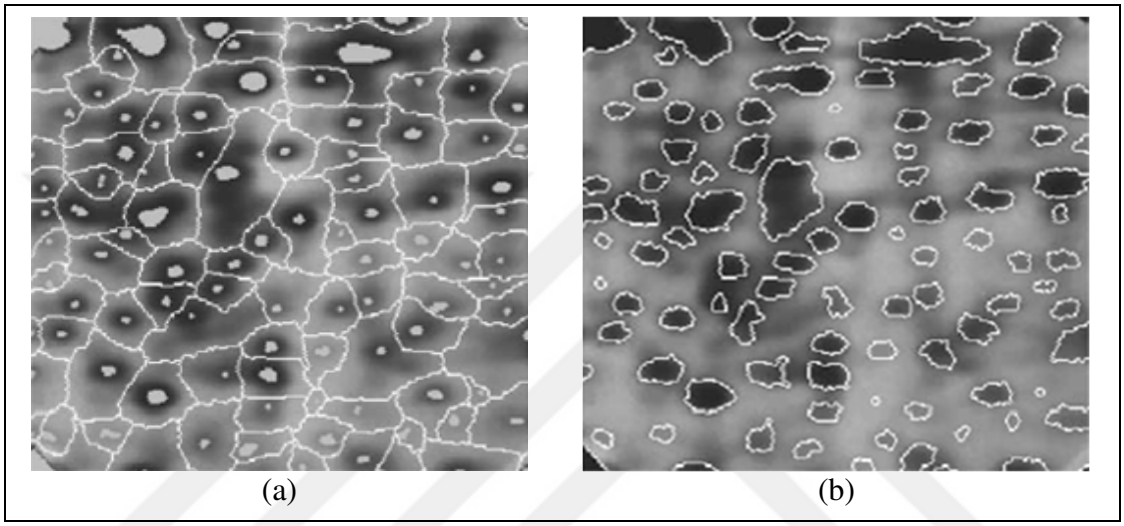

Figure 5. Marker-controlled segmentation principle [160]. Internal (light grey regions) and external (watershed lines) markers (a), segmentation result (b)

Another approach to avoid over-segmentation is to use markers. A marker is a connected component of an image. Internal markers are associated with image objects, whereas external markers are associated with the background. A marker selection procedure generally includes two steps; pre-processing and specification of criteria that should be met by markers. Internal markers are defined as regions surrounded by points of higher 'elevation' (or whatever the feature is) [160]. A connected component is composed of the points inside a region. All points in this connected component have the same intensity. The watershed algorithm is implemented on the smoothed image by considering the internal markers as the only regional minima. Resulting watershed lines are defined as external markers. An example for this situation can be seen in Figure 5. As seen in Figure 5 (a), each region contains an internal marker and some part of the background. In such cases, the object and background should be separated by using a segmentation technique. Another approach is to apply the WS to each region to separate the object and background [160].

The OTB software uses two parameters to perform the WS; the depth threshold parameter specifies the maximum depth in the image and the flood level parameter generates the merge tree from the initial segmentation.

2. APPLICATION

2.1. Study Area and Data Preparation

Three test sites were chosen in the Firat University campus, which is located in the city of Elazig (38° 17´ - 39° 11´ N, 38° 30´ - 40° 21´ E), eastern Turkey. All test sites have a slight slope and are dominated by sequentially planted deciduous and coniferous urban trees such as *Pinus pinea, Picea pungens, Cedrus libani* and *Abies nordmanniana ssp. equi-trojani* etc. Most of the trees in these sites are interlocking with each other.

Prior to the conduction of the flight, 7 GCPs (Ground Control Point) were established in the test sites. It should be noted that plenty of attention was paid to distribute the GCPs evenly over the campus. Then, 3D positions of these GCPs were measured with the RTK (Real Time Kinematik) GPS technique. Once the flight plan was made, 321 stereo aerial photos were taken over the campus with an FC300X digital camera mounted on a DJI Phantom 3 UAS. The aerial photos were captured along 19 flight lines from an altitude of 141 m. After the flight, acquired aerial photos were processed by using the APP software. The software allows the users to check if acquired aerial photos suffer from negative effects (low-contrast, brightness, striping, noise etc.) prior to processing. Photos with low quality should be discarded to avoid their negative effects on the process. Evaluations showed that none of the aerial photos were inappropriate for processing. The software links GCP coordinates to the photos with time settings of the camera that is synchronized with GPS time before the flight. Geotagged photos enable the software to specify overlapped parts of the photos to be used in point matching [161]. The APP software employs the Structure from Motion (SfM) approach to align the photos in order to produce a 3D sparse point cloud representing the geometry of the process area [162,163]. The software solves the relative orientation of camera positions and the internal camera parameters (i.e. focal length, skew, principal point location and tangential distortion coefficients) [163]. As a result of the SfM process, the software extracted a point cloud with a density of 0.3 point/m^2. Visual examination of the generated point cloud revealed some outliers resulted from point matching procedure. These outliers were removed manually. The software builds the 3D geometry of the process area by applying a dense Multiview stereo reconstruction on the aligned photos [164,165]. The APP software offers a number of settings, which enables the

reconstruction of detailed geometry. Since the main goal of this study was to predict the stand parameters with a high accuracy, the point cloud was densified using the APP software. The software determines depth information for each camera position and combines them to form a denser point cloud [112,166]. As a result, a point cloud with a density of 154.6 point/m^2 was generated. The APP software produces the 3D model as a polygonal mesh, visualized in a solid, shaded and wireframe mode. The software also determines a colour for each vertex of the model by using the colour information of the source photos. These colour values are interpolated for each polygon face [163]. A DSM with a spatial resolution of 15 cm was produced in the APP software.

Since the PFB methodology and segmentation-based approaches estimate the crown diameters from the CHM, which is calculated by subtracting the DTM from DSM, the point cloud was filtered to remove the points belonged to the above-ground objects to retrieve only the ground points used to interpolate the DTM. The APP software was used to filter the point cloud. The software uses the ATIN algorithm [104,167] to perform ground filtering. Ground filtering performance of the APP software was investigated through randomly selected test points. The minimum number of required test points n was estimated with the multinomial distribution approach [168], which was proposed as;

$$n = \frac{B\Pi_i(1-\Pi_i)}{b_i^2} \tag{2.1}$$

where, $B = \propto/k$, k is the total number of classes, $\propto$ is the confidence interval and b_i is the desired accuracy. Π_i denotes the ratio of the area of the i^{th} class and entire area [112,169]. If there is no information regarding the area of the classes (Π_i), n is estimated as [112,168];

$$n = \frac{B}{4b^2} \tag{2.2}$$

It should be noted that there are two classes (i.e. ground and non-ground) in the point cloud and the confidence interval was set to 95%. Since it is hard to tell the area of each class in the test sites, the Equation (2.2) was used to estimate the minimum number of required test points. Hence, B was computed as 0.025 ($\propto/k = 0.05/2$). χ^2 distribution table

reveals that the value of 0.025 corresponds to 5.02 at one degree of freedom. Hence, n was determined as 502 ($B/4b^2 = 5.02/4(0.05^2)$). As a result, it was decided to use 600 randomly selected test points for each test site. Actual classes of the test points were found by visual examination of the very high-resolution orthophoto. It was found that 422, 277 and 196 out of 600 test points belonged to the ground surface in the sites 1, 2 and 3, respectively. 178, 323 and 404 of the test points were found to be belong to the above ground objects in the sites 1, 2 and 3, respectively. The T1E, T2E and TE metrics were computed by using the omission and commission errors given in Figure 6. As seen in the figure, the ATIN algorithm committed 14, 20 and 11 omission errors in the sites 1, 2 and 3, respectively. On the other hand, 84, 108 and 93 commission errors were found in the test sites 1, 2 and 3, respectively. It can be clearly seen from Figure 7 that the ATIN algorithm preserved the ground points with T1Es of 0.03, 0.07 and 0.06 in the sites 1, 2 and 3, respectively. However, it was not that successful in removing the non-ground points, especially in the sites 1 and 2. The algorithm committed TEs of 0.16, 0.21 and 0.17 in the test sites 1, 2 and 3, respectively.

Once the ground points were retrieved, they interpolated with the Bi-linear interpolation algorithm to generate a 15-cm DTM of the campus. Afterwards, a 15-cm CHM was generated from the DSM and DTM. Finally, a 15-cm orthophoto was produced with the APP software for the entire campus. The produced orthophoto and CHM were cropped with respect to the boundaries of the test sites, which can be seen in Figure 8.

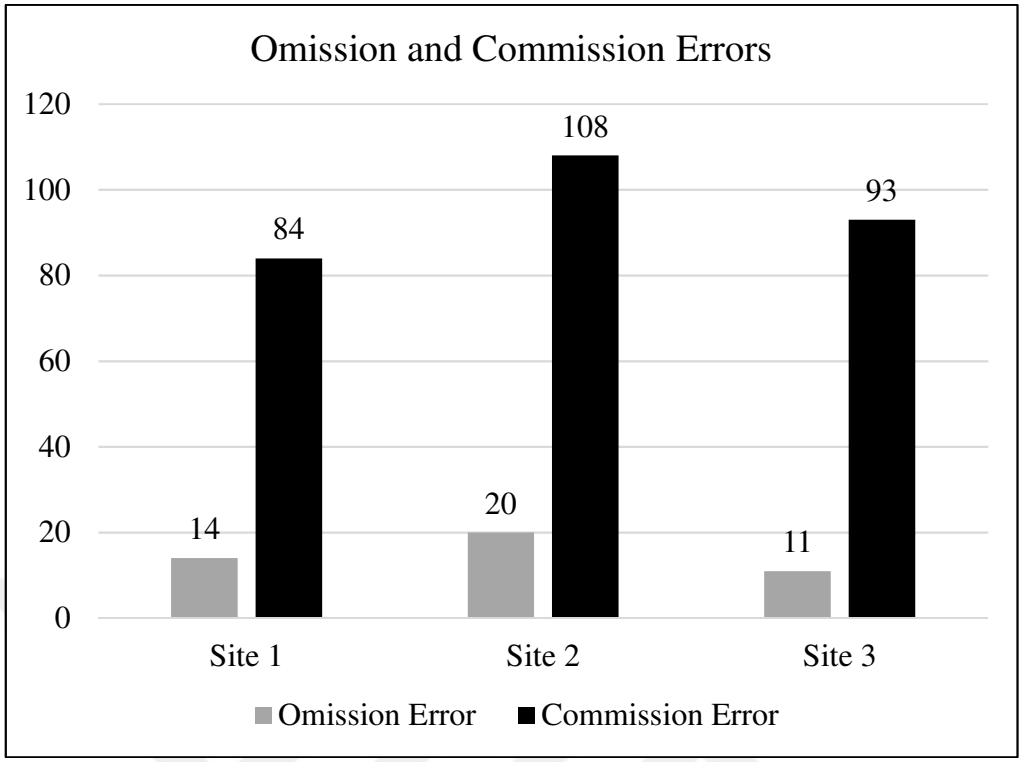

Figure 6. Calculated omission and commission errors

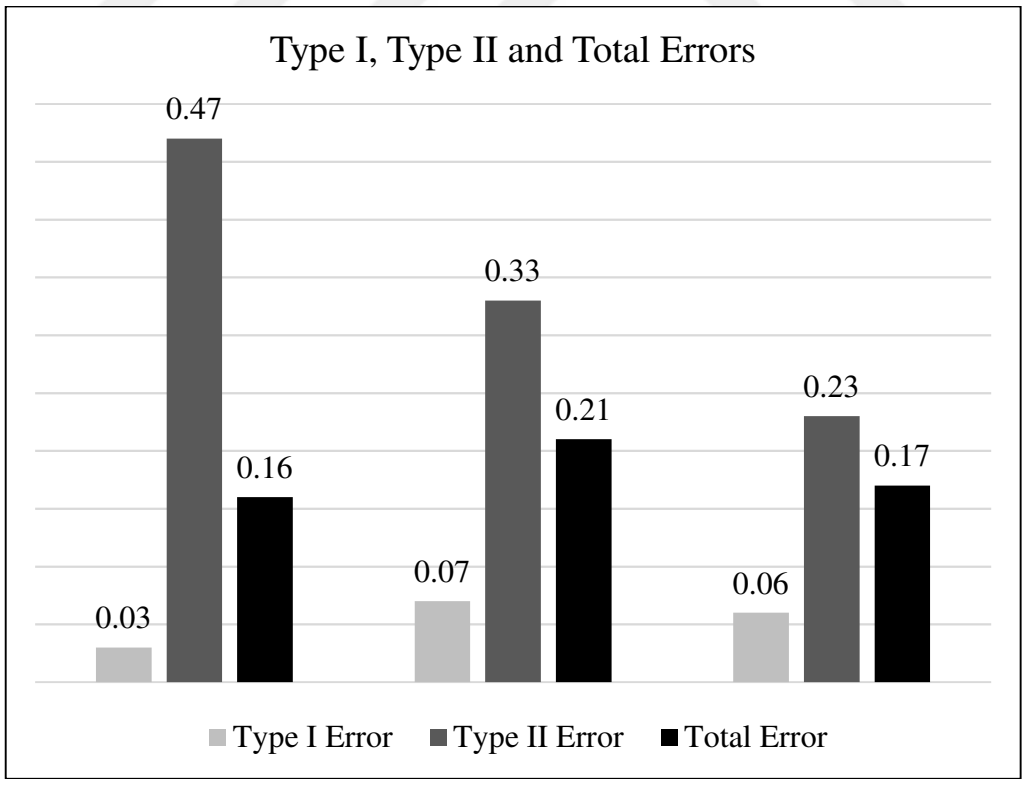

Figure 7. Calculated T1E, T2E and TE values

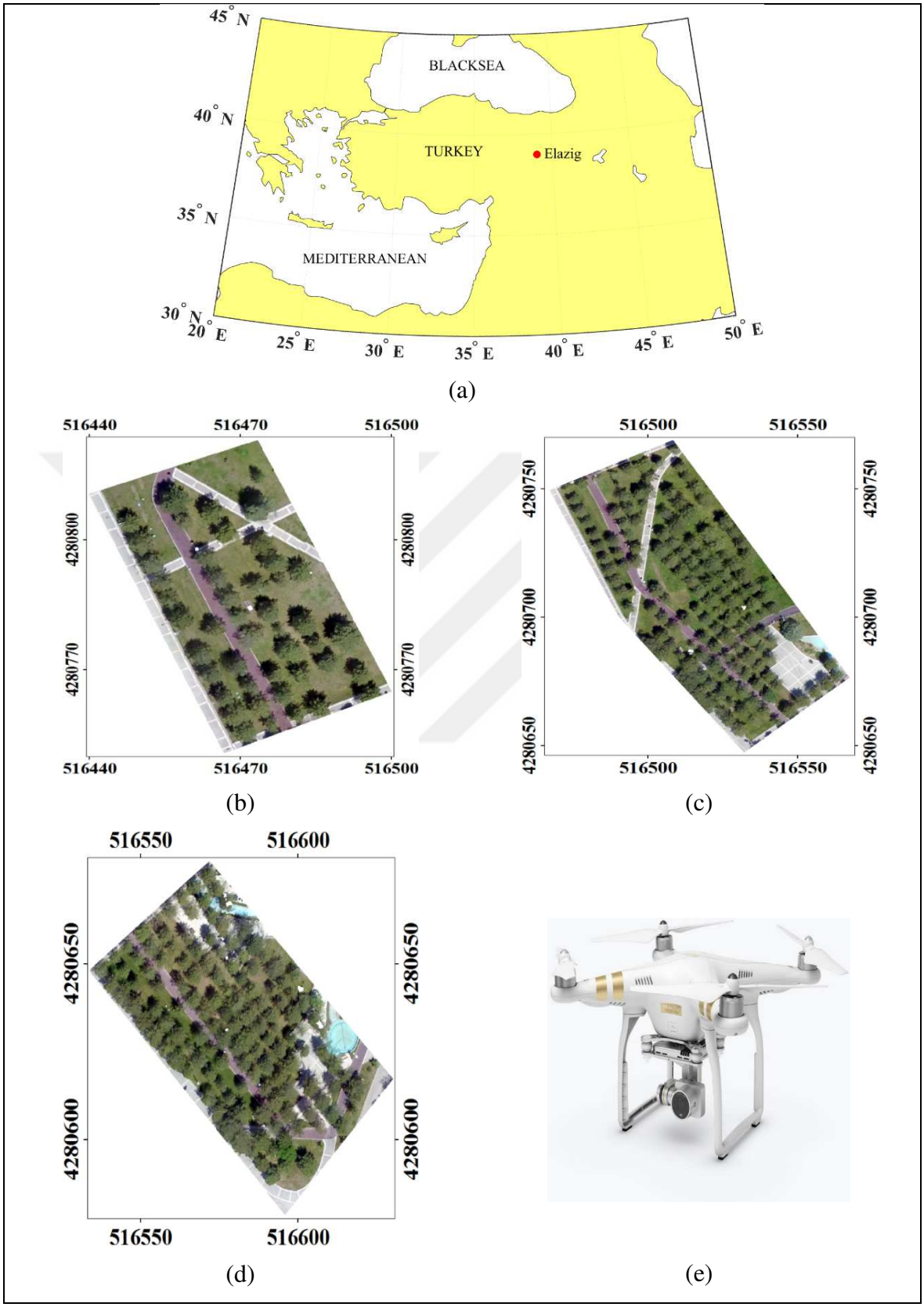

Figure 8. Location of the city of Elazig in Turkey (a), Test site 1 (b), Test site 2 (c), Test site 3 (d), DJI Phantom 3 UAS [170] (e).

2.2. Methodology

2.2.1. Crown Closure Map Production

The very high-resolution orthophotos were classified by using the SVM classification algorithm to identify the forested areas. Each classified image was used as a base to generate the crown closure map of each test site. To do so, a sliding window was employed in MATLAB environment to compute the crown closure ratio. For each window position, the crown closure ratio was determined by the ratio between the forested and non-forested areas within the window. As mentioned before, a closure ratio between 11% and 40% indicates sparse density, whereas a closure ratio between 41% and 70% refers to a moderate density. A closure ratio greater than 71% refers to a high density. Hence, the closure maps were produced and coloured with respect to the determined crown closure ratios. Figures 9, 10 and 11 show the classified images as well as the crown closure maps of the test sites 1, 2 and 3, respectively.

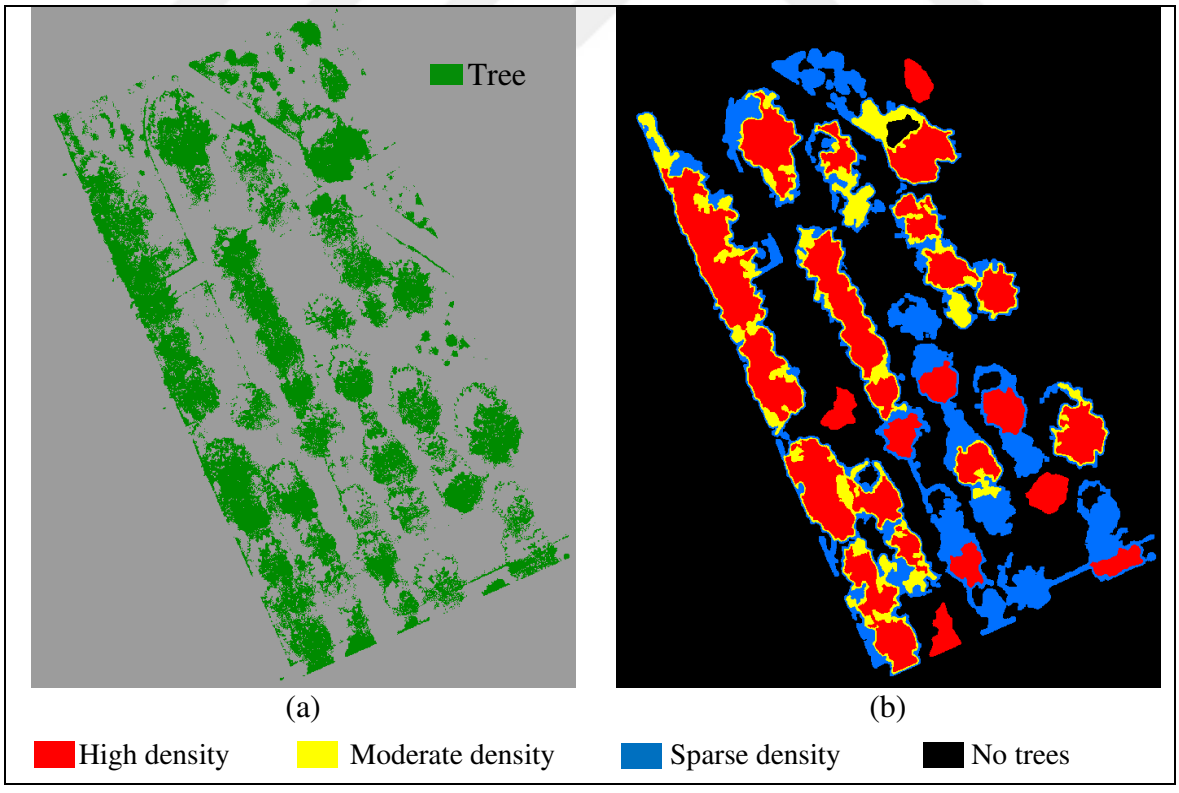

Figure 9. Classified orthophoto of the site 1 (a), crown closure map of the site 1 (b)

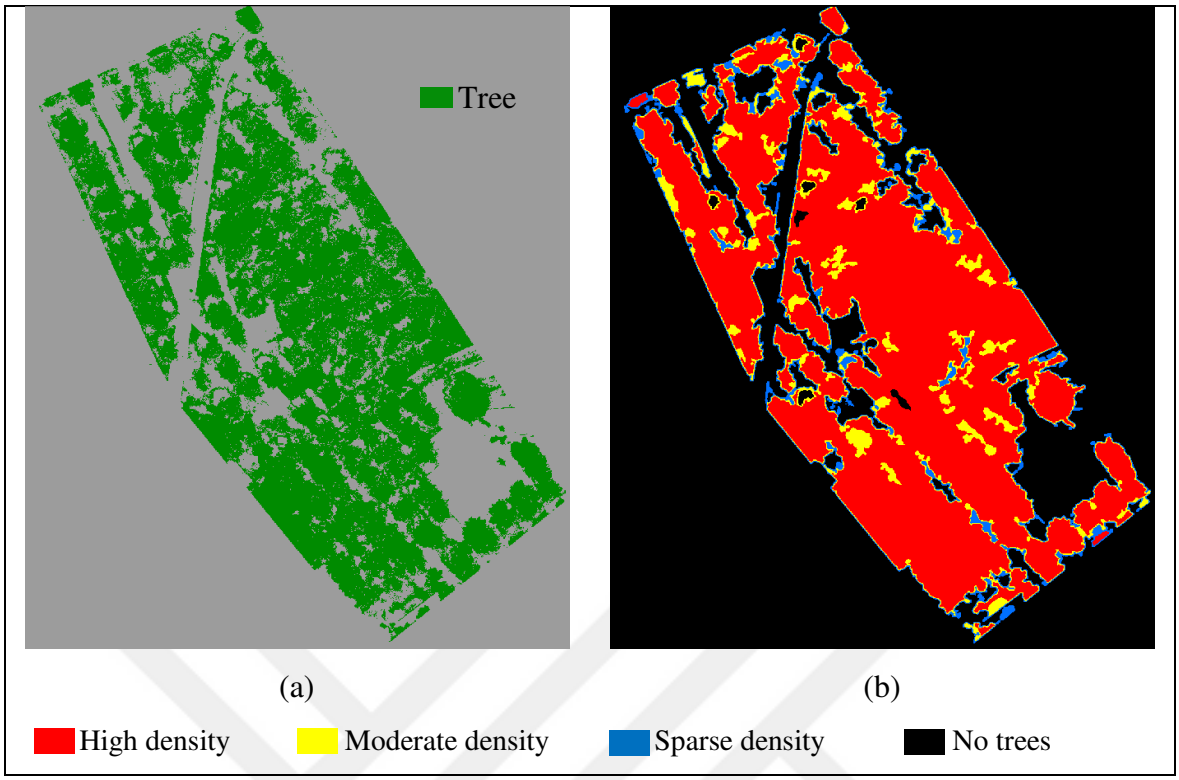

Figure 10. Classified orthophoto of the site 2 (a), crown closure map of the site 2 (b)

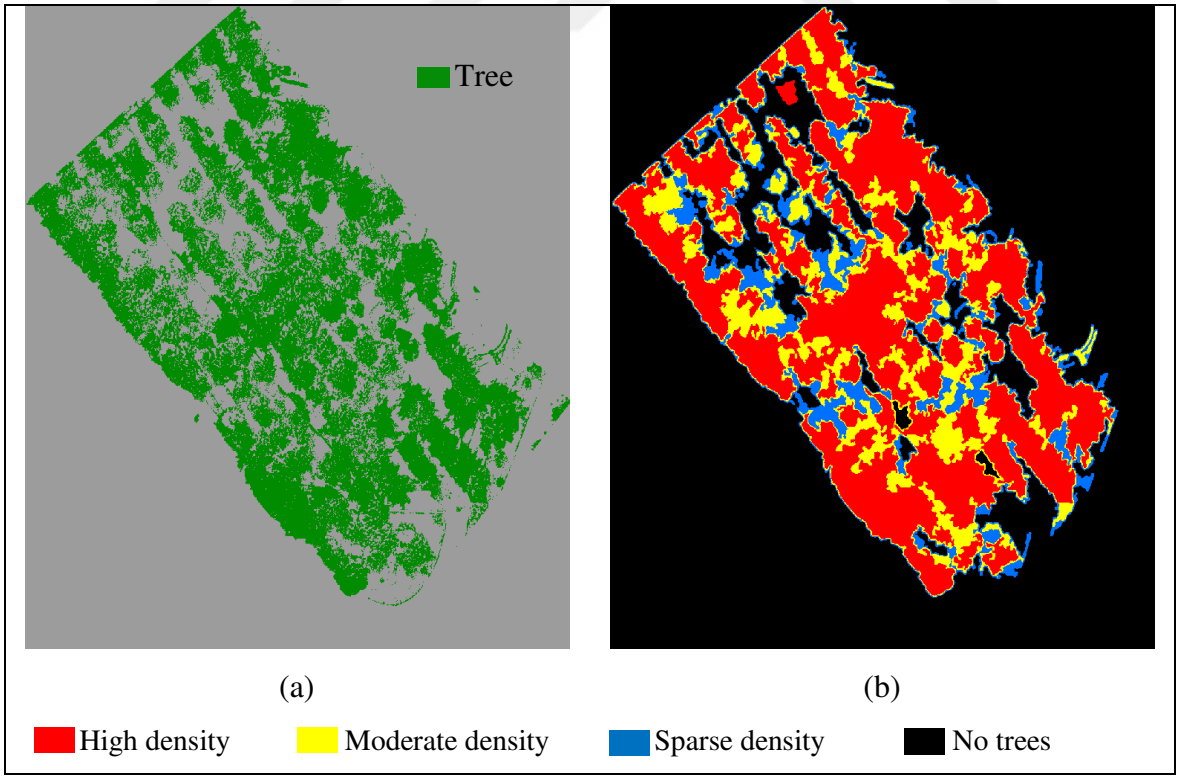

Figure 11. Classified orthophoto of the site 3 (a), crown closure map of the site 3 (b)

2.2.2. Tree Crown Segmentation

The MSS, MPBS, MRS, SRGS and WS algorithms were applied to the produced CHMs to delineate the trees in the test sites. As mentioned before, the very high-resolution CHMs were interpolated from a very dense point cloud, which means that they had a tendency to contain a large amount of noise. This, of course, would affect the segmentation performance in a negative way. Hence, the CHMs were smoothed with a Gaussian filter prior to the segmentation in order to eliminate the adverse effects of the noises. The parameters used by these algorithms were specified by trial-and-error procedure. Benz et al [131] and Platt and Rapoza [137] pointed out that there is no such thing as optimal parameters in image segmentation. Hence, different parameter values were tried until the tree segments were appropriately sized and shaped.

The range radius, spatial radius and minimum region size are the most effective parameters of the MSS algorithm. The range radius parameter should be selected greater than the maximum elevation difference between intra-segment pixel pairs and lower than the elevation difference between the pixels in the segment and surrounding pixels outside the segment. Chehata et al [171] indicated that the spatial radius parameter should be selected close to the size of the segments of interest. However, under-segmentation was observed in many parts of the test sites when the spatial radius parameter was selected this way. This may be due to the high-resolution of the CHMs. Reducing this parameter resulted in more natural tree segments. Since the crown area of a few of the smallest trees in the test sites were measured on the orthophotos about 2 m^2 and the CHM had a spatial resolution of 15 cm, the minimum region size parameter was set to 100 pixels in all test sites. 100 iterations were found to be adequate for the test sites, hence, the maximum number of iterations parameter was set to 100.

The profile size and initial radius are the most effective parameters of the MPBS algorithm. Since the very high-resolution CHMs were produced by interpolating a very dense point cloud, it was necessary to select the parameters that were sensitive to small local elevation differences. Hence, the initial radius, radius step and decision threshold parameters were set to smaller values in the test sites. The profile size parameter was selected 12, 16 and 4 for the test sites 1, 2 and 3, respectively. Since the trees in the site 3 has similar crown areas, a smaller profile size value was thought to be adequate for this site, which also made the segmentation process more time-efficient.

The most effective parameter of the MRS algorithm is the scale. Definition of this parameter is very challenging [172]. Tian and Chen [173] indicated that choosing smaller or larger values for this parameter will probably result in unnatural segments. Smaller scale values produce smaller segments, whereas larger segments are obtained with larger values [173]. In this thesis, the scale parameter was chosen close to the average crown diameter of the trees to generate tree segments with realistic crown sizes. Note that the average crown diameter was defined by measuring a few of the crown diameters on the orthophotos, which had the same spatial resolution as the CHMs (15 cm). Since the trees in the test sites had an average crown diameter of approximately 4.5 m, the values close to 30 were tried for the scale parameter. As a result, 20, 22 and 18 values were found to generate realistic tree segments for the sites 1, 2 and 3, respectively. Platt and Rapoza [137] stated that the optimum compactness parameter is dependent on the size and type of the objects of interest. The authors also indicated that the objects with similar grey values would ideally have high compactness. Adapting this to our case, higher compactness values were used to delineate the trees, since they had similar heights. Tests revealed that a value of 0.9 resulted in natural tree segments in all test sites. The shape parameter used by the MRS algorithm was found to have no significant effect on the segmentation result.

The seeds used to grow the tree segments through the SRGS were generated by the 'Seed Generation' tool of the SAGA software. The tool was used to calculate the local maxima of the CHMs, which were then used as seed points. In fact, there has not been any specific recommendation about the use of the variance in feature space, variance in position space and similarity threshold parameters used by the SRGS algorithm, which was integrated in the SAGA software. Hence, great effort was put into the specification of the optimum values for these parameters.

The depth threshold parameter used by the WS algorithm was found to control the over-segmentation effect, which is almost inevitable in the WS. Increasing this parameter not only tackled the over-segmentation problem and resulted in more natural tree segments, but also reduced the computation time. Setting the flood level parameter to a low value causes over-segmentation problem and yields softer segment boundaries [174]. Hence, this parameter was increased to produce larger tree segments with more defined boundaries. However, greater flood level values increased the computation time. Table 1 shows the optimum parameters used by all segmentation algorithms.

Table 1. The optimum parameters used in the segmentation algorithms

Test Site	Method	Parameters			
1	MSS	spat. radius 10	range radius 0.35	mode conv. thres. 0.3	min. reg. size 100
	MPBS	profile size 12	initial radius 1	radius step 1	decision thres. 0.3
	MRS	scale 20	shape 0.3	compactness 0.9	
	SRGS	var. in feat. space 2	var. in posit. space 3.5	sim. thres. 0.7	
	WS	depth thres. 0.6	flood level 0.5		
2	MSS	spat. radius 10	range radius 0.35	mode conv. thres. 0.3	min. reg. size 100
	MPBS	profile size 16	initial radius 1	radius step 1	decision thres. 0.3
	MRS	scale 22	shape 0.3	compactness 0.9	
	SRGS	var. in feat. space 1	var. in posit. space 4	sim. thres. 0.5	
	WS	depth thres. 0.6	flood level 0.5		
3	MSS	spat. radius 10	range radius 0.1	mode conv. thres. 0.3	min. reg. size 100
	MPBS	profile size 4	initial radius 5	radius step 2	decision thres. 0.05
	MRS	scale 18	shape 0.3	compactness 0.9	
	SRGS	var. in feat. space 0.55	var. in posit. space 0.25	sim. thres. 0.2	
	WS	depth thres. 0.5	flood level 0.65		

Once the trees in the test sites were delineated with the segmentation algorithms, each segment (i.e. tree) was used to estimate the crown diameter of each tree. To do so, the circle enclosing each segment was generated. The diameter of the circle gave the diameter of the tree crown. The next step was to estimate the crown diameters by using the PFB methodology, which is introduced in the following subsection. The estimates of the PFB methodology were compared either to the reference data or to the estimates obtained based on the other segmentation-based approaches.

2.2.3. Crown Diameter Estimation

Since the test sites include various deciduous and coniferous urban trees such as *Pinus pinea, Picea pungens, Cedrus libani* and *Abies nordmanniana ssp. equi-trojani* etc., a brief literature review is provided in Subsection 2.2.3.1 to comprehend what the researchers have done to estimate the crown diameters of urban trees by means of remotely-sensed data. Subsection 2.2.3.2 presents the PFB methodology.

2.2.3.1. Estimation of Crown Diameters of Urban Trees in the Literature

The literature reports various studies in which crown diameters of urban trees were estimated with remotely sensed data. Shrestha and Wynne [175] used small footprint discrete-return LiDAR data to estimate biophysical parameters of trees in an urban environment. They developed prediction models for over two thousand individual trees by using best subsets multiple linear regression. As a result, the crown diameters were estimated with a high accuracy (R^2=0.9).

Lee et al [176] estimated the crown diameters of 802 urban trees from 20 different tree species by digitizing their boundaries on aerial photos. The estimated crown diameters were compared against terrestrial measurements. It was concluded that the trees of all species were estimated with RMSEs ranging from 0.62 m to 1.35 m. The overall RMSE was calculated 1.07 m.

In a recent study, Yilmaz et al [177] estimated the crown diameters of urban trees from a UAS-based CHM. The authors estimated the crown diameters from the tree segments produced with the MRS and SRGS techniques. Reference crown diameters were obtained from manually delineated tree segments. The MRS- and SRGS-based approaches estimated the crown diameters with RMSEs of 1.59 m and 1.76 m, respectively.

Schreyer et al [178] used a LiDAR-derived CHM to estimate the crown diameters of urban trees. They estimated the crown diameters by using the local maxima as starting points to derive 16 radii, which were 16 cardinal directions radiating from each tree. The authors did not evaluate the estimation results quantitatively. They used the estimated crown diameters to compute the DBH of trees. The computed DBH values were then used to estimate the carbon storage. Further information about the approach used by the authors can be found in [178].

Alonzo et al [179] derived some stand parameters including crown diameter from a number of urban tree segments obtained from the manual delineation of airborne LiDAR data. The derived crown diameters were found to be in good agreement with terrestrial measurements with an RMSE of 0.77 m and an R^2 value of 0.95. The stand parameter estimates were then used to train a LiDAR model to predict the leaf area. The model was applied to all WS-based tree segments to predict the LAI (Leaf Area Index), which is a key ecosystem structural attribute for urban areas [179]. In a similar study, Alonzo et al [180] used LiDAR data to estimate the crown diameters of urban trees for LAI mapping.

Zhang [181] estimated the crown diameters of urban trees with LiDAR data by using the 'donut expanding and sliding' method, which computes the diameter of the outermost 'donut' and considers it as the estimated crown diameter. The RMSE and R^2 values between the estimated and field-measured crown diameters were determined as 1.9 m and 0.84, respectively.

Wu et al [81] used MLS data to predict the crown diameters of street trees with a voxel-based methodology. In the study, laser scanning points of each tree object were projected onto the horizontal plane. Afterwards, they computed the range of the projected points for each tree object in *x* and *y* directions. The crown diameters were determined by taking the average of the differences between the minimum and maximum *x* and *y* coordinates of the projected points. The RMSE between the estimated and field-measured crown diameters were computed 0.19 m and 0.13 m in the test sites 1 and 2, respectively.

Fernández-Sarría et al [182] investigated the potential of the TLS (Terrestrial Laser Scanning) data in the determination of dendrometric parameters and biomass yielded from pruning of urban forests. The authors manually selected the tree crown and stem points from the point cloud. The point cloud was projected to the ground. For each tree trunk, a reference point was selected, which was considered as the center of the trunk. The point cloud was divided into 72 circular sections with an interval of 5°. A radius was then calculated for each section. The crown diameters were calculated by the arithmetic mean of the longest diameter and diameters perpendicular to it. The crown diameter estimates were found to correspond well with the field measurements with an R^2 value of 0.906.

Lin et al [183] used MLS data for understory tree characterization in urban forests. In the study, the authors projected the point cluster of each tree onto the ground plane. The crown diameter of each individual tree was predicted by considering the boundary of crown projection as a symmetrical circle fitting to it. The estimation results were compared against

the estimates from TLS data. As a result, the MLS- and TLS-based crown diameters were found to be comparable with an R^2 value of 0.64.

Pokharel [184] expressed the crown volumes of urban trees as a function of crown diameter and crown frontal area, which were estimated from LiDAR data. The crown diameters were estimated in different height levels from outline polygon of crown frontal view. Further details about the author's methodology can be found in [184]. In conclusion, the author found out a high relationship between the estimated and field-measured crown diameters with an RMSE of 0.18 m and an R^2 value of 0.98.

Chen [185] applied the WS algorithm on an ALS data-based CHM to delineate the tree crowns of urban trees. The crown diameters were then estimated from the tree segments. The RMSE between the crown diameter estimates and terrestrial measurements was computed 1.47 m.

Wang [186] used MLS data to estimate the crown diameters of urban roadside trees. They used segmentation techniques to delineate the trees. The crown diameters of the trees with a rounded crown were estimated by means of the RANSAC shape detection method, whereas the spoke method was used to estimate the crown spread of the trees with an irregular shape. The author concluded that the followed methodology was successful in estimating the crown diameters. Further information can be found in [186].

2.2.3.2. PFB Crown Diameter Estimation Methodology

The very first step of the PFB methodology is to find the tree tops, which will then be used as seed points to calculate the crown diameters. Except some abnormal situations, top point of a tree is located at the top centre of the tree crown, no matter it is a coniferous or a deciduous tree. A leaning tree is a good example of an abnormal tree. Top of a leaning tree may not be at the top centre.

Canopy closure is the main factor that influences the detection accuracy of the tree tops. If trees are located far from each other, they can spread their branches freely. In such cases, it is a lot easier to detect their top points. However, if trees are interlocking to some extent, then they cannot spread their branches freely and their top points get closer to each other, which makes the detection of their top points more challenging. This phenomenon is illustrated in Figure 12.

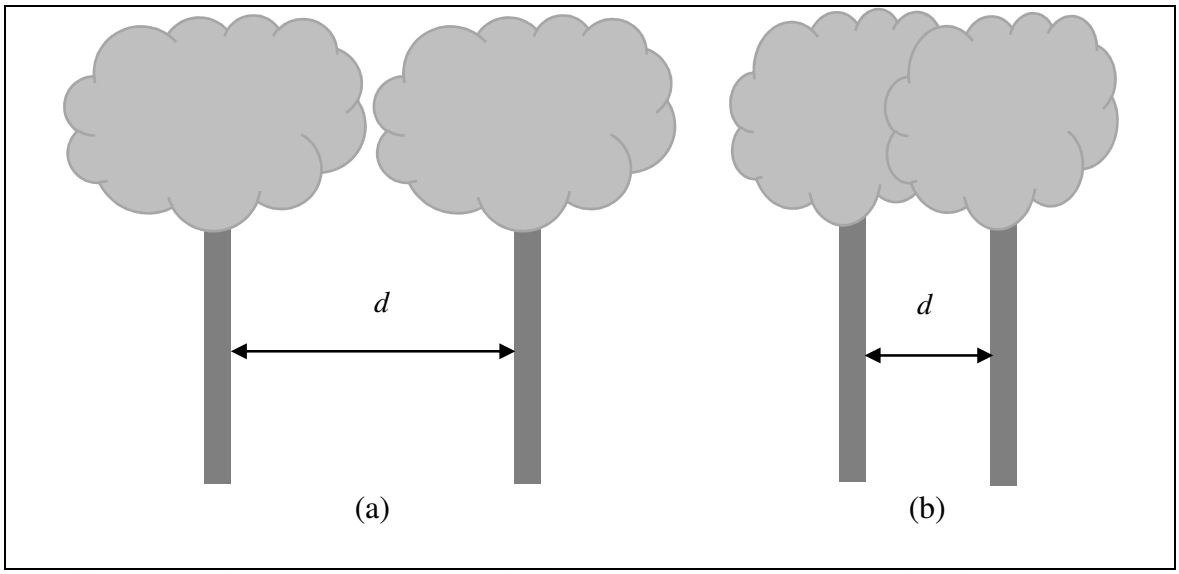

Figure 12. Non-interlocking tree crowns (a), interlocking tree crowns (b). d is the distance between two tree stems

CHMs, calculated by subtracting the DTM from DSM [86,187], have been used in a large number of studies in the literature [85-89] owing to its ability to provide useful information for the estimation of physical characteristics of trees. Local maxima of the CHM are generally calculated to find the tree top points. Before calculating the local maxima, the PFB methodology sets the elevation values lower than a predefined threshold (zt) to 0. This is because the DTM used to calculate the CHM is produced by using the ground points obtained from a point cloud filtering procedure, which may introduce some filtering errors, i.e. some ground points may not be kept or some non-ground points may be retained. This, of course, affects the 3D accuracy of the produced DTM, as well as CHM. The zt threshold parameter should be smaller than the height of the smallest tree in the site. Otherwise, the algorithm misses a number of trees. This parameter can be easily defined by reading the heights of a few of the smallest trees on the CHM. Another pre-processing procedure that the PFB methodology carries out before the determination of local maxima is the filtering of the CHM with a Gaussian filter to reduce the local height variations. This procedure has been used in various tree detection-themed studies to smooth the CHM [86,88,188]. It should be noted that all segmentation algorithms used in this study were applied on the CHMs that were filtered with a Gaussian filter.

After these pre-processing procedures, local maxima are calculated by employing a sliding window on the smoothed CHM. The size of the window is identified as the smallest

crown diameter ($minr$) in processing area so that the algorithm can find all possible tree tops. The user should define the $minr$ by manually measuring the smallest crown diameter in pixels. In most cases, a single tree falls in multiple window positions (see Figure 13), which leads to multiple top points for a single tree. For such cases, the PFB methodology uses two thresholds (dt and ht) to determine the correct tree top. If the horizontal distance between two candidate top points is smaller than dt and the elevation difference between these candidate points is smaller than ht, then these points can be considered to be belong to the same tree crown. In such cases, the point with the maximum elevation value is said to be the top of the tree.

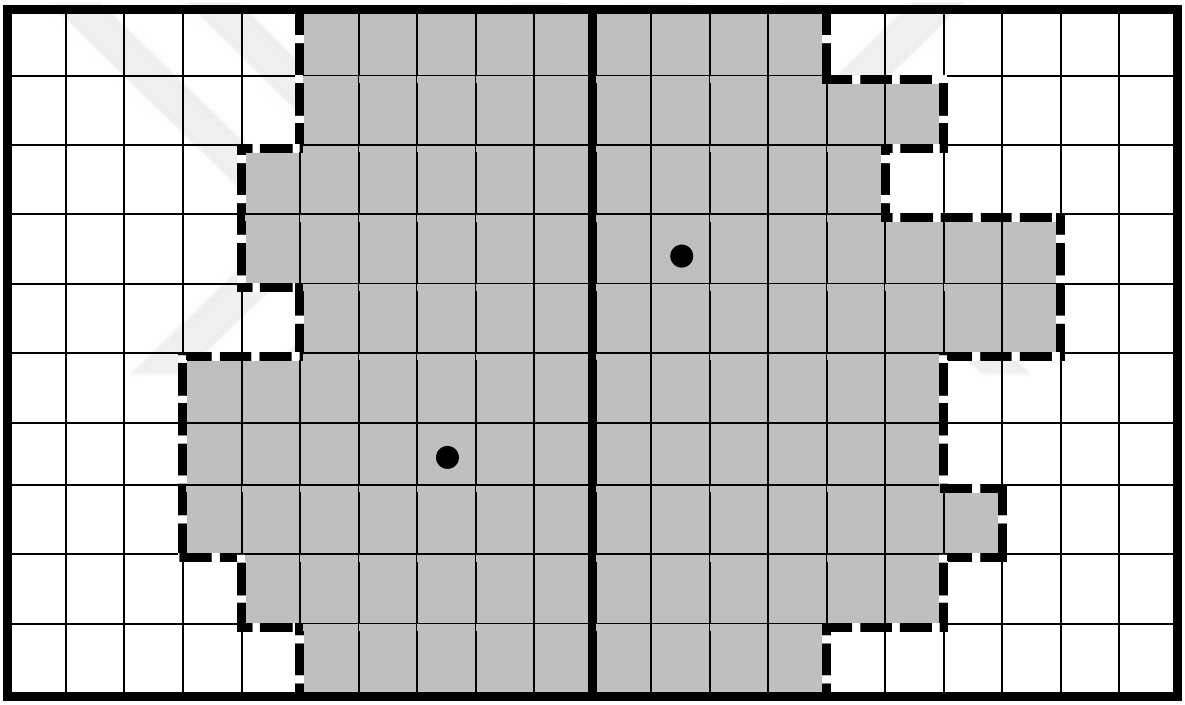

Figure 13. A single tree falling in multiple window positions (black dots are the local maxima of the window positions)

The PFB methodology determines the diameter of each tree crown with a polynomial fitting-based approach. The methodology takes the elevation values from the tree top position to the boundary of the tree in four cardinal directions (i.e. north, south, east and west), forming four profiles for each tree. The elevation should decrease from the top of the tree towards the edge of the tree. If a tree is interlocking with another one, the elevation values start to increase from the point where two trees interact. In the light of this, a polynomial fitting-based approach is used to find the point where two interlocking trees

meet. A polynomial is fit through each profile, making four polynomials for each tree crown. The minimum critical point is then determined for each polynomial. This is the point where two trees interact. Figure 14 illustrates this situation.

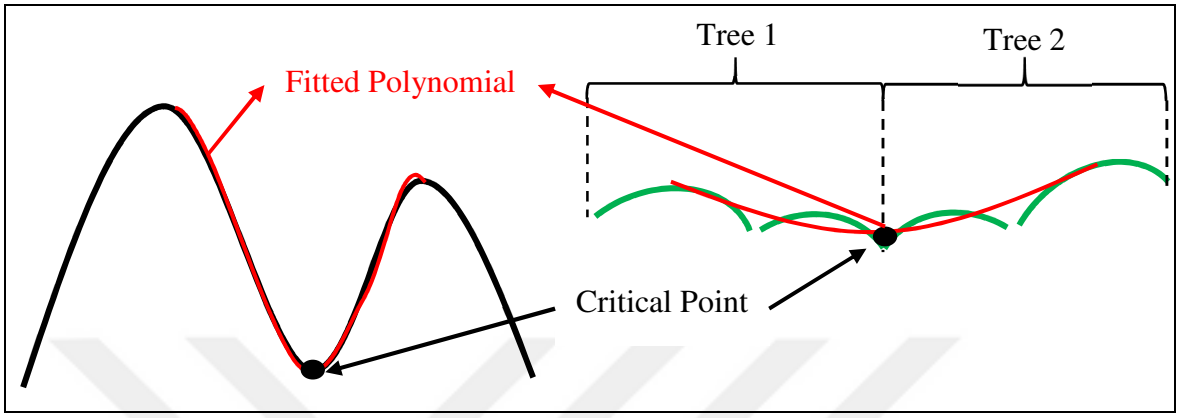

Figure 14. PFB crown diameter estimation theory

Degree of the polynomial plays an important role in finding the critical point precisely. A linear polynomial may present a poor approximation for a complex data. On the other hand, a high-degree polynomial may result in an unnecessarily complex model. Hence, a compromise should be made between the complexity and precision of the polynomial model. The PFB methodology estimates the optimal degree for a polynomial with respect to Akaike's Information Criterion (AIC), which was defined by Akaike [189]. The AIC was defined in a least-squares sense as [190];

$$AIC = 2(N+1) + (d+1)\left[\ln\left(2\pi\frac{RSS}{d+1}\right) + 1\right] \tag{2.3}$$

RSS is the residual sum of squares and is defined by;

$$RSS = \sum_{i=0}^{N}\left(y_i - p(x_i)\right)^2 \tag{2.4}$$

where, N is the total number of data points y_x, p_x is the polynomial and d is the degree of the polynomial. If a polynomial is fit with a high precision as in Figure 14 (a), then the

positions of the critical points can be used to determine the crown diameters. The PFB methodology utilizes the RMSE to investigate whether or not a polynomial is fit with a high accuracy. The RMSE is determined between each vector and the vector yielded by substituting the values into the fitted polynomial. If calculated RMSE value is smaller than a predefined threshold, then the polynomial can be said to have a good fit. The RMSE is calculated between two vectors as;

$$RMSE = \sqrt{\frac{1}{n}\sum_{j=1}^{n}(o-f)^2} \tag{2.5}$$

where, o is the original vector, f is the estimated vector and n is the total number of the elements in the vector. If a polynomial does not have a good fit, then this means that the profile contains some values breaking the increasing/decreasing trend of the profile (large branches can be the reason for this). In such cases, the PFB methodology finds the point where the trend is broken by subtracting each element from the previous one, which yields a positive/negative trend. The algorithm determines all values breaking the trend and ignores them prior to polynomial fitting. The least squares approach is used to determine the coefficients of the polynomials. Minimum critical points of the polynomials are then specified. The distances between the critical points and tree top are then used to compute the crown diameters. Crown diameter of a tree is calculated by averaging the distances in east-west and north-south directions. The PFB methodology was developed in MATLAB environment. The parameters used by the PFB methodology are given in Table 2.

Table 2. Parameters used in the PFB methodology

Test site	**Parameters**				
	zt	***minr***	***dt***	***ht***	***RMSE thres.***
1	2	20	20	20	0.1
2	2	14	14	16	0.1
3	2	20	20	24	0.1

Popescu et al [77] determined the crown diameters by fitting 4th-degree polynomials to elevation profiles. However, a degree of 4 may not always be appropriate for all tree types,

especially when using a very high-resolution CHM. In order to illustrate this situation, two example profiles from the site 2 are given in Figure 15. As seen in the figure, a 4^{th}-degree polynomial does not fit through the data points, making it more challenging to determine its critical points. The PFB methodology tackles this issue by using the AIC metric to estimate an appropriate degree for each polynomial. This criterion revealed that degrees of 21 and 18 were more appropriate for these polynomials. It is a lot easier to find the critical points of such polynomials. In addition, the PFB methodology does not centre the polynomial on tree top positions like Popescu et al [77], instead, it fits polynomials starting from tree top positions in four cardinal directions, generating four polynomials for each tree. This approach constitutes a huge advantage when estimating the crown diameters of interlocking trees. In this way, it becomes sufficient to fit a polynomial between the tree top point and the point where two trees meet, which also makes it a lot easier to determine the critical points of polynomials. This approach also makes the process more time-efficient.

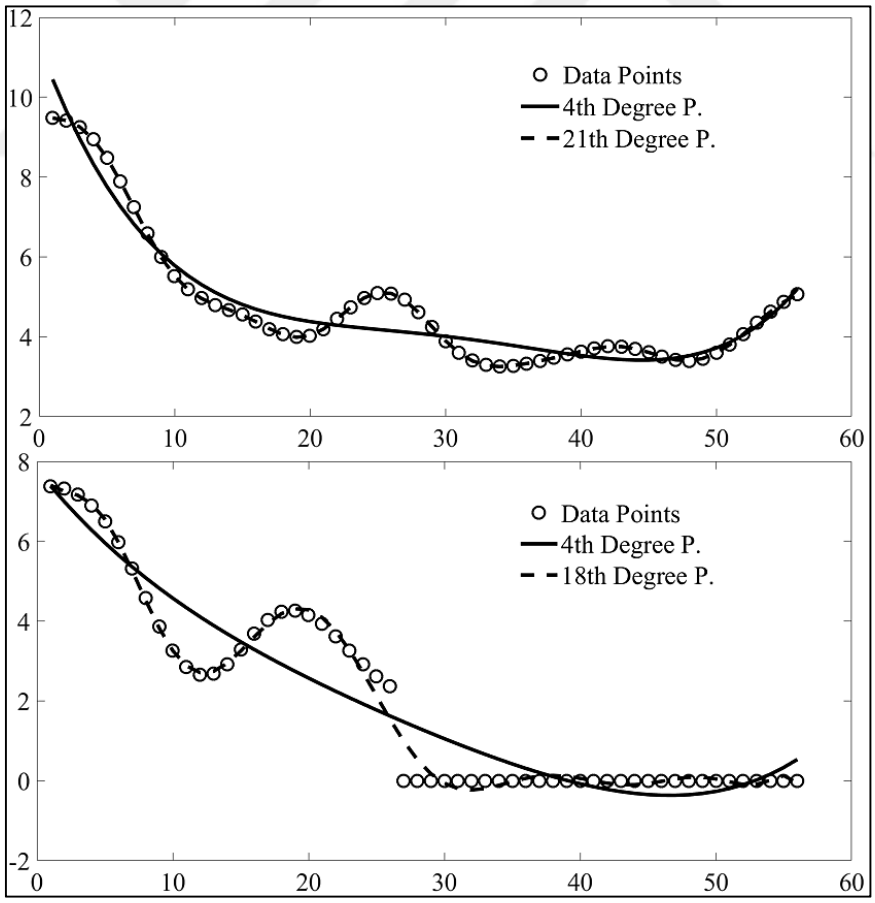

Figure 15. Examples for fitted polynomials

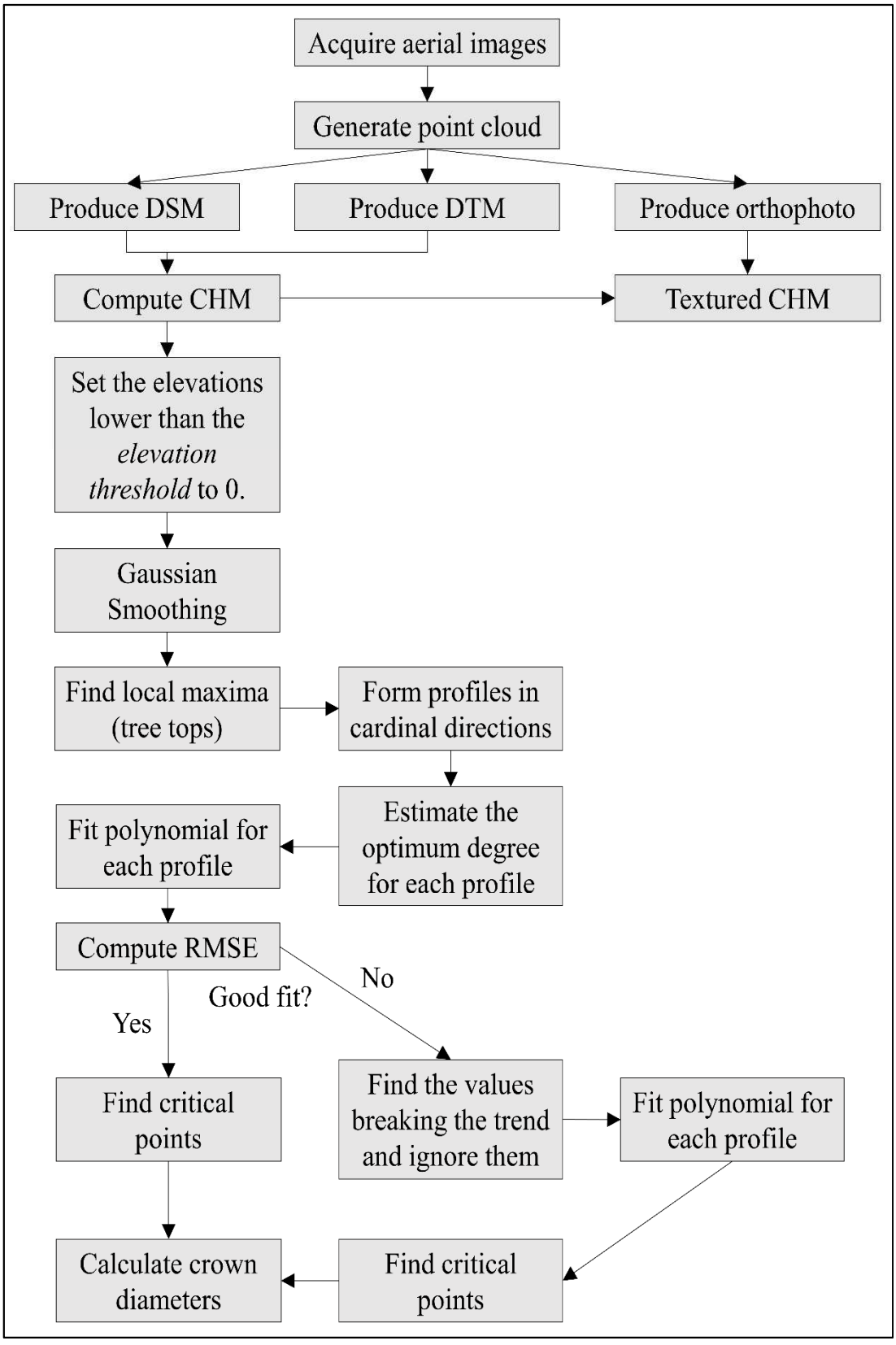

Figure 16. Workflow of the PFB methodology

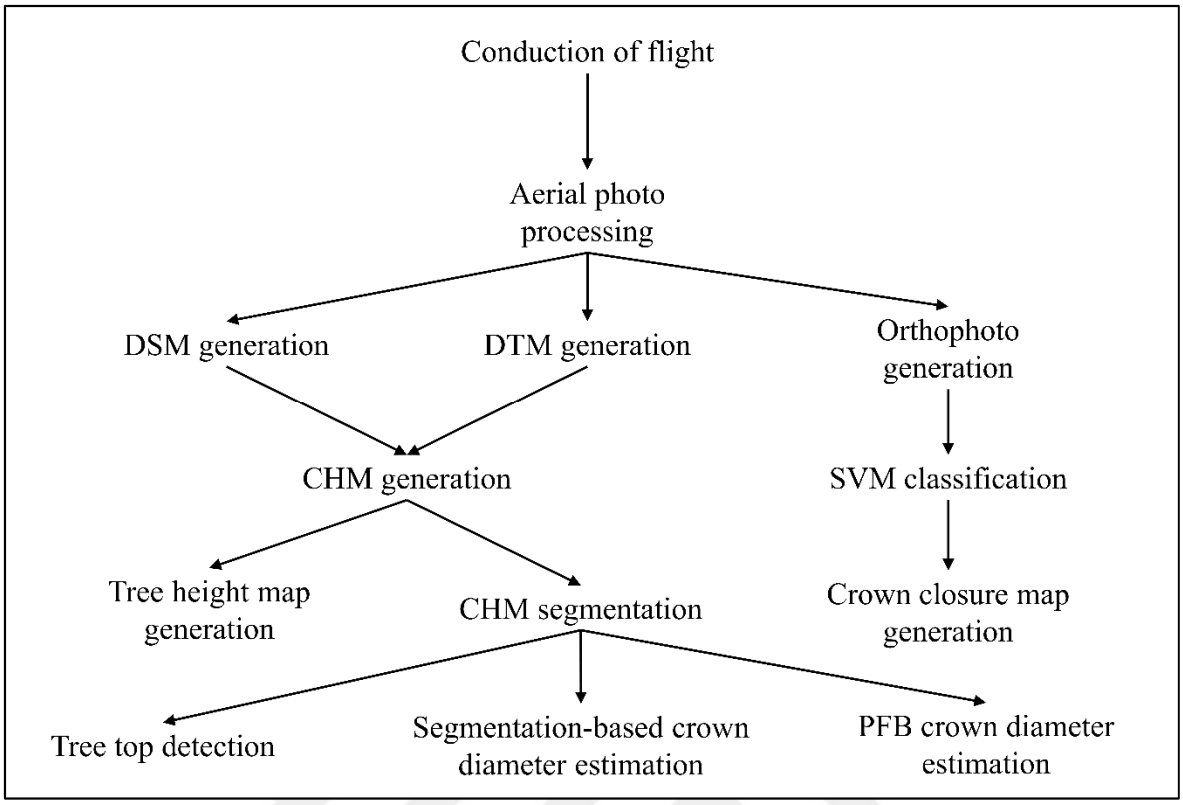

Figure 17. General workflow of the thesis

3. RESULTS AND DISCUSSION

This section presents the estimated stand parameters and investigates their accuracies qualitatively and quantitatively.

3.1. Qualitative Investigation

Figure 18 shows the tree height maps, which were generated from the CHMs of the test sites. As seen in the figure, the heights of the trees vary between 0-12 m in the test sites 1 and 2, whereas between 0-14 m in the test site 3. Tree delineation results for the test sites are shown in Figures 19, 20, 21, 22, 23, 25, 26, 27, 28, 29, 31, 32, 33, 34 and 35. The crown circles obtained from the PFB methodology are given in Figures 24, 30 and 36. These figures also depict the reference tree segments, reference crown circles and crown circles enclosing the tree segments. Since the DSMs and orthophotos have a very high resolution, reference tree segments were obtained by manually delineating the trees on the orthophotos draped on the DSMs. Many previous studies used manually delineated tree segments as reference data [20,191-194]. A method is considered successful if its resultant crown segments and circles perfectly overlap with the reference crown segments and circles. Visual investigations revealed that there are 46, 144 and 133 trees in the sites 1, 2 and 3, respectively.

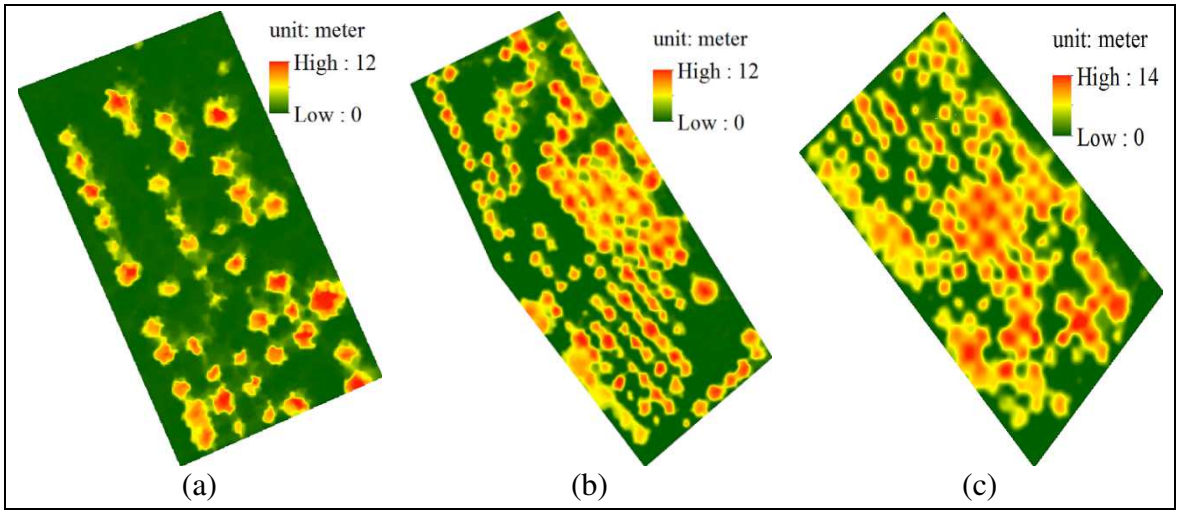

Figure 18. Tree height maps of the test sites 1 (a), 2 (b) and 3 (c)

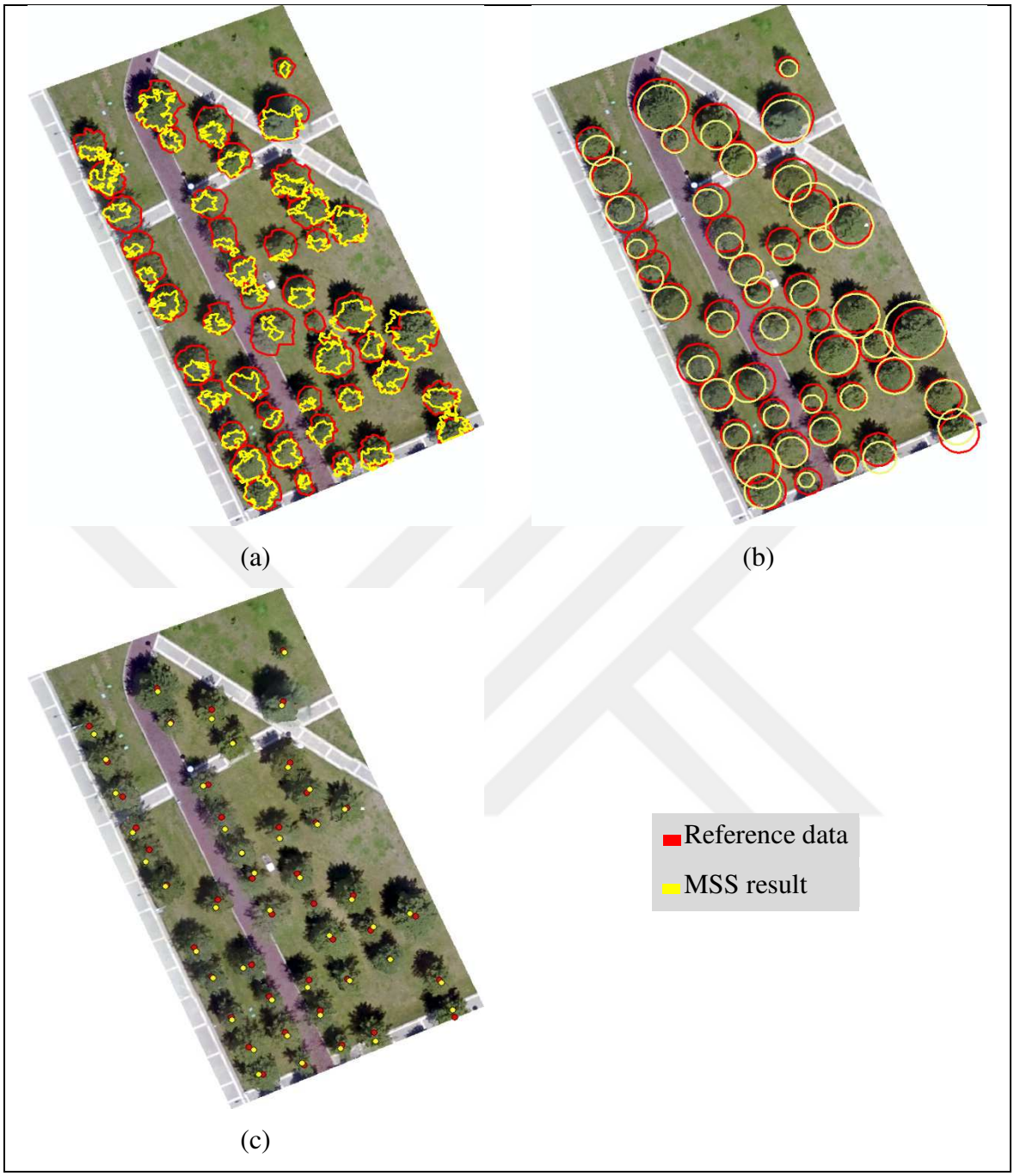

Figure 19. Reference tree segments and MSS delineation result for the site 1 (a), Reference and MSS-derived crown circles for the site 1 (b), Reference and MSS-derived crown circle centres for the site 1 (c)

As seen in Figure 19, the MSS algorithm missed just one tree in the site 1. This algorithm delineated only a small part of some of the trees, which resulted in smaller crown diameters, compared to the reference data. In general sense, the MSS algorithm can be considered successful in the site 1.

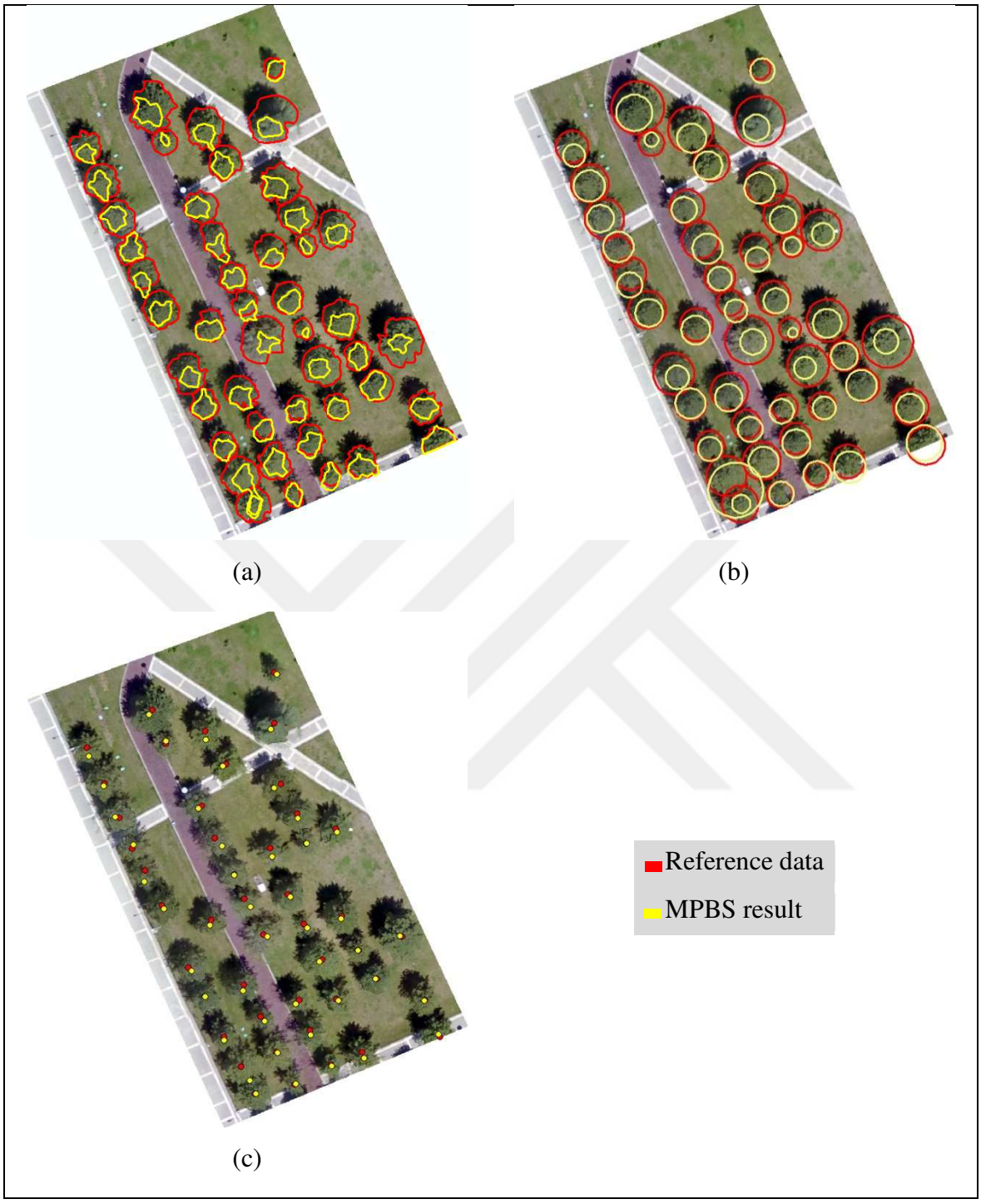

Figure 20. Reference tree segments and MPBS delineation result for the site 1 (a), Reference and MPBS-derived crown circles for the site 1 (b), Reference and MPBS-derived crown circle centres for the site 1 (c)

As seen in Figure 20, the MPBS algorithm managed to detect all trees in the site 1. The most noticeable thing about the MPBS result in the site 1 was that the crown diameters estimated with this algorithm were smaller than those in the reference data.

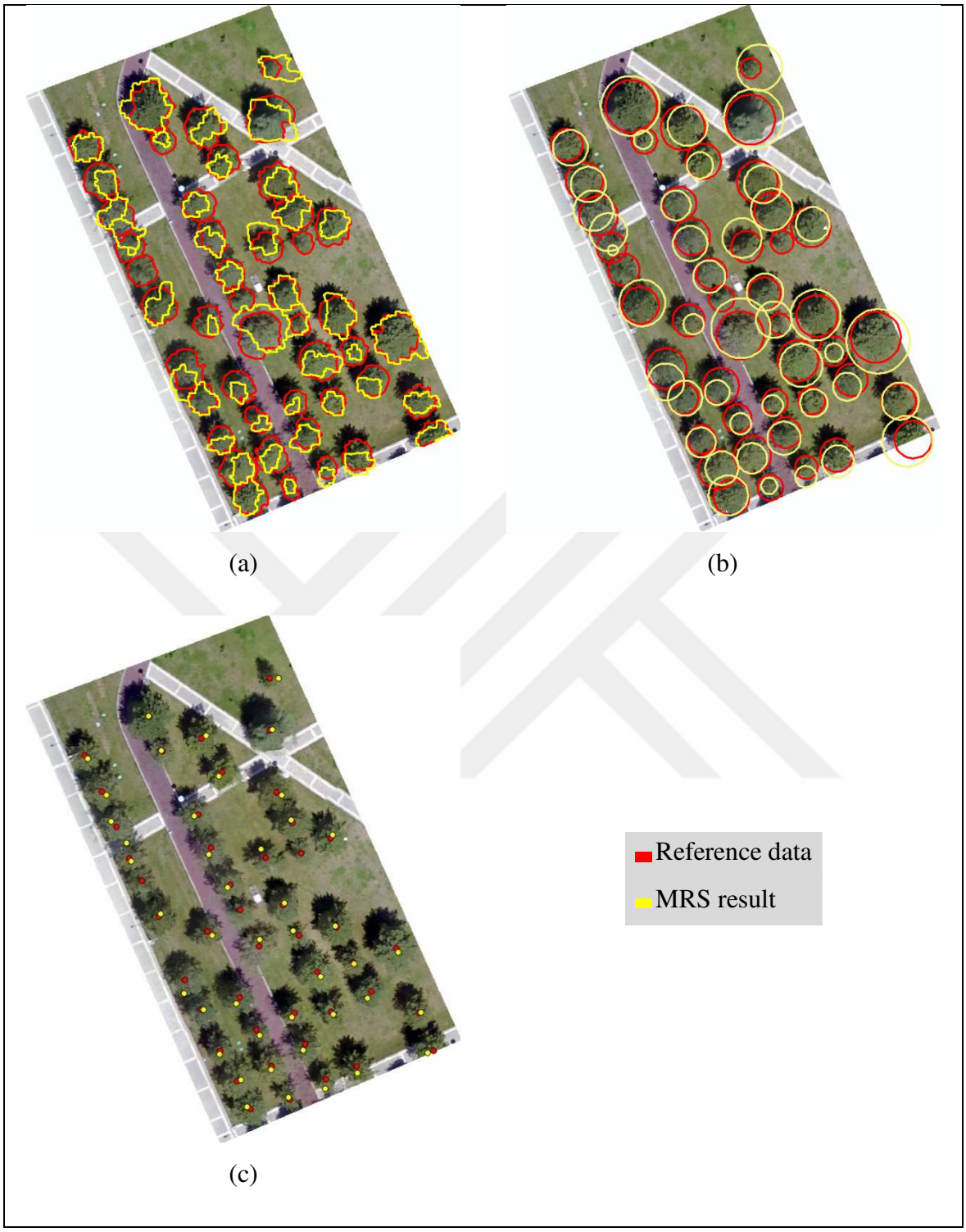

Figure 21. Reference tree segments and MRS delineation result for the site 1 (a), Reference and MRS-derived crown circles for the site 1 (b), Reference and MRS-derived crown circle centres for the site 1 (c)

As seen in Figure 21, the MRS algorithm missed 3 of the trees in the site 1. The figure also depicts that this algorithm merged some tree segments with some non-tree segments.

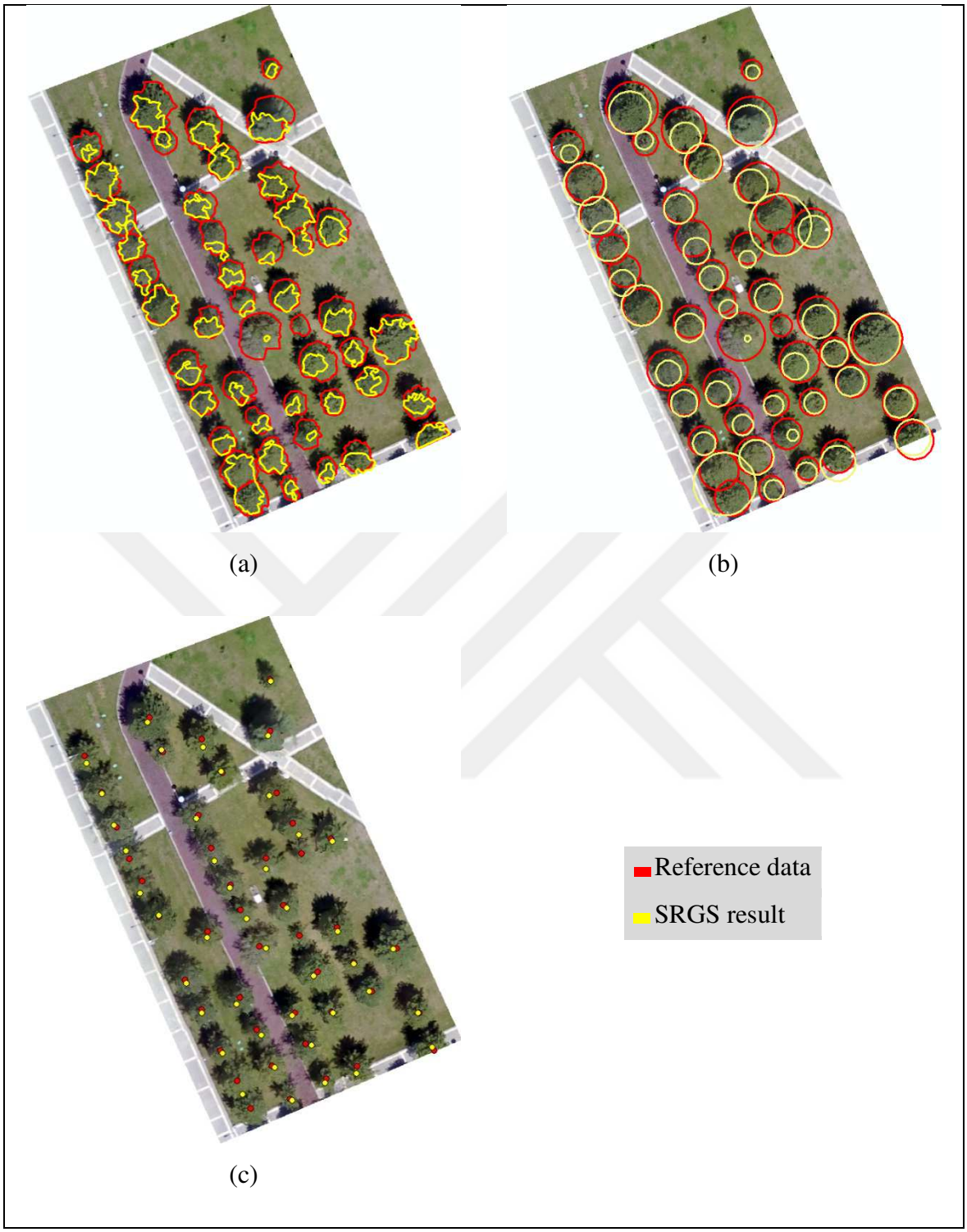

Figure 22. Reference tree segments and SRGS delineation result for the site 1 (a), Reference and SRGS-derived crown circles for the site 1 (b), Reference and SRGS-derived crown circle centres for the site 1 (c)

The SRGS algorithm missed 3 of the trees in the site 1, as shown in Figure 22. As seen in the figure, the SRGS algorithm merged some of the tree crowns.

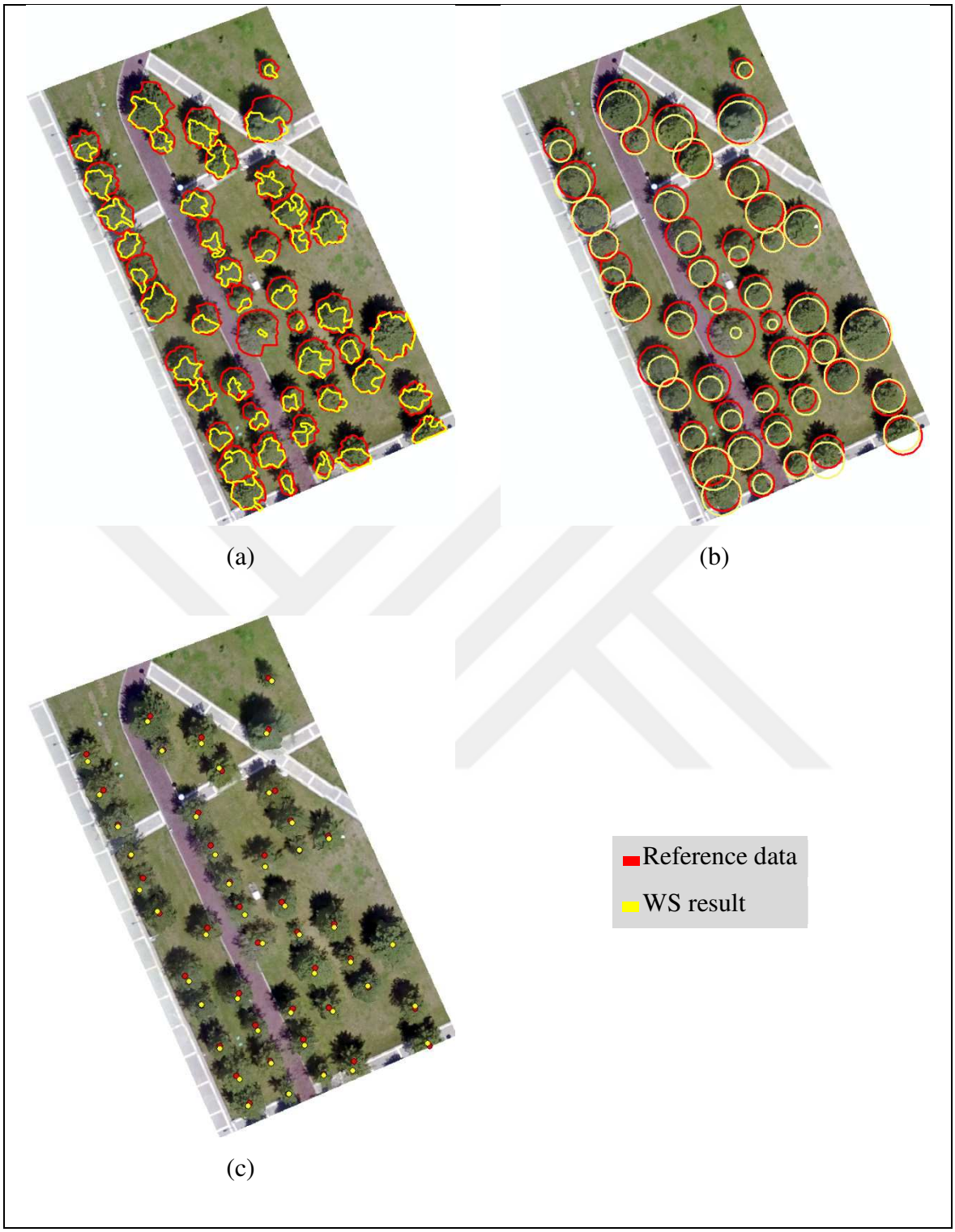

Figure 23. Reference tree segments and WS delineation result for the site 1 (a), Reference and WS-derived crown circles for the site 1 (b), Reference and WS-derived crown circle centres for the site 1 (c)

The WS algorithm detected all trees in the site 1. As seen in Figure 23, this algorithm was successful in estimating most of the crown diameters in the site 1.

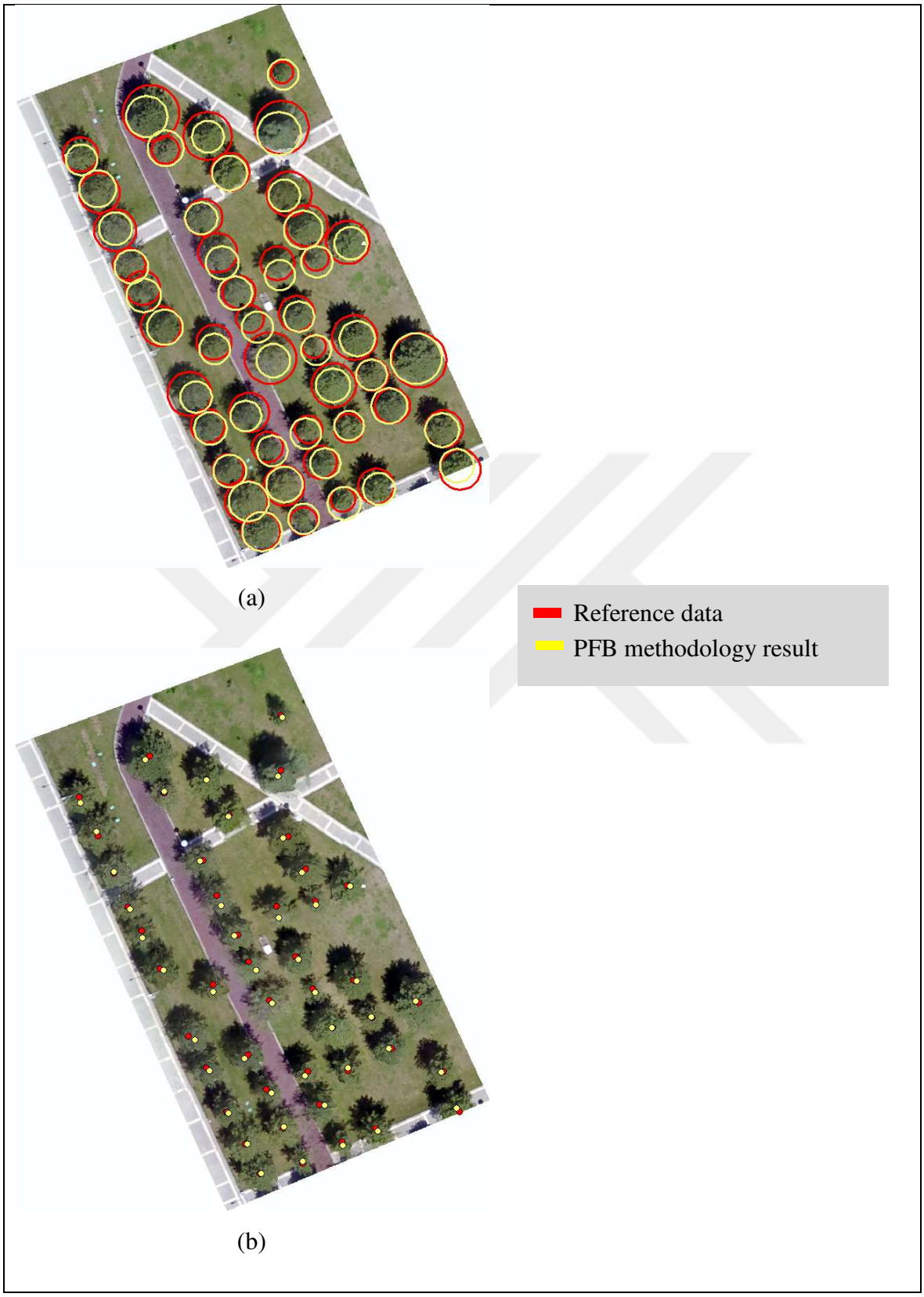

Figure 24. Reference and PFB methodology-derived crown circles for the site 1 (a), Reference and PFB methodology-derived crown circle centres for the site 1 (b)

Figure 25. Reference tree segments and MSS delineation result for the site 2 (a), Reference and MSS-derived crown circles for the site 2 (b), Reference and MSS-derived crown circle centres for the site 2 (c)

Figure 25 shows that the MSS algorithm missed 9 of the trees in the site 2. Compared to the site 1, the MSS algorithm performed worse in the site 2.

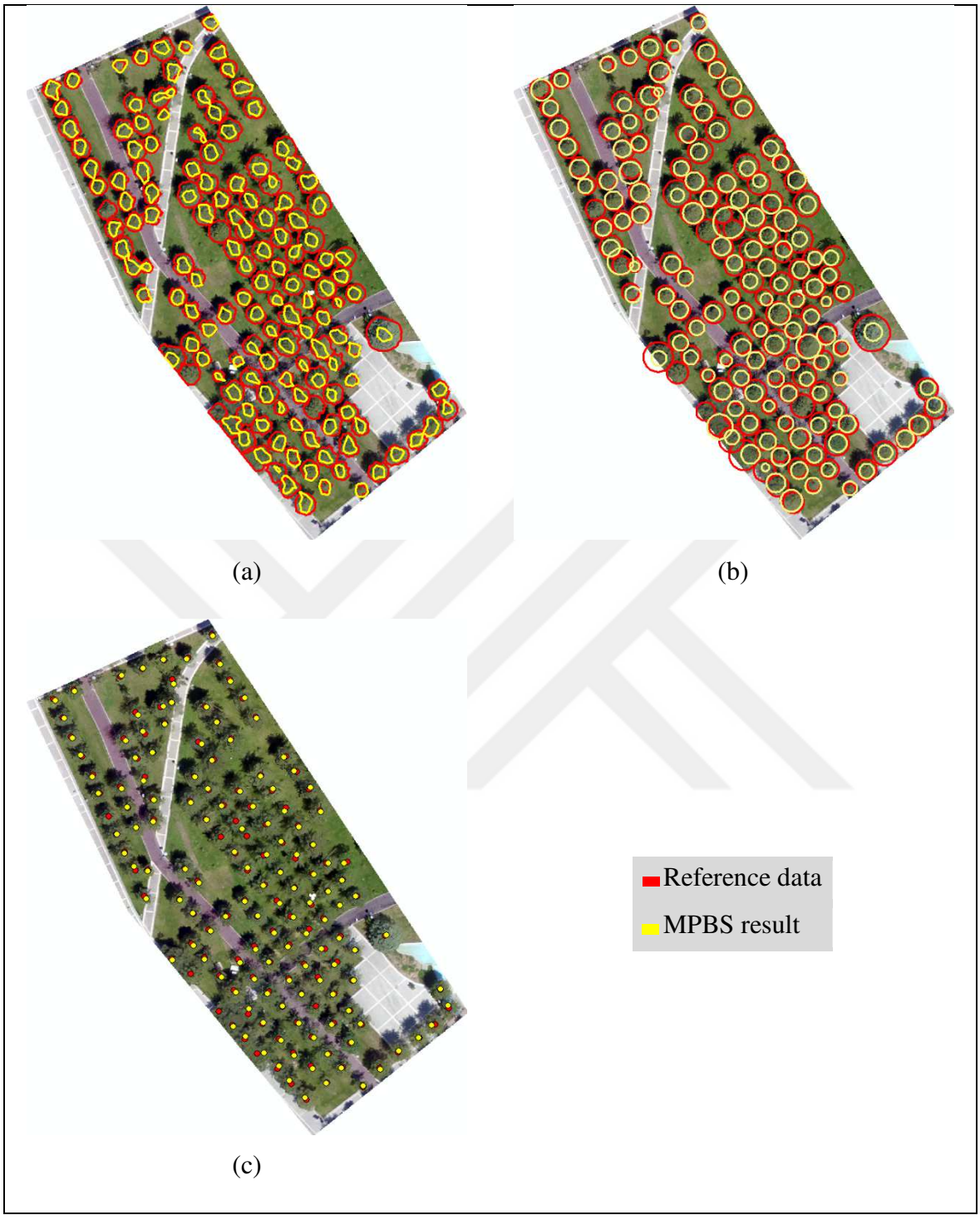

Figure 26. Reference tree segments and MPBS delineation result for the site 2 (a), Reference and MPBS-derived crown circles for the site 2 (b), Reference and MPBS-derived crown circle centres for the site 2 (c)

The MPBS algorithm missed 6 of the trees in the site 2, which can also be seen in Figure 26. As seen in the figure, this algorithm generated smaller crown circles compared to the reference data, as was the case in the site 1.

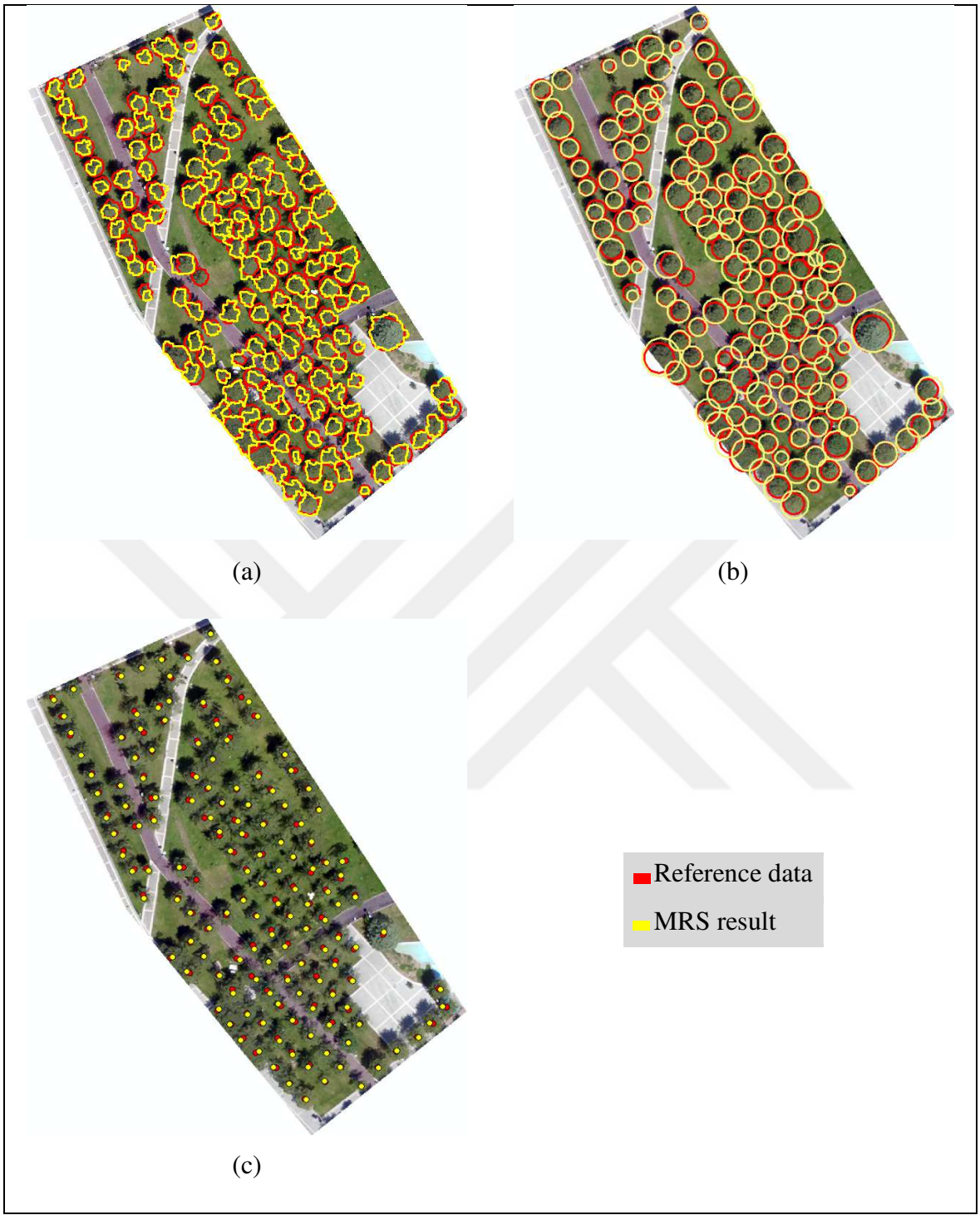

Figure 27. Reference tree segments and MRS delineation result for the site 2 (a), Reference and MRS-derived crown circles for the site 2 (b), Reference and MRS-derived crown circle centres for the site 2 (c)

As seen in Figure 27, the MRS algorithm missed just one tree in the site 2. The MRS algorithm was found to be successful in estimating the crown diameters of the most of the trees in this site.

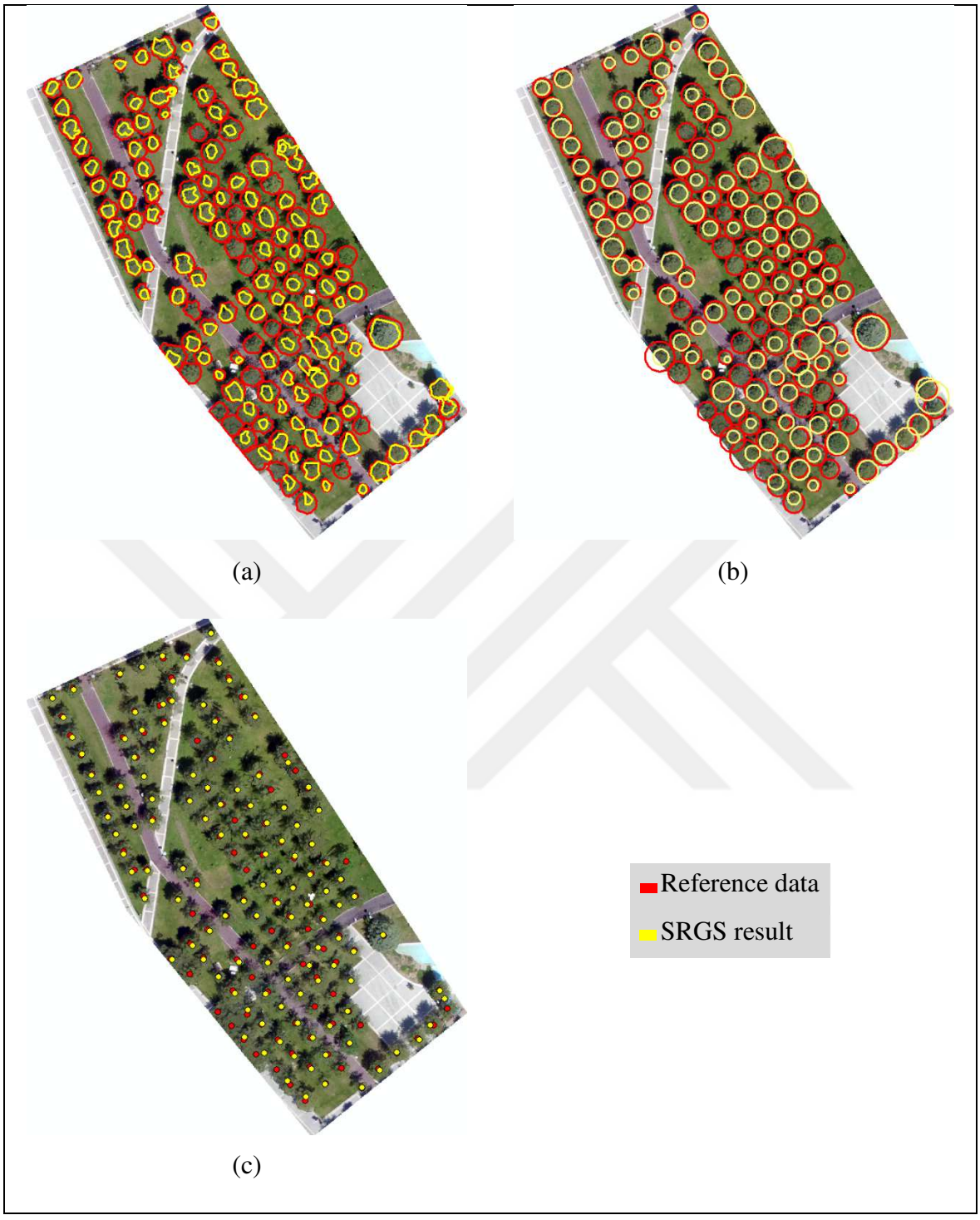

Figure 28. Reference tree segments and SRGS delineation result for the site 2 (a), Reference and SRGS-derived crown circles for the site 2 (b), Reference and SRGS-derived crown circle centres for the site 2 (c)

Figure 28 depicts that the SRGS algorithm performed worse in the site 2, compared to the site 1. This algorithm missed 20 of the trees in the site 2. In addition, the SRGS algorithm underestimated the crown diameters of the most of the trees in this site.

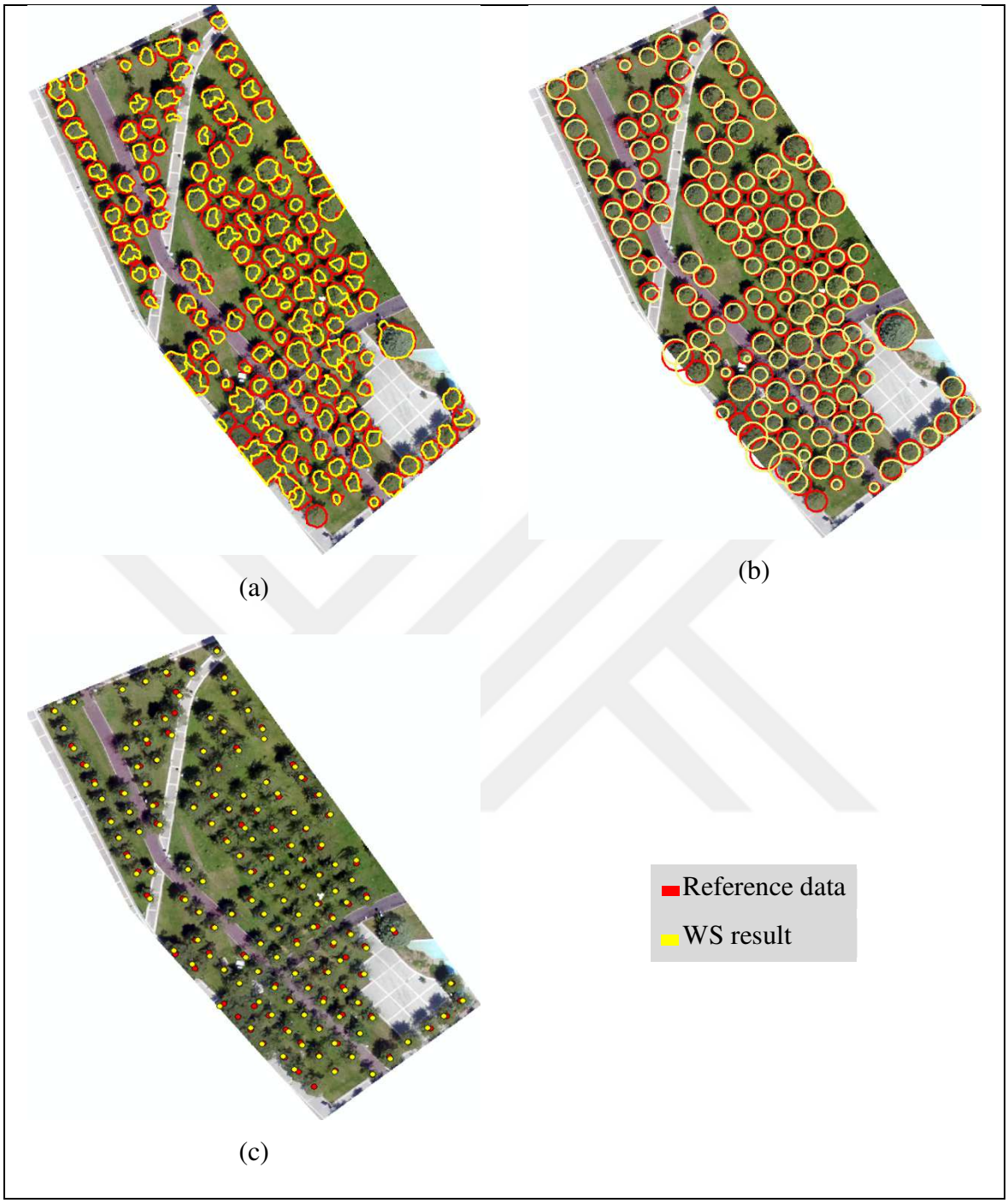

Figure 29. Reference tree segments and WS delineation result for the site 2 (a), Reference and WS-derived crown circles for the site 2 (b), Reference and WS-derived crown circle centres for the site 2 (c)

As seen in Figure 29, the WS algorithm missed 3 of the trees in the site 2. The figure also depicts that the crown circles generated based on the WS approach overlap with those of the reference data, which shows that this algorithm presented a good performance in the site 2.

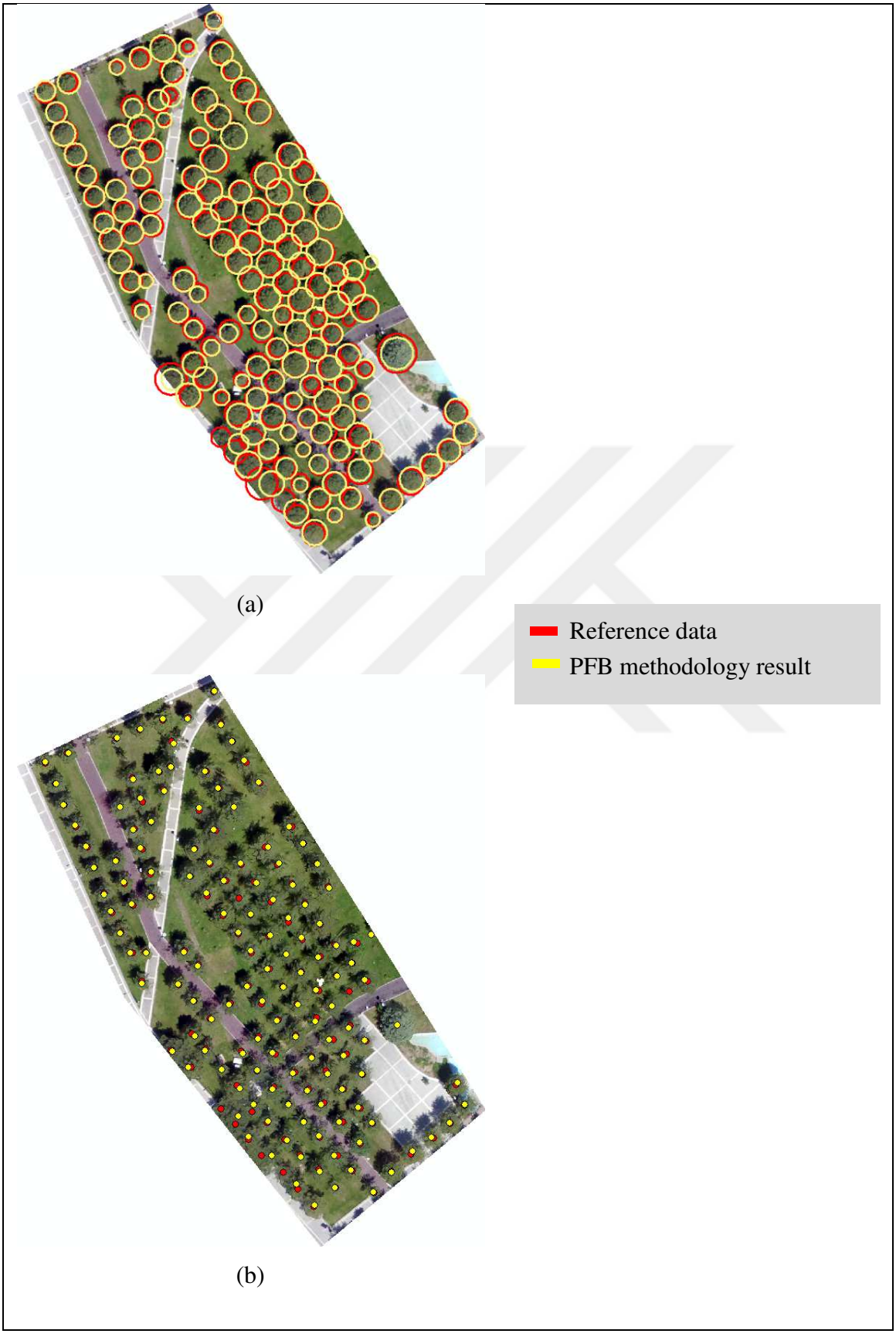

Figure 30. Reference and PFB methodology-derived crown circles for the site 2 (a), Reference and PFB methodology-derived crown circle centres for the site 2 (b)

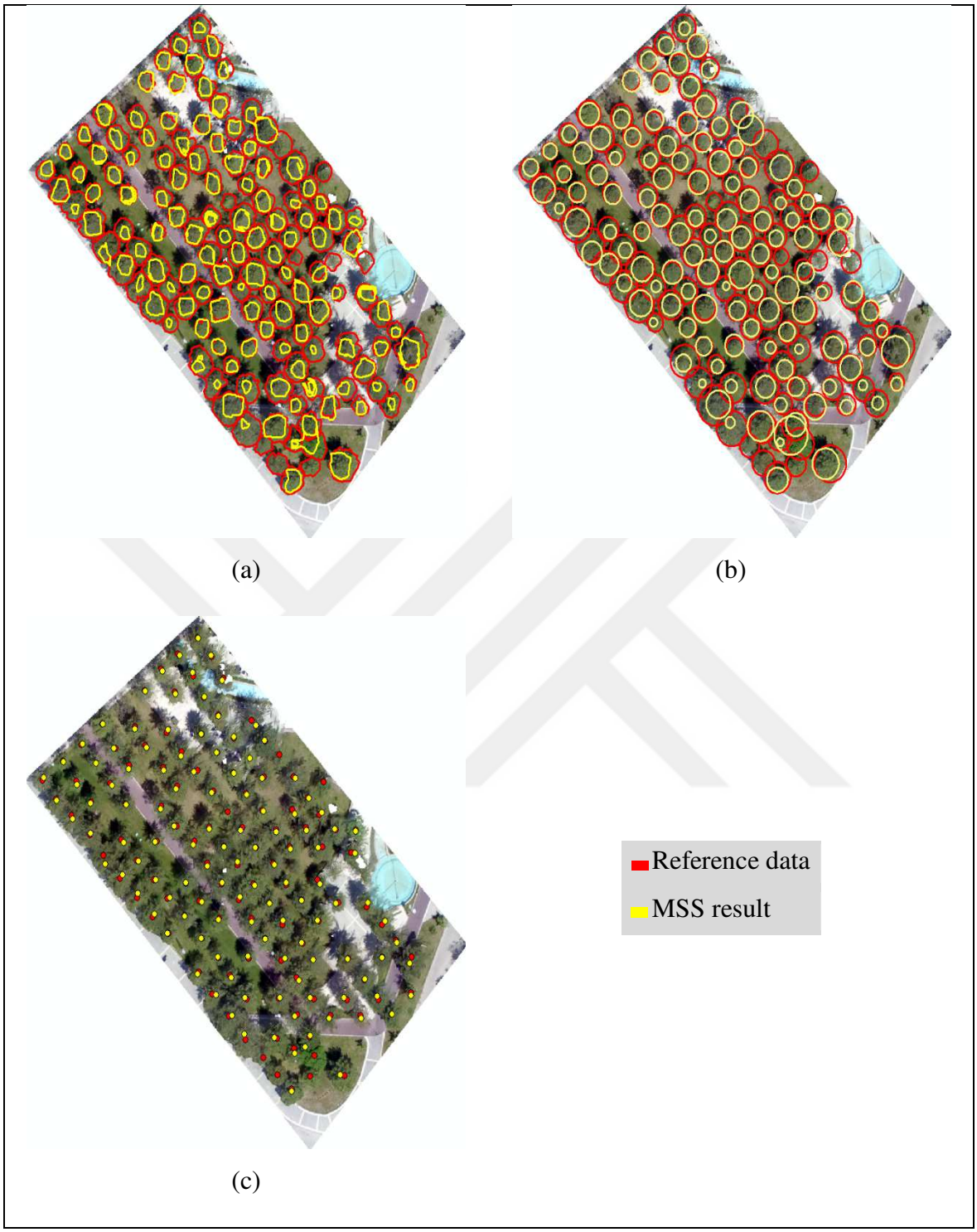

Figure 31. Reference tree segments and MSS delineation result for the site 3 (a), Reference and MSS-derived crown circles for the site 3 (b), Reference and MSS-derived crown circle centres for the site 3 (c)

Figure 31 shows that the MSS algorithm missed 9 trees in the site 3. As seen in the figure, this algorithm underestimated the crown diameters of the most of the trees.

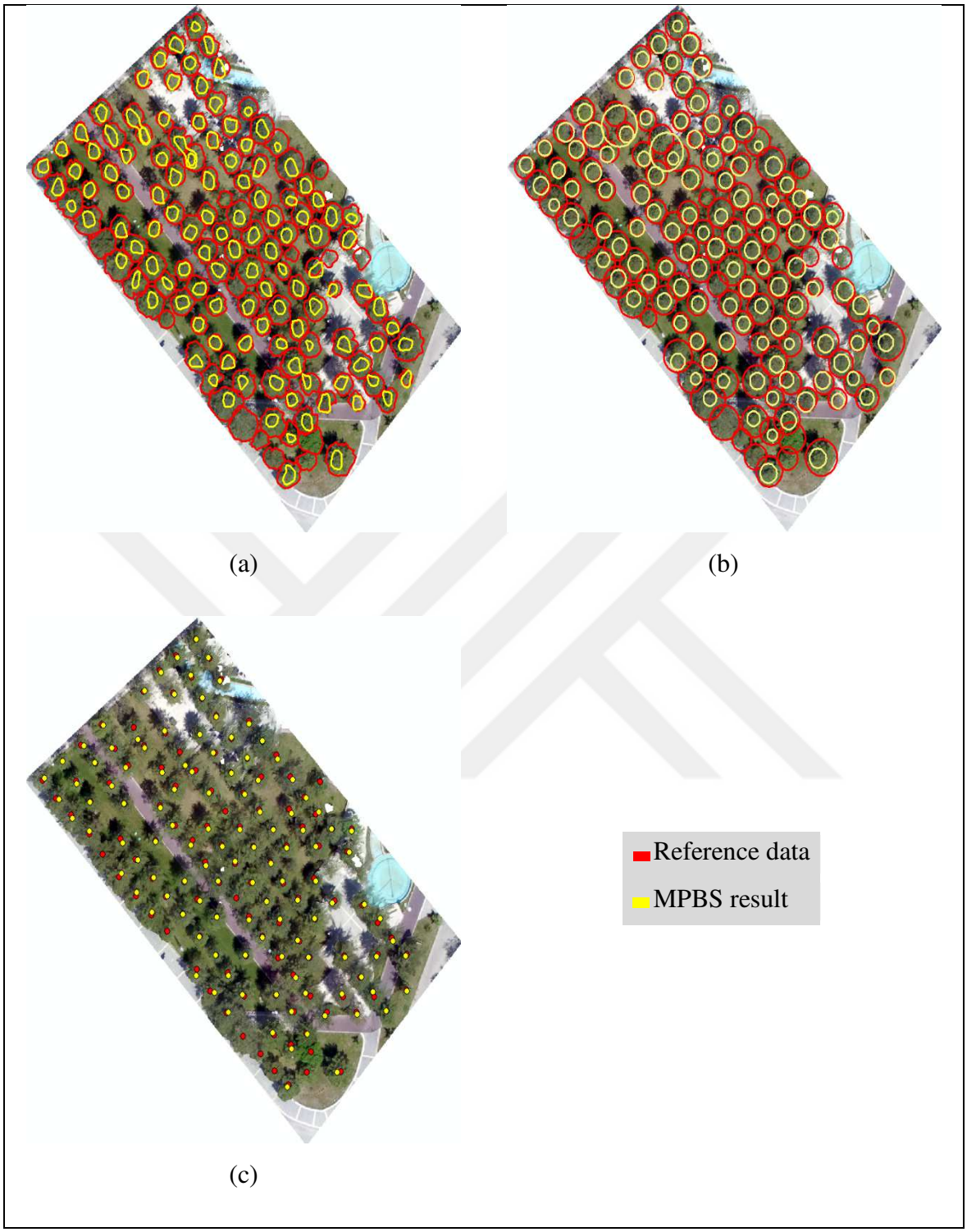

Figure 32. Reference tree segments and MPBS delineation result for the site 3 (a), Reference and MPBS-derived crown circles for the site 3 (b), Reference and MPBS-derived crown circle centres for the site 3 (c)

The MPBS algorithm missed 13 trees in the site 3, which can be seen in Figure 32. This algorithm, again, generated smaller crown circles, which was the case in the other sites.

Figure 33. Reference tree segments and MRS delineation result for the site 3 (a), Reference and MRS-derived crown circles for the site 3 (b), Reference and MRS-derived crown circle centres for the site 3 (c)

As seen in Figure 33, the MRS algorithm missed 3 of the trees in the site 3. The crown diameters estimated from this algorithm can be said to be similar to those of the reference data.

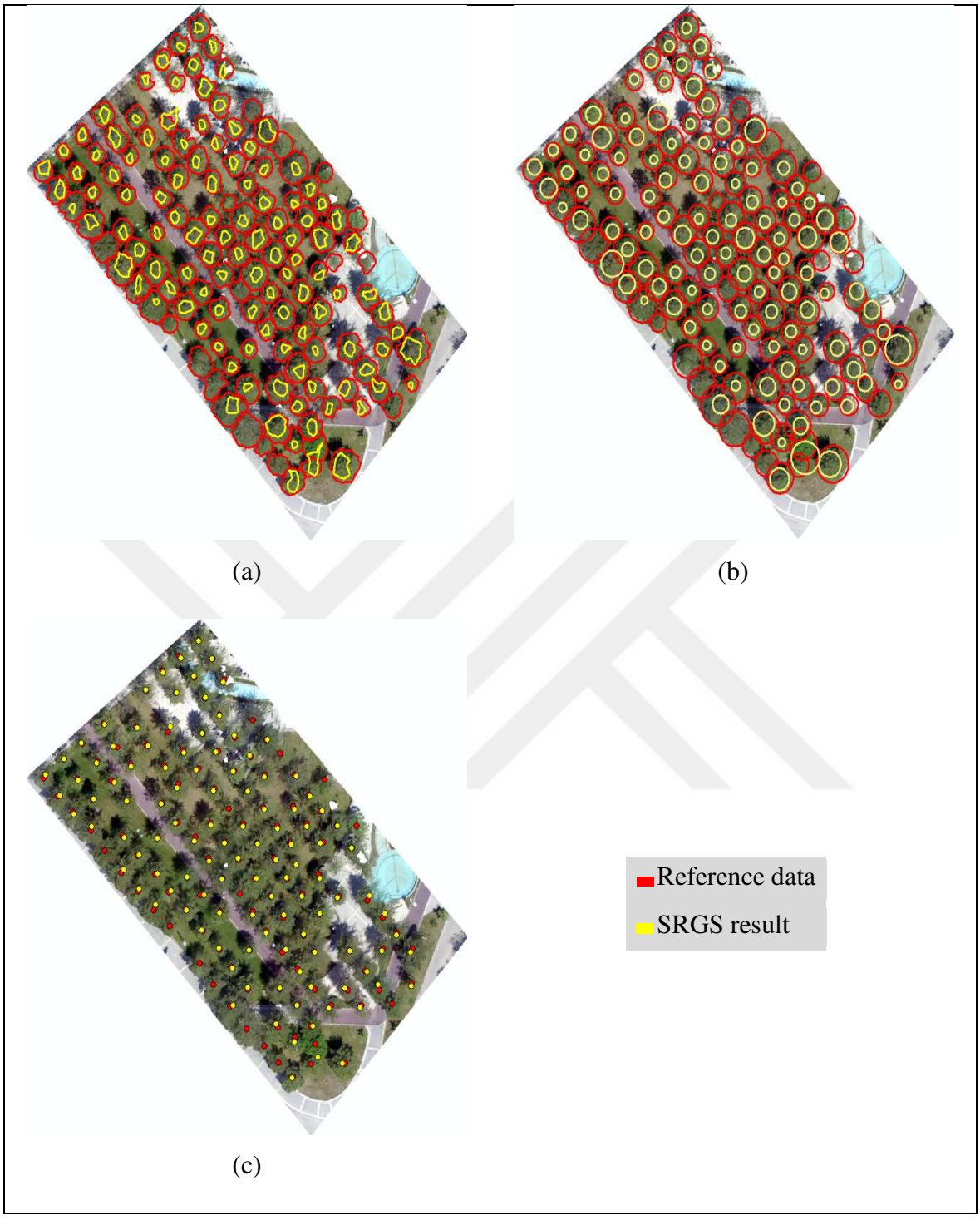

Figure 34. Reference tree segments and SRGS delineation result for the site 3 (a), Reference and SRGS-derived crown circles for the site 3 (b), Reference and SRGS-derived crown circle centres for the site 3 (c)

The SRGS algorithm missed 17 of the trees in the site 3, which can also be seen in Figure 34. This algorithm, again, presented the worst performance in this site, compared to the other algorithms.

Figure 35. Reference tree segments and WS delineation result for the site 3 (a), Reference and WS-derived crown circles for the site 3 (b), Reference and WS-derived crown circle centres for the site 3 (c)

As seen in Figure 35, the WS algorithm missed 5 of the trees in the site 3. The WS algorithm can be said to have a good performance in estimating the crown diameters of the trees in this site.

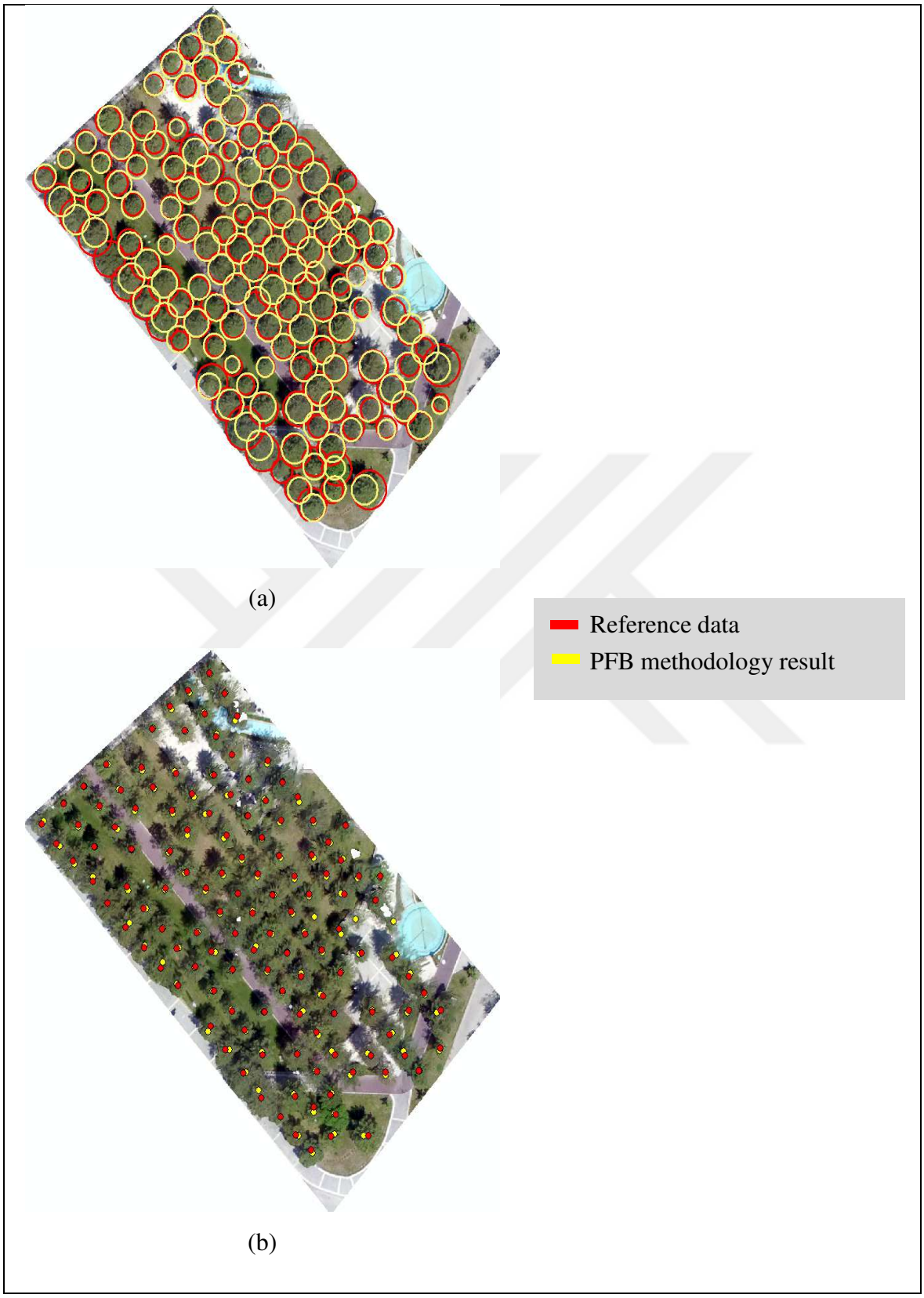

Figure 36. Reference and PFB methodology-derived crown circles for the site 3 (a), Reference and PFB methodology-derived crown circle centres for the site 3 (b)

3.2. Quantitative Investigation

Despite the fact that qualitative investigations give some clues about the performances of the used methodologies, their results are highly dependent on the perspective of the analyst. Hence, some additional quantitative evaluations are essential for more robust and comprehensive performance investigations.

3.2.1. Tree Detection Accuracies

Tree detection results were quantitatively investigated by means of the Precision, Recall and F-measure metrics, which have been used in various object detection studies [195-198]. The Precision is the ratio between the number of correctly detected trees and the number of all detected trees. The Recall is calculated by dividing the number of correctly detected trees to the number of trees in the reference data. The F-measure is a harmonic mean between the Precision and Recall. It is used as an overall performance investigation metric [195]. These metrics are calculated based on the terms True Positives (TP), False Positives (FP) and False Negatives (FN). The TP is the number of correctly detected trees. The FP is the number of trees detected in the spots where there are no trees and the FN is the number of trees that are not detected [195]. Srestasathiern and Rakwatin [195] presented the Precision, Recall and F-measure metrics as;

$$Precision = \frac{TP}{TP + FP}$$
$$Recall = \frac{TP}{TP + FN} \tag{3.1}$$
$$F - measure = \frac{(1 + a) \times Precision \times Recall}{a \times Precision + Recall}$$

where, a is a positive scalar, which was set to 0.5 as in [195] and [196]. Tree detection results can be seen in Table 3. As seen in the table, all approaches managed to detect the trees in the site 1 with an accuracy higher than 90%. The MPBS, WS and PFB methodologies detected all trees in this site, whereas the MSS, MRS and SRGS algorithms missed 1, 3 and 3 of the trees, respectively. None of the algorithms except the MRS committed false positives in the site 1. The MRS algorithm detected a very small tree in a location where there is no

tree. Since the MPBS, WS and PFB methodologies detected all the trees in the site 1, the F-measure scores calculated from their outcomes were found 1.

In the site 2, all algorithms except the SRGS achieved to detect more than 90% of all trees. The SRGS algorithm missed 20 trees in this site, which can be considered significant compared to the results of the other methodologies. The MSS, MPBS and SRGS algorithms presented a higher performance in the site 1, which shows that the performance of these algorithms tends to decrease as the canopy closure rate increases. The MSS, MPBS, MRS, WS and PFB approaches missed 9, 6, 1, 3 and 4 of the trees in the site 2, respectively. The MSS, WS and PFB methodologies committed 2, 1 and 1 false positives in this site, whereas the others did not commit any. The MRS, WS, MPBS and PFB methodologies gave higher F-measure scores while the other approaches resulted in relatively smaller scores.

Table 3. Tree detection statistics calculated for each approach

Test site	Approach	Detection accuracy (%)	TP	FP	FN	Precision	Recall	F-measure
1 (46 trees)	**MSS**	97.83	45	0	1	1.000	0.978	0.993
	MPBS	100.00	46	0	0	1.000	1.000	1.000
	MRS	93.48	43	1	3	0.977	0.935	0.963
	SRGS	93.48	43	0	3	1.000	0.935	0.977
	WS	100.00	46	0	0	1.000	1.000	1.000
	PFB	100.00	46	0	0	1.000	1.000	1.000
2 (144 trees)	**MSS**	93.75	135	2	9	0.985	0.938	0.969
	MPBS	95.83	138	0	6	1.000	0.958	0.986
	MRS	99.31	143	0	1	1.000	0.993	0.998
	SRGS	86.11	124	0	20	1.000	0.861	0.949
	WS	97.92	141	1	3	0.993	0.979	0.988
	PFB	97.22	140	1	4	0.993	0.972	0.986
3 (133 trees)	**MSS**	93.23	124	0	9	1.000	0.932	0.976
	MPBS	90.23	120	0	13	1.000	0.902	0.965
	MRS	97.74	130	0	3	1.000	0.977	0.992
	SRGS	87.22	116	0	17	1.000	0.872	0.953
	WS	96.24	128	0	5	1.000	0.962	0.987
	PFB	97.74	130	0	3	1.000	0.977	0.992

In the site 3, all algorithms except the SRGS presented a tree detection accuracy higher than 90%, as was the case in the site 2. The MSS, MPBS, MRS, SRGS, WS and PFB approaches missed 9, 13, 3, 17, 5 and 3 of the trees in the site 3, respectively. None of the used methods committed false positives in this site. The MRS and PFB methods resulted in

the greatest F-measure scores in the site 3, which shows that these algorithms were the most successful ones in detecting the trees. The SRGS and MPBS algorithms gave the worst performances in this regard.

Figure 37 shows the overall tree detection accuracies and F-measure scores calculated for the test sites. As seen in the figure, the PFB methodology was found to be the most successful one in detecting the trees with an overall detection accuracy of 98.32% and an F-measure score of 99.27%. The WS algorithm followed the PFB methodology with a small margin. The figure also shows that the MRS and MPBS algorithms presented similar performances to the WS and PFB methodologies. The SRGS and MSS algorithms detected less number of trees.

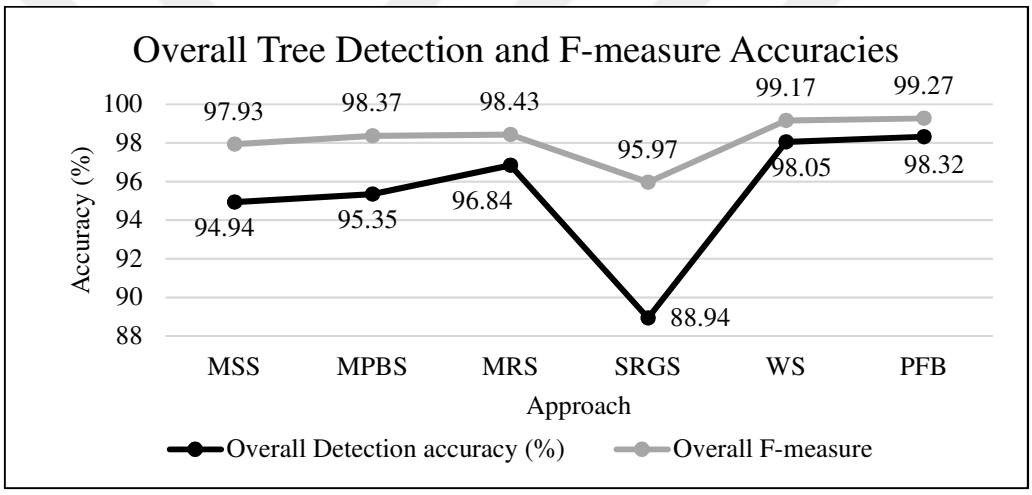

Figure 37. Calculated overall tree detection accuracies and F-measure values

3.2.2. Evaluation of Tree Segments

Since another important aim of this thesis was to predict the crown diameters directly from the tree segments produced with the segmentation algorithms, the quality of the produced tree segments had to be evaluated. Hence, the tree crown delineation results were evaluated with the over-segmentation (OS) [199-201], under-segmentation (US) [199-201], RMSE [199-201], area fit index (AFI) [199,202-204] and quality rate (QR) [205,206] metrics.

Let A_{R_j} and A_{S_i} be the total area of the reference and estimated tree segments, respectively. The OS, US, RMSE, AFI and QR are given as;

$$OS = 1 - \frac{A_{R_j} \cap A_{S_i}}{A_{R_j}}$$

$$US = 1 - \frac{A_{R_j} \cap A_{S_i}}{A_{S_i}}$$

$$RMSE = \sqrt{\frac{(OS)^2 + (US)^2}{2}} \tag{3.2}$$

$$AFI = \frac{A_{R_j} - A_{S_i}}{A_{R_j}}$$

$$QR = \frac{A_{R_j} \cap A_{S_i}}{A_{R_j} \cup A_{S_i}}$$

It should be noted that the optimum value for the OS, US, RMSE and AFI metrics is 0, whereas 1 for the QR metric.

Table 4. Metric scores calculated from the segmentation results

Test Site	Approach	OS	US	RMSE	AFI	QR
1	**MSS**	0.547	0.078	0.390	0.508	0.437
	MPBS	0.506	0.056	0.360	0.477	0.480
	MRS	0.410	0.196	0.321	0.266	0.516
	SRGS	0.624	0.051	0.442	0.603	0.369
	WS	0.533	0.051	0.379	0.508	0.455
2	**MSS**	0.518	0.067	0.369	0.483	0.466
	MPBS	0.414	0.060	0.296	0.377	0.564
	MRS	0.326	0.139	0.251	0.218	0.607
	SRGS	0.599	0.036	0.424	0.584	0.395
	WS	0.628	0.030	0.444	0.616	0.368
3	**MSS**	0.579	0.035	0.410	0.564	0.414
	MPBS	0.426	0.056	0.304	0.392	0.552
	MRS	0.235	0.153	0.198	0.096	0.669
	SRGS	0.712	0.020	0.504	0.706	0.286
	WS	0.799	0.010	0.565	0.797	0.201

Table 4 presents the metric scores determined from the segmentation results. Out of all algorithms, the MRS produced the most natural tree segments in the site 1. The tree segments produced with the MRS algorithm got the best scores from almost all metrics in this site. Despite its success, the MRS algorithm caused a greater amount of under-segmentation in the site 1, which can also be seen from the US scores given in Table 4. The

OS, RMSE, AFI and QR metrics indicated that the MPBS algorithm was the second most successful one in producing tree segments in the site 1. The MSS and MPBS algorithms caused a fair amount of over-segmentation in this site. These algorithms also caused a very small amount of under-segmentation in the site 1. The SRGS and WS algorithms got the best US score of 0.051 in this site. The AFI scores indicated that the MRS-based tree segments corresponded well with the reference tree segments in the site 1. The overall performance evaluation metrics RMSE and QR indicated that the MRS and SRGS algorithms produced the most and least natural tree segments in the site 1.

In the sites 2 and 3, the MRS algorithm, again, got the best scores from the OS, RMSE, AFI and QR metrics, as seen in Table 4. The MPBS algorithm was the second most successful one in these sites with respect to the OS, RMSE, AFI and QR metrics. The WS algorithm caused the least amount of under-segmentation in the sites 2 and 3. The MRS algorithm got an AFI score of 0.096 in the site 3, which shows that this algorithm produced tree segments that corresponded well with the reference tree segments. The SRGS and WS algorithms presented the worst performances in these sites, as was also the case in the site 1.

3.2.3. Evaluation of Crown Diameter Estimation Results

The crown diameters estimated based on the MSS, MPBS, MRS, SRGS, WS and PFB methodologies were compared against the reference data with respect to the MAE (Mean Absolute Error), RMSE and SDD statistics.

Let cd_e, cd_r and n be the estimated crown diameter, reference crown diameter and total number of trees, respectively;

$$MAE = \frac{1}{n}\sum_{i=1}^{n}|cd_e - cd_r|$$

$$RMSE = \sqrt{\frac{1}{n}\sum_{i=1}^{n}(cd_e - cd_r)^2} \tag{3.3}$$

$$SDD = \sqrt{\frac{\sum_{i=1}^{n}(cd_e - cd_r)^2 - \frac{(\sum_{i=1}^{n} cd_e - cd_r)^2}{n}}{n-1}}$$

Table 5 shows the metric scores computed between the reference and estimated crown diameters. According to the SDD scores, the crown diameters estimated based on the PFB methodology showed the smallest deviation (SDD of 0.82 m) from the reference crown diameters in the site 1, which indicated that this algorithm was the most successful one in this site. In addition, the PFB methodology got the best MAE and RMSE scores in the site 1. The MSS algorithm got the second best SDD (0.86 m), MAE (0.75 m) and RMSE (0.98 m) scores in the site 1. The SDD and MAE scores calculated between the reference and WS- and MSS-based crown diameters were found to be smaller than 1 m, which showed the success of these methods in this site. The SRGS algorithm got relatively lower SDD, MAE and RMSE scores in the site 1.

Table 5. Metric scores calculated for crown diameter estimates

Test site	Approach	SDD (m)	MAE (m)	RMSE (m)
1	**MSS**	0.86	0.75	0.98
	MPBS	1.06	1.26	1.56
	MRS	1.13	0.89	1.13
	SRGS	1.44	1.21	1.60
	WS	0.95	0.81	1.15
	PFB	0.82	0.71	0.92
2	**MSS**	0.93	0.98	1.18
	MPBS	0.94	1.11	1.33
	MRS	0.81	0.81	0.87
	SRGS	0.98	1.20	1.40
	WS	0.80	0.72	0.90
	PFB	0.66	0.53	0.69
3	**MSS**	1.05	1.30	1.60
	MPBS	1.13	1.80	2.06
	MRS	0.72	0.80	1.00
	SRGS	0.86	2.14	2.30
	WS	0.92	0.86	1.03
	PFB	0.79	0.63	0.79

In the site 2, the PFB methodology resulted in an SDD score of 0.66 m, an MAE score of 0.53 m and an RMSE score of 0.69 m, which were the best ones out of all algorithms. The performance of the MSS algorithm was found to be relatively lower in the site 2, compared to the site 1. The WS algorithm got the second best SDD (0.80 m) and MAE (0.72 m) scores, whereas the MRS algorithm yielded the second best RMSE score (0.87 m) in the site 2. The

SDD, MAE and RMSE scores given in Table 5 revealed that all algorithms except the MSS performed better in the site 2, compared to the site 1. The SRGS algorithm, again, presented the worst performance in the site 2. It yielded the worst SDD (0.98 m), MAE (1.20 m) and RMSE (1.40 m) scores in this site.

In the site 3, the MSS algorithm got the best SDD score (0.72 m). The PFB methodology resulted in the second best SDD score of 0.79 m. On the other hand, the PFB methodology was found to be the most successful one in estimating the crown diameters in the site 3 with an MAE score of 0.63 m and an RMSE score of 0.79 m. The MRS algorithm yielded the second best MAE (0.80 m) and RMSE (1 m) scores in this site. Considering the SDD, MAE and RMSE scores, the performances of the PFB and WS approaches in the site 3 were found to be lower than those in the site 2 and be higher than those in the site 1. The MPBS approach got the worst SDD score (1.13 m) in the site 3, whereas the SRGS algorithm resulted in the worst MAE (2.14 m) and RMSE (2.30 m) scores as seen in Table 5.

Statistical significance of the differences between the reference and estimated crown diameters was investigated with the ANOVA test, which compares group means [207] and has been used in various disciplines [208-211]. To do this, the one-way ANOVA test was conducted for each reference-estimated crown diameter pairs in all test sites. The null hypothesis in our case was that the means of the reference and estimated crown diameters were equal. The null hypothesis is rejected when determined *p*-value is less than 0.05 (95% confidence interval), which indicates a significant difference between groups [208-211].

Table 6. ANOVA test results for crown diameter estimates

Test site	MSS	MPBS	MRS	SRGS	WS	PFB
1	0.040	2.6E-07	0.740	0.010	0.011	0.620
2	2.2E-10	6.1E-20	0.030	5.2E-20	0.021	0.480
3	1.3E-19	2.0E-38	0.012	5.5E-50	0.010	0.510

Table 6 presents the one-way ANOVA test results, which were used to investigate if there was any statistically significant difference between the reference and estimated crown diameters. As seen in the table, the *p*-values calculated between the reference and PFB-estimated crown diameters were found 0.62, 0.48 and 0.51 for the test sites 1, 2 and 3, respectively. Since these values were greater than 0.05, it was concluded that there was no significant difference between the reference and PFB-estimated crown diameters in the test

sites. A high relationship (*p*-value of 0.74) was also found between the reference and MRS-based crown diameters in the site 1. The *p*-values given in Table 6 revealed statistically significant differences between the reference and MSS-, MPBS-, SRGS- and WS-based crown diameters in the test sites.

An algorithm is considered successful if the positions of the estimated crown circles match to those of the reference data. In order to investigate this phenomenon, the SDD, MAE and RMSE statistics were computed with the distances between the estimated crown circle centres and corresponding reference crown circle centres. Calculated statistics are presented in Table 7. As seen in the table, all methodologies generated the crown circles with a position accuracy better than 1 m. It was also concluded that the PFB methodology was the most successful one in this regard. The MSS and WS algorithms followed the PFB methodology with a small margin. The MRS and SRGS algorithms were the least successful ones in this regard.

Table 7. Calculated statistics for crown circle centres

Test Site	Method	SDD (m)	MAE (m)	RMSE (m)
1	**MSS**	0.41	0.69	0.80
	MPBS	0.46	0.63	0.79
	MRS	0.36	0.68	0.78
	SRGS	0.49	0.74	0.89
	WS	0.40	0.62	0.74
	PFB	0.33	0.53	0.62
2	**MSS**	0.28	0.45	0.53
	MPBS	0.29	0.49	0.56
	MRS	0.32	0.57	0.66
	SRGS	0.36	0.47	0.59
	WS	0.31	0.48	0.57
	PFB	0.30	0.41	0.51
3	**MSS**	0.35	0.49	0.60
	MPBS	0.39	0.52	0.64
	MRS	0.30	0.58	0.67
	SRGS	0.32	0.50	0.59
	WS	0.38	0.54	0.66
	PFB	0.27	0.48	0.55

3.3. General Evaluation

Despite the fact that plenty of attention was paid to choose appropriate parameters for the segmentation algorithms, crown delineation results were not perfect, which, of course, affected the accuracy of the estimated crown diameters. Point cloud filtering procedure plays a vital role in the production of a CHM. If the points belong to the above-ground objects are not removed properly, then the resultant DTM may not be accurate as needed, which influences the 3D accuracy of the generated CHM. Since none of the ground filtering algorithms reported in the literature are able to perform perfectly, there will likely be filtering errors to some extent. Hence, prior to the segmentation, CHMs were filtered with the same Gaussian filter to minimize the errors due to the point cloud filtering procedure.

The MSS algorithm focuses on finding local maximum density, hence, the magnitude of the Gaussian filter parameter should be chosen carefully when smoothing the CHM prior to the segmentation. A larger magnitude reduces the height variations more than needed. In such cases, the MSS algorithm produces excessive-sized tree crown segments, especially for small trees in the close vicinity of larger ones. The minimum region size parameter used by the MSS algorithm was found to be effective in producing tree segments whose sizes were consistent with the reference tree crowns. Since the MSS is a non-parametric algorithm, users do not have to define the number of classes (segments), unlike in the case of many clustering algorithms such as the k-means. Moreover, owing to the use of a joint feature space, the MSS algorithm is able to produce segments with the aid of the elevation and position information. The most straightforward downside of this algorithm is that it is not time-efficient, especially working with high-resolution data [212], as was also the case in this thesis.

As shown in Figure 8, there are a large number of interlocking trees in the site 3, which made it very challenging to define an appropriate size for the structuring element used in the MPBS algorithm. Since the trees in this site have similar heights, the algorithm tended to consider some of the trees as a large tree. Increasing the size of the structuring element facilitated to detect a huge amount of the trees in this site, however, the algorithm eroded a considerable amount of the trees more than needed, which resulted in crown diameters smaller than reality. This is the main reason that the MPBS algorithm performed worst in the site 3. The MPBS algorithm performs well in complex image scenes and on the images with relatively low spatial resolution. The main advantage of the MPBS algorithm is that it

does not use image gradient and can be applied in single- or multi-scale segmentation applications. It was also found to reduce the over-segmentation effect dramatically. The MPBS algorithm generally performs a large number of opening and closing by reconstruction operations, which is the main disadvantage of this algorithm.

The main drawback of the MRS algorithm is the difficulty to choose an appropriate scale parameter, which is the most effective parameter of this algorithm. The analysts need to try different values for this parameter until the optimum segmentation result is obtained. Despite this disadvantage, the MRS algorithm performed well in the test sites. The crown diameters estimated based on this algorithm corresponded well with the reference crown diameters, especially in the sites 2 and 3, where there are a large number of interlocking trees. Despite the fact that the canopy closure ratio is lower in the site 1, it was very challenging to find the optimum scale parameter value for this site. This is the reason that the MRS algorithm performed worst in this site. Greater scale values yielded large segments, whereas smaller ones produced smaller segments. The shape and compactness parameters did not play a significant role in the segmentation process. Trying different values for these parameters caused no significant changes in the boundary of the segments.

The Gaussian filtering procedure reduced the height variations in the CHMs, which caused the seed generation algorithm used by the SAGA software to miss some of the shorter trees. This is the main reason that the SRGS algorithm failed to detect a considerable amount of the trees. Another drawback of the SRGS algorithm is that it is very challenging to find an appropriate similarity threshold value for this algorithm. The similarity threshold values used for the sites 2 and 3 did not help delineate the tree crowns properly. As seen in Figures 28 and 34, the crown diameters estimated by the SRGS-based approach were smaller than those in the reference data. Greater values were tried for the similarity threshold parameter to enlarge the size of the segments. However, using greater values caused the tree crown segments to merge with neighboring non-crown segments, which increased the crown diameters in no small measure. Hence, smaller similarity threshold values were used to produce the tree segments.

The result of the WS algorithm is highly sensitive to noise, which constitutes a huge drawback for this algorithm. This, of course, attaches importance to the smoothing of the data prior to the segmentation. The WS algorithm is also sensitive to local minima, which increases its tendency to end up with over-segmented tree segments in most cases. On the other hand, the WS method divides the data into closed and connected segments, regardless

of the spatial resolution of the data. Unlike many segmentation algorithms, the WS algorithm does not require any post-processing procedures to produce closed regions, which is a fact also confirmed by Beucher and Meyer [213] and Hill et al [214]. The WS algorithm was found to be very time-efficient, compared to the others.

The PFB methodology detects the tree tops with a sliding window whose size is set to the crown diameter of the smallest tree. This enabled the detection of the most of the tree tops (see Table 3). The PFB methodology is directly based on the fact that trees' elevation values decrease from top point towards to edge of crowns, which provides accurate estimates of crown diameters of trees, no matter they are in open or closed area. The PFB methodology outperformed the other segmentation-based approaches in all test sites, which can be observed either from qualitative (Figures 24, 30 and 36) or quantitative (Tables 5 and 6) evaluation results. Another important advantage of the PFB methodology is that it estimates the optimum degree for the polynomial fit through each profile formed in each cardinal direction. This approach enables the consideration of even small elevation differences in the profiles, which makes the methodology flexible for trees with different size and shapes. The main disadvantage of the PFB methodology is that it is not fully automated. It uses five parameters to perform. However, its parameters are not hard to define. The elevation threshold, smallest crown diameter and horizontal distance parameters can be easily defined by making a few measurements on a textured CHM, which is produced by draping an orthophoto over a CHM. Measurements can, of course, be made on a CHM without the texture data. However, using a textured CHM would be more helpful to define the parameters precisely, owing to its ability to provide the elevation of a specific point and the distance between two specific points. Definition of the parameters used by the PFB methodology took a shorter span of time, compared to the time spent to find the optimum parameters used by the segmentation-based approaches. A few simple measurements are enough to define the parameter values used by the PFB methodology, whereas the optimum parameter values of the used segmentation algorithms are found after a large number of trials. Hence, the PFB methodology can be considered time-efficient, compared to the other methods. However, it may take longer to process CHMs with higher spatial resolutions.

Since the estimates of the PFB methodology were compared either to the reference data or to the estimates from five segmentation approaches in terms of four performance criteria (the SDD, MAE, RMSE and *p*-value) employed in three different test sites, it may be hard to comprehend all evaluation results to decide which algorithm outperformed which.

In order to make it easier to interpret all evaluation results, each methodology was given a score with respect to its success within each criterion. Since a total of six approaches were used to estimate the crown diameters, each algorithm got a score between 1 and 6. For each performance criterion, the most successful approach got the score of 6, whereas the least successful one got the score of 1. The average scores were used to interpret the performance of each approach.

Table 8. Crown diameter estimation performance scores

Test site	Method	Criterion				
		SDD score	MAE score	RMSE score	*p*-value score	Average score
1	**MSS**	5	5	5	4	4.75
	MPBS	3	1	2	1	1.75
	MRS	2	3	4	6	3.75
	SRGS	1	2	1	2	1.50
	WS	4	4	3	3	3.50
	PFB	6	6	6	5	5.75
2	**MSS**	3	3	3	3	3.00
	MPBS	2	2	2	2	2.00
	MRS	4	4	5	5	4.50
	SRGS	1	1	1	1	1.00
	WS	5	5	4	4	4.50
	PFB	6	6	6	6	6.00
3	**MSS**	2	3	3	3	2.75
	MPBS	1	2	2	2	1.75
	MRS	6	5	5	5	5.25
	SRGS	4	1	1	1	1.75
	WS	3	4	4	4	3.75
	PFB	5	6	6	6	5.75

Table 8 shows the scores given to each algorithm with respect to its crown diameter estimation success. The table also presents the overall scores calculated for each algorithm in all test sites. As seen in the table, the PFB methodology outperformed the other approaches in all test sites. It got the average scores of 5.75, 6 and 5.75 in the test sites 1, 2 and 3, respectively. The MSS-based approach was found to be the second most successful one in the site 1 with an average score of 4.75. The MRS approach was ranked as second in the sites 2 and 3 with average scores of 4.5 and 5.25, respectively. The MSS approach got the second highest average score (4.75) in the site 1. The WS algorithm was found to be another

successful one in estimating the crown diameters with average scores of 3.5, 4.5 and 3.75 in the sites 1, 2 and 3, respectively. The SRGS and MPBS algorithms presented the poorest performances in all test sites, which can be clearly seen from their average scores given in Table 8. Figure 38 shows the average performance scores of each approach.

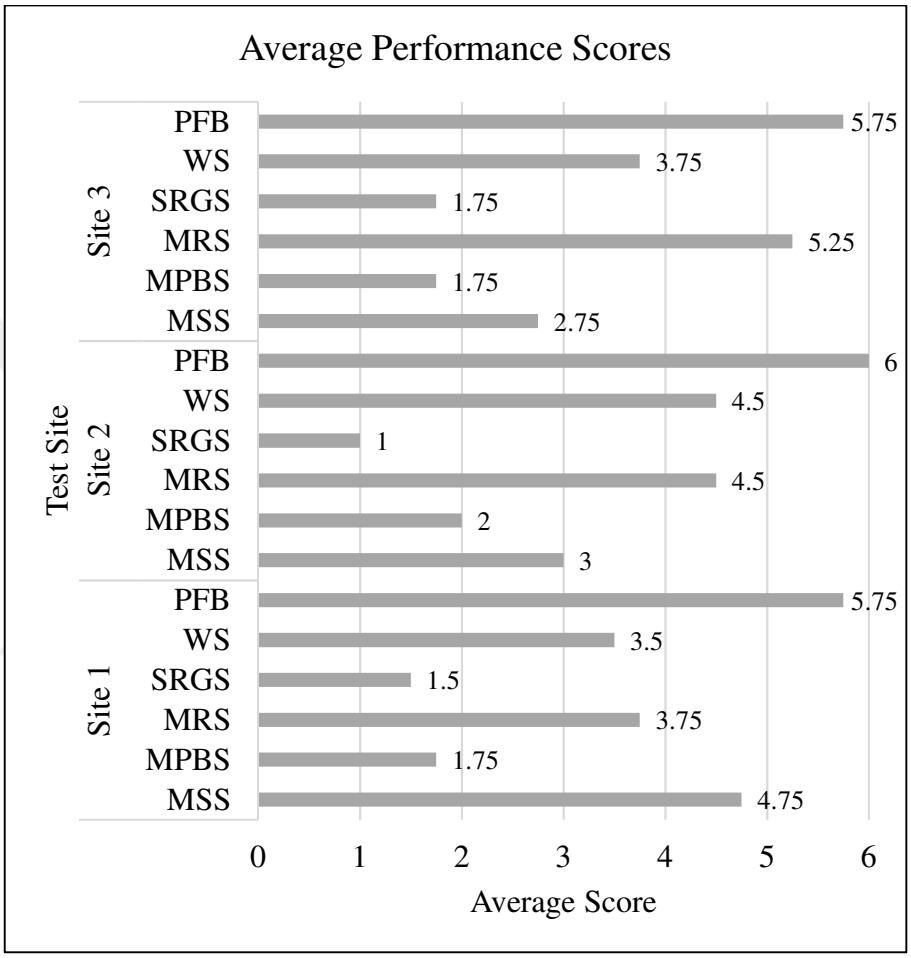

Figure 38. Average performance scores for each approach

4. CONCLUSIONS

Estimation of forest characteristics plays a vital role in forest management. Estimated forest stand parameters are used to generate forest management plans, which are used as basis to take actions in order to maintain the sustainability of forests and to ensure the continuity of the service offered by forests. Owing to their advantages to offer accurate measurements of the physical characteristics of tree stands, terrestrial measurements are often utilized to collect forest inventory. However, conduction of field measurements may not always be cost- and time-efficient. On the other hand, today's sophisticated satellite and photogrammetry systems offer very comprehensive and accurate information about the features on the surface of the earth. Advanced LiDAR systems and UASs are able to provide 3D position accuracies up to a few centimetres. Hence, they have been used in numerous studies to estimate forest stand parameters. In the literature, a wide variety of studies have revealed the fact that forest characteristics derived from LiDAR- or photogrammetry-based point clouds compare well with terrestrial measurements. Further information about the studies in which forest stand parameters were estimated from satellite imageries and UAS data can be found in Section 1.

The aim of this thesis is to estimate some critical stand parameters (i.e. location, number, height, crown closure and crown diameter of trees) by using point clouds generated from stereo aerial photos acquired from UASs. Since crown diameter information is very useful to specify tree species, it is of huge importance when producing a forest management plan. Hence, it should be estimated with high accuracy to ensure robust identification of tree species. This thesis proposes a novel polynomial fitting-based methodology to estimate the crown diameters. The PFB methodology utilizes UAS-derived CHMs to perform. Further details about the PFB methodology can be found in Section 2.2.3.2. The performance of the PFB methodology was evaluated by comparing its estimates against reference data, which were obtained from manual delineation of trees. The estimates of the PFB methodology were also compared to those of some widely-used segmentation-based approaches (MSS, MPBS, MRS, SRGS and WS), whose details can be found in Section 1.7.

The results showed that the PFB methodology achieved to detect a huge amount of the trees in the test sites. Its tree detection accuracy was 100%, 97.22% and 97.74% in the test sites 1, 2 and 3, respectively, which makes an overall tree detection accuracy of 98.32% for

all test sites. The overall tree detection accuracy of the WS algorithm was found 98.05% for all test sites. The MRS and MPBS algorithms detected the trees in the test sites with overall accuracies of 96.84% and 95.35%, respectively. The SRGS algorithm presented an overall tree detection accuracy of 88.94%. It can be concluded from the results that the WS, MRS and PFB methodologies are able to detect the trees in highly closed areas. The PFB methodology was also found to be successful in estimating the crown diameters of trees. It outperformed the other methodologies in all test sites. As seen in Table 5, it estimated the crown diameters with RMSEs of 0.92 m, 0.69 m and 0.79 m, in the test sites 1, 2 and 3, respectively. The MRS-based approach estimated the crown diameters with RMSEs of 1.13 m, 0.87 m and 1 m in the test sites 1, 2 and 3, respectively; whereas the WS-based approach presented RMSEs of 1.15 m, 0.9 m and 1.03 m in the test sites 1, 2 and 3, respectively. The SDD and MAE values computed between the estimated and reference crown diameters revealed that the PFB methodology estimated the crown diameters with high accuracies in all test sites. It estimated the crown diameters with MAEs of 0.71 m, 0.53 m and 0.63 m; and with SDDs of 0.82 m, 0.66 m and 0.79 m in the test sites 1, 2 and 3, respectively. The MRS- and WS-based approaches were found to be the other successful ones after the PFB methodology. Comparing the positions of the circles enclosing the estimated and reference tree segments can give some hints about the position accuracy of crown circles. Hence, the positions of the centres of the estimated and reference crown circles were compared with respect to the SDD, MAE and RMSE. The PFB methodology showed its success in this regard too. It surpassed the other approaches in almost all cases in terms of the SDD, MAE and RMSE statistics (see Table 7). The main advantage of the PFB methodology is that it is able to estimate the locations and crown diameters of trees in just a couple of seconds. The biggest disadvantage of the PFB methodology is that it is not a fully-automated process and it uses five parameters to perform. However, defining these parameters is not challenging. It is possible to define these parameters by making a few simple measurements on the orthophotos and CHMs.

The main conclusion drawn from this thesis is that it is possible to estimate stand parameters with accuracies comparable to terrestrial measurements. Making use of remotely-sensed data decreases the time and labour force needed to collect forest inventory, especially in large-scaled areas. This, of course, enables the foresters to renew forest measurements and produce forest management plans in a shorter span of time. The use of low-cost UASs in forest management reduces the expenditure needed to collect forest inventory.

The stand parameter estimation methodologies used in this study were conducted to estimate the physical characteristics of urban trees with mostly moderate density. Stand parameter estimation in denser tree stands would, of course, be more challenging. The use of LiDAR data may be more reasonable in denser forests, since LiDAR point clouds result in multiple returns, which enables more accurate 3D reconstruction of trees.

5. REFERENCES

1. Kadıoğulları, A., İ., Orman Kaynaklarındaki Zamansal Değişimin Uzaktan Algılama ve Coğrafi Bilgi Sistemleri Yardımıyla Ortaya Konulması (İnegöl ve Gümüşhane Devlet Orman İşletmeleri Örneği), Yüksek Lisans Tezi (M.Sc. Thesis), Karadeniz Teknik Üniversitesi, Fen Bilimleri Enstitüsü, Trabzon, 2005.
2. Borucu, S., Orman Kaynaklarındaki Zamansal Değişimin ve Meşcere Parametrelerinin Uzaktan Algılama Teknikleriyle Belirlenmesi (Dereli Orman İşletme Müdürlüğü Örneği), Yüksek Lisans Tezi (M.Sc. Thesis), Karadeniz Teknik Üniversitesi, Fen Bilimleri Enstitüsü, Trabzon, 2014.
3. http://www.environmentforbeginners.com/content/view/52/49/, 2 October 2017.
4. https://www.mnn.com/earth-matters/wilderness-resources/blogs/21-reasons-why-forests-are-important, 2 October 2017.
5. http://www.earthshare.org/2013/07/treebenefits.html, 2 October 2017.
6. www.ogm.gov.tr, 2 October 2017.
7. Yilmaz, V., Serifoglu, C. and Gungor, O., Determining Stand Parameters from UAS-Based Point Clouds, International Society for Photogrammetry and Remote Sensing (ISPRS) Symposium, 2016, Prague, Czech Republic, 413-416.
8. Türkiye Orman Varlığı Kitabı, Orman İdaresi ve Planlama Dairesi Başkanlığı, Orman Genel Müdürlüğü, Orman ve Su İşleri Bakanlığı, 2014.
9. Çil, B., Bazı Meşcere Parametrelerinin Farklı Uydu Görüntüleri Yardımıyla Tahmin Edilmesi: Kelkit ve İğdir Planlama Birimi Örneği, Yüksek Lisans Tezi (M.Sc. Thesis), Karadeniz Teknik Üniversitesi, Fen Bilimleri Enstitüsü, Trabzon, 2014.
10. Fırat, F., Dendrometri, Dördüncü Baskı, Kutulmuş Matbaası, İstanbul Üniversitesi Yayın No 1800, Orman Fakültesi Yayın No 193, İstanbul, 359 s, 1973.
11. Schreuder, H., T., Gregoire, T., G. and Wood, G., B., Sampling Methods for Multiresource Forest Inventory, John Wiley & Sons Inc., USA, 446 s, 1993.
12. Kangas, A., Gove, J., H. and Scott, C., T., Introduction, Forest Inventory Methodology and Applications, Kangas, A., Maltamo, M., (Eds.) Springer, Netherlands, 13-38, 2006.
13. Alkan, O., Meşcere Bazlı Orman Envanterinde Optimal Örnekleme Tasarımı; Sinop-Ayancık Orman İşletme Şefliğinde Bir Uygulama Çalışması, Yüksek Lisans Tezi (M.Sc. Thesis), Süleyman Demirel Üniversitesi, Fen Bilimleri Enstitüsü, 2013.
14. Hyyppä, J., Hyyppä, H., Inkinen, M., Engdahl, M., Linko, S., and Zhu, Y., H., Accuracy comparison of various remote sensing data sources in the retrieval of forest stand attributes, Forest Ecology and Management, 128, 1 (2000) 109-120.
15. Diedershagen, O., Koch, B. and Weinacker, H., Automatic segmentation and characterisation of forest stand parameters using airborne lidar data, multispectral and

fogis data, International Archives of Photogrammetry, Remote Sensing and Spatial Information Sciences, 36 (2004) 208-212.

16. Lu, D., Mausel, P., Brondızio, E. and Moran, E., Relationships between forest stand parameters and Landsat TM spectral responses in the Brazilian Amazon Basin, Forest Ecology and Management, 198, 1 (2004) 149-167.

17. Günlü, A., Sivrikaya, F., Baskent, E., Z., Keles, S., Çakir, G. and Kadiogullari, A., İ., Estimation of stand type parameters and land cover using Landsat-7 ETM image: A case study from Turkey, Sensors, 8, 4 (2008) 2509-2525.

18. Günlü, A., Landsat TM Uydu Görüntüsü Yardımıyla Bazı Meşcere Parametreleri (Gelişim Çağı ve Kapalılık) ve Arazi Kullanım Sınıflarının Belirlenmesi, Kastamonu Üniversitesi Orman Fakültesi Dergisi, 12, 1 (2012) 71-79.

19. Stellingwerf, D., A. and Hussin, Y., A., Measurements and estimations of forest stand parameters using remote sensing, VSP, 1997.

20. Pouliot, D., A., King, D., J., Bell, F., W. and Pitt, D., G., Automated tree crown detection and delineation in high-resolution digital camera imagery of coniferous forest regeneration, Remote Sensing of Environment, 82, 2 (2002) 322-334.

21. Culvenor, D., S., TIDA: an algorithm for the delineation of tree crowns in high spatial resolution remotely sensed imagery, Computers & Geosciences, 28, 1 (2002) 33-44.

22. de Wulf, R., R., Goossens, R., E., de Roover, B., P. and Borry, F., C., Extraction of forest stand parameters from panchromatic and multispectral SPOT-1 data, International Journal of Remote Sensing, 11, 9 (1990) 1571-1588.

23. Cohen, W., B. and Spies, T., A., Estimating structural attributes of Douglas-fir/western hemlock forest stands from Landsat and SPOT imagery, Remote Sensing of Environment, 41, 1 (1992), 1-17.

24. Tokola, T., Pitkänen, J., Partinen, S. and Muinonen, E., Point accuracy of a non-parametric method in estimation of forest characteristics with different satellite materials, International Journal of Remote Sensing, 17, 12 (1996) 2333-2351.

25. Holmgren, J., Joyce, S., Nilsson, M. and Olsson, H., Estimating stem volume and basal area in forest compartments by combining satellite image data with field data, Scandinavian Journal of Forest Research, 15, 1 (2000) 103-111.

26. Astola, H., Bounsaythip, C., Ahola, J., Häme, T., Parmes, E., Sirro, L. and Veikkanen, B., Highforest-forest parameter estimation from high resolution remote sensing data, In Proceedings of the International Society for Photogrammetry and Remote Sensing Twentieth Congress, 2004, 12-23.

27. Sivanpillai, R., Smith, C., T., Srinivasan, R., Messina, M., G. and Wu, X., B., Estimation of managed loblolly pine stand age and density with Landsat ETM+ data, Forest Ecology and Management, 223, 1 (2006) 247-254.

28. Hall, R., J., Skakun, R., S., Arsenault, E., J. and Case, B., S., Modeling forest stand structure attributes using Landsat ETM+ data: Application to mapping of aboveground biomass and stand volume, Forest Ecology and Management, 225, 1 (2006) 378-390.

29. Kayitakire, F., Hamel, C. and Defourny, P., Retrieving forest structure variables based on image texture analysis and IKONOS-2 imagery, Remote Sensing of Environment, 102, 3 (2006) 390-401.

30. Peuhkurinen, J., Maltamo, M., Vesa, L. and Packalén, P., Estimation of forest stand characteristics using spectral histograms derived from an IKONOS satellite image, Photogrammetric Engineering & Remote Sensing, 74, 11 (2008) 1335-1341.

31. Ozdemir, I. and Karnieli, A., Predicting forest structural parameters using the image texture derived from WorldView-2 multispectral imagery in a dryland forest, Israel, International Journal of Applied Earth Observation and Geoinformation, 13, 5 (2011) 701-710.

32. Kilkki, P. and Päivinen, R., Reference sample plots to combine field measurements and satellite data in forest inventory, Department of Forest Mensuration and Management, University of Helsinki, Research Notes, 19, 210-215, 1987.

33. Hagner, O., Computer aided forest stand delineation and inventory based on satellite remote sensing, In Proceedings from SNS/IUFRO Workshop on the Usability of Remote Sensing for Forest Inventory and Planning, 1990, Swedish University of Agricultural Sciences, Remote Sensing Laboratory, Umeå, 26-28.

34. Reese, H., Nilsson, M., Sandström, P. and Olsson, H., Applications using estimates of forest parameters derived from satellite and forest inventory data, Computers and Electronics in Agriculture, 37, 1 (2002) 37-55.

35. Couteron, P., Pelissier, R., Nicolini, E., A. and Paget, D., Predicting tropical forest stand structure parameters from Fourier transform of very high-resolution remotely sensed canopy images, Journal of Applied Ecology, 42, 6 (2005) 1121-1128.

36. Wolter, P., T., Townsend, P., A. and Sturtevant, B., R., Estimation of forest structural parameters using 5 and 10 meter SPOT-5 satellite data, Remote Sensing of Environment, 113, 9 (2009) 2019-2036.

37. Günlü, A., Ercanlı, İ., Sönmez, T. and Başkent, E., Z., Prediction of Some Stand Parameters using Pan-Sharpened IKONOS Satellite Image, European Journal of Remote Sensing, 47 (2014) 329-342.

38. Günlü, A., Ercanlı, İ., Keleş, S. and Anlar, H., C., Modelling of stand volume and tree density using Spot-4 satellite image: a case study in Devrez planning unit, International Journal of Global Warming, 7, 4 (2015) 454-465.

39. Kwak, D., A., Lee, W., K., Lee, J., H., Biging, G., S. and Gong, P., Detection of individual trees and estimation of tree height using LiDAR data, Journal of Forest Research, 12, 6 (2007) 425-434.

40. Rahman, M., Z., A. and Gorte, B., G., H., Tree crown delineation from high resolution airborne lidar based on densities of high points, InProceedings of the ISPRS Workshop Laserscanning, 1-2 September 2009, France, XXXVIII (3/W8).

41. Suárez, J., C., Ontiveros, C., Smith, S. and Snape, S., Use of airborne LiDAR and aerial photography in the estimation of individual tree heights in forestry, Computers & Geosciences, 31, 2 (2005) 253-262.

42. Li, W., Guo, Q., Jakubowski, M., K. and Kelly, M., A new method for segmenting individual trees from the lidar point cloud, Photogrammetric Engineering & Remote Sensing, 78, 1 (2012) 75-84.

43. Liu, J., Shen, J., Zhao, R. and Xu, S. Extraction of individual tree crowns from airborne LiDAR data in human settlements, Mathematical and Computer Modelling, 58, 3 (2013) 524-535.

44. Morsdorf, F., Meier, E., Allgöwer, B. and Nüesch, D. Clustering in airborne laser scanning raw data for segmentation of single trees, International Archives of the Photogrammetry, Remote Sensing and Spatial Information Sciences, 34 (2003).

45. Gupta, S., Weinacker, H. and Koch, B., Comparative analysis of clustering-based approaches for 3-D single tree detection using airborne fullwave lidar data, Remote Sensing, 2, 4 (2010) 968-989.

46. Lee, H., Slatton, K., C., Roth, B., E. and Cropper Jr, W., P., Adaptive clustering of airborne LiDAR data to segment individual tree crowns in managed pine forests, International Journal of Remote Sensing, 31, 1 (2010) 117-139.

47. Pascual, C., García-Abril, A., García-Montero, L., G., Martín-Fernández, S. and Cohen, W., B., Object-based semi-automatic approach for forest structure characterization using lidar data in heterogeneous Pinus sylvestris stands, Forest Ecology and Management, 255, 11 (2008) 3677-3685.

48. Reitberger, J., Krzystek, P. and Stilla, U., Combined tree segmentation and stem detection using full waveform lidar data, International Archives of Photogrammetry, Remote Sensing and Spatial Information Sciences, 36 (2007) 332-337.

49. Díaz-Varela, R., A., de la Rosa, R., León, L. and Zarco-Tejada, P., J., High-Resolution Airborne UAV Imagery to Assess Olive Tree Crown Parameters Using 3D Photo Reconstruction: Application in Breeding Trials, Remote Sensing, 7, 4 (2015) 4213-4232.

50. Ismail, S., Peterson, L., D., Hinkle, J., D. and Friedman, E., Applications of deployable telescopes for earth-observing lidar, In Proceedings of the ESTO earth science technology conference, College Park, 2005, pp. 27-28.

51. Kattenborn, T., Sperlich, M., Bataua, K. and Koch, B., Automatic Single Palm Tree Detection In Plantations Using UAV-Based Photogrammetric Point Clouds, International Archives of the Photogrammetry, Remote Sensing and Spatial Information Sciences, 2014, XL-3, 5-7 September, Zurich, Switzerland.

52. Sperlich, M., Kattenborn, T., Koch, B. and Kattenborn, G., Potential of Unmanned Aerial Vehicle Based Photogrammetric Point Clouds for Automatic Single Tree Detection, In Gemeinsame Tagung 2014 der DGfK, 2014, der DGPF, der GfGI und des GiN (DGPF Tagungsband 23/2014).

53. https://fennerschool-associated.anu.edu.au/mensuration/number.htm, 2 October 2017.

54. McCombs, J., W., Roberts, S., D. and Evans, D., L., Influence of fusing lidar and multispectral imagery on remotely sensed estimates of stand density and mean tree height in a managed loblolly pine plantation, Forest Science, 49, 3 (2003) 457-466.

55. Yılmaz, V., Güngör, O. and Kadıoğulları, A., İ., Görüntü İşleme Teknikleri ile Ağaçların Boy, Tepe Çapı ve Tepe Hacimlerinin Belirlenmesi, Türkiye Uluslararası Fotogrametri ve Uzaktan Algılama Birliği Sempozyumu, 2015, Konya, Türkiye.

56. https://fennerschool-associated.anu.edu.au/mensuration/s_height.htm, 2 October 2017.

57. Nilsson, M., Estimation of tree heights and stand volume using an airborne lidar system, Remote Sensing of Environment, 56, 1 (1996) 1-7.

58. Naesset, E., Determination of mean tree height of forest stands using airborne laser scanner data, ISPRS Journal of Photogrammetry and Remote Sensing, 52, 2 (1997) 49-56.

59. Næsset, E. and Økland, T., Estimating tree height and tree crown properties using airborne scanning laser in a boreal nature reserve, Remote Sensing of Environment, 79, 1 (2002) 105-115.

60. Holmgren, J., Prediction of tree height, basal area and stem volume in forest stands using airborne laser scanning, Scandinavian Journal of Forest Research, 19, 6 (2004) 543-553.

61. Olofsson, K. and Holmgren, J., Forest stand delineation from lidar point-clouds using local maxima of the crown height model and region merging of the corresponding Voronoi cells, Remote Sensing Letters, 5, 3 (2014) 268-276.

62. http://fennerschool-associated.anu.edu.au/mensuration/BrackandWood1998/CROWN.HTM, 2 October 2017.

63. Anonim, Ana Ağaç Türlerimizde Özel Gençleştirme Sürelerinin Uzatılması ve Değer Artışına Gidilmesine Ait 177-A/EK:7 Sayılı Tebliği, T.C. Orman Bakanlığı, Orman Genel Müdürlüğü Silvikültür Dairesi Başkanlığı, 1996, Ankara.

64. Özen, F. ve Türk, M., Ormaniçi merada ağaç sıklığının bitki örtüsü üzerine etkileri, Süleyman Demirel Üniversitesi Orman Fakültesi Dergisi, 15, 1 (2014) 9-14.

65. Mo, L., He, Y., Liu, Y., Zhao, J., Tang, S., J., Li, X., Y. and Dai, G., Canopy closure estimates with GreenOrbs: sustainable sensing in the forest. In Proceedings of the 7th ACM Conference on Embedded Networked Sensor Systems, 2009, 99-112.

66. Fiala, A., C., Garman, S., L. and Gray, A., N., Comparison of five canopy cover estimation techniques in the western Oregon Cascades, Forest Ecology and Management, 232, 1 (2006) 188-197.

67. Korhonen, L., Korhonen, K., T., Rautiainen, M. and Stenberg, P., Estimation of forest canopy cover: a comparison of field measurement techniques, Silva Fennica, 40, 4 (2006) 577-588.

68. Huang, C., Yang, L., Wylie, B., K. and Homer, C., A strategy for estimating tree canopy density using Landsat 7 ETM+ and high resolution images over large areas, In proceedings of the Third International Conference on Geospatial Information in Agriculture and Forestry, 5-7 November 2001, Colorado, Denver.

69. Hansen, M., C., DeFries, R., S., Townshend, J., R., G., Carroll, M., Dimiceli, C. and Sohlberg, R., A., Global percent tree cover at a spatial resolution of 500 meters: First

results of the MODIS vegetation continuous fields algorithm, Earth Interactions, 7, 10 (2003) 1-15.

70. Hansen, M., C. and DeFries, R., S., Detecting long-term global forest change using continuous fields of tree-cover maps from 8-km advanced very high resolution radiometer (AVHRR) data for the years 1982–99, Ecosystems, 7, 7 (2004) 695-716.

71. Hansen, M., C., Townshend, J., R., DeFries, R., S. and Carroll, M., Estimation of tree cover using MODIS data at global, continental and regional/local scales, International Journal of Remote Sensing, 26, 19 (2005) 4359-4380.

72. Rokhmatuloh, R., Nitto, D., Al-Bilbisi, H. and Tateishi, R., Percent Tree Cover Estimation Using Regression Tree Method: A Case Study of Africa with Very-High Resolution QuickBird Images as Training Data, In Geoscience and Remote Sensing Symposium Proceedings 2005 (IGARSS'05), 3 (2005), 2157-2160.

73. Rokhmatuloh, R., Al-Bilbisi, H., Arihara, K., Kobayashi, T., Nitto, D., Erdene, B., Hirabayashi, K., Javzandulam, T., A., Lee, S., A., Migita, E., Soliman, N., Ouma, Y., Aslam, M. and Tateishi, R., Application of Regression Tree Method for Estimating Percent Tree Cover of Asia with QuickBird Images as Training Data. In the 11th CEReS International Symposium on Remote Sensing, 2005, Chiba University, Chiba, Japan.

74. Tunay, M. ve Ateşoğlu, A., Uydu Görüntüleri Kullanılarak Meşcere Kapalılık Derecesi Haritalanması, 4. Coğrafi Bilgi Sistemleri Bilişim Günleri, 13–16 Eylül 2006, Fatih Üniversitesi, İstanbul, Türkiye.

75. Meydan, H., S., T. ve Berberoğlu, S., Yukari Seyhan Havzası' nda Uzaktan Algılama Yöntemleri ile Arazi Örtüsünün Sınıflandırılması ve Bazı Orman Meşcerelerinde Verimliliğin Modellenmesi, Çanakkale Üniversitesi Fen Bilimleri Enstitüsü, 18, 1 (2008).

76. Günlü, A., Keleş, S., Kadıoğulları, A., İ. ve Başkent, E., Z., Landsat 7 ETM+ Uydu Görüntüsü Yardımıyla Arazi Kullanımı, Meşcere Gelişim Çağı ve Meşcere Kapalılığın Tahmin Edilmesi; Kastamonu-Kızılcasu İşletme Şefliği Örneği, 1. Ulusal Akdeniz Orman ve Çevre Sempozyumu, 26-28 Ekim 2011, Kahramanmaraş, Türkiye, 660-667.

77. Popescu, S., C., Wynne, R., H. and Nelson, R., F., Measuring individual tree crown diameter with lidar and assessing its influence on estimating forest volume and biomass, Canadian Journal of Remote Sensing, 29, 5 (2003) 564-577.

78. Falkowski, M., J., Smith, A., M., Hudak, A., T., Gessler, P., E., Vierling, L., A. and Crookston, N., L., Automated estimation of individual conifer tree height and crown diameter via two-dimensional spatial wavelet analysis of lidar data, Canadian Journal of Remote Sensing, 32, 2 (2006) 153-161.

79. Popescu, S., C. and Zhao, K., A voxel-based lidar method for estimating crown base height for deciduous and pine trees, Remote Sensing of Environment, 112, 3 (2008) 767-781.

80. Ke, Y. and Quackenbush, L., J., Individual tree crown detection and delineation from high spatial resolution imagery using active contour and hill-climbing methods, In

Proceedings of 2009 ASPRS Annual Conference, American Society of Photogrammetry and Remote Sensing, 9-13 March 2009, Baltimore, Maryland.

81. Wu, B., Yu, B., Yue, W., Shu, S., Tan, W., Hu, C., Huang, Y., Wu, J. and Liu, H., A voxel-based method for automated identification and morphological parameters estimation of individual street trees from mobile laser scanning data, Remote Sensing, 5, 2 (2013) 584-611.

82. Panagiotidis, D., Abdollahnejad, A., Surový, P. and Chiteculo, V., Determining tree height and crown diameter from high-resolution UAV imagery, International Journal of Remote Sensing, 38, 8-10 (2017), 2392-2410.

83. Özgün, M., Landsat TM Uydu Görüntüsü Yardımıyla Bazı Meşcere Parametrelerinin Tahmin Edilmesi (Yapraklı Orman İşletme Şefliği Örneği), Yüksek Lisans Tezi (M.Sc. Thesis), Çankırı Karatekin Üniversitesi, Fen Bilimleri Enstitüsü, 2014.

84. Ün, C., İstanbul ili orman kaynaklarında meydana gelen zamansal değişimin uzaktan algılama ve CBS ile belirlenmesi, Yüksek Lisans Tezi (M.Sc. Thesis), Karadeniz Teknik Üniversitesi, Fen Bilimleri Enstitüsü, Trabzon, 2006.

85. Popescu, S., C., Wynne, R., H. and Nelson, R., F., Estimating plot-level tree heights with lidar: local filtering with a canopy-height based variable window size, Computers and Electronics in Agriculture, 37, 1 (2002) 71-95.

86. Pitkänen, J., Maltamo, M., Hyyppä, J. and Yu, X., Adaptive methods for individual tree detection on airborne laser based canopy height model, International Archives of Photogrammetry, Remote Sensing and Spatial Information Sciences, 36, 8 (2004) 187-191.

87. Popescu, S., C., Estimating biomass of individual pine trees using airborne lidar, Biomass and Bioenergy, 31, 9 (2007) 646-655.

88. Zhao, K. and Popescu, S., Hierarchical watershed segmentation of canopy height model for multi-scale forest inventory, ISPRS Workshop on Laser Scanning and SilviLaser 2007, 2007, Espoo, Finland, 436-442.

89. Gaulton, R. and Malthus, T., J., LiDAR mapping of canopy gaps in continuous cover forests: A comparison of canopy height model and point cloud based techniques, International Journal of Remote Sensing, 31, 5 (2010) 1193-1211.

90. Meng, X., Wang, L., Silván-Cárdenas, J., L. and Currit, N., A multi-directional ground filtering algorithm for airborne LIDAR, ISPRS Journal of Photogrammetry and Remote Sensing, 64 (2009) 117–124.

91. Serifoglu Yilmaz, C. and Gungor, O., Comparison of the performances of ground filtering algorithms and DTM generation from a UAV-based point cloud, Geocarto International, 2016, pp. 1-16.

92. Kilian, J., Haala, N. and Englich, M., Capture and evaluation of airborne laser scanner data, International Archives of Photogrammetry and Remote Sensing, 31 (1996) 383–388.

93. Vosselman, G., Slope based filtering of laser altimetry data, International Archives of Photogrammetry and Remote Sensing, 33 (2000) 935–942.

94. Roggero, M., Airborne Laser Scanning: Clustering in Raw Data, International Archives of Photogrammetry and Remote Sensing, 34 (2001) 227–232.

95. Sithole, G., Filtering of laser altimetry data using a slope adaptive filter, International Archives of Photogrammetry, Remote Sensing and Spatial Information Sciences, 34 (2001) 203–210.

96. Zhang, K., Chen, S., C., Whitman, D., Shyu, M., L., Yan, J. and Zhang, C., A progressive morphological filter for removing nonground measurements from airborne LIDAR data, IEEE Transactions on Geoscience and Remote Sensing, 41 (2003) 872–882.

97. Kim, K. and Shan, J., Adaptive morphological filtering for DEM generation, IEEE International Geoscience and Remote Sensing Symposium (IGARSS) 2011, 24-29 July 2011, Vancouver, 2539–2542.

98. Zhang, J. and Lin, X., Filtering airborne LiDAR data by embedding smoothness-constrained segmentation in progressive TIN densification, ISPRS Journal of Photogrammetry and Remote Sensing, 81 (2013) 44-59.

99. Tóvári, D. and Pfeifer, N., Segmentation based robust interpolation-a new approach to laser data filtering, International Archives of Photogrammetry, Remote Sensing and Spatial Information Sciences, 36 (2005) 79–84.

100. Wang, C., K. and Tseng, Y., H., DEM generation from airborne LIDAR data by an adaptive dual-directional slope filter, ISPRS Commission VII Mid-Term Symposium '100 Years ISPRS – Advancing Remote Sensing Science', 2010, 38, 628–632.

101. Kraus, K. and Pfeifer, N., Determination of terrain models in wooded areas with airborne laser scanner data, ISPRS Journal of Photogrammetry and Remote Sensing, 53 (1998) 193–203.

102. Evans, J., S. and Hudak, A., T., A multiscale curvature algorithm for classifying discrete return LiDAR in forested environments, IEEE Transactions on Geoscience and Remote Sensing, 45 (2007) 1029–1038.

103. Kobler, A., Pfeifer, N., Ogrinc, P., Todorovski, L., Oštir, K. and Džeroski, S., Repetitive interpolation: a robust algorithm for DTM generation from aerial laser scanner data in forested terrain, Remote Sensing of Environment, 108 (2007) 9–23.

104. Axelsson, P., DEM generation from laser scanner data using adaptive TIN models, International Archives of Photogrammetry and Remote Sensing, 33, B4/1 (2000), 110–117.

105. Zhang, K. and Cui, Z., Airborne LIDAR Data Processing and Analysis Tools, ALDPAT 1.0. Miami, FL, USA: National Center for Airborne Laser Mapping, 81 pp, 2007.

106. Serifoglu, C., Gungor, O. and Yilmaz, V., Performance Evaluation of Different Ground Filtering Algorithms for UAV-Based Point Clouds, International Archives of the Photogrammetry, Remote Sensing and Spatial Information Sciences, 41 (2016).

107. Sithole, G. and Vosselman, G., Experimental comparison of filter algorithms for bare-earth extraction from airborne laser scanning point clouds, ISPRS Journal of Photogrammetry and Remote Sensing, 59 (2004) 85–101.

108. Zhang, K. and Whitman, D., Comparison of three algorithms for filtering airborne LiDAR data, Photogrammetric Engineering and Remote Sensing, 7 (2005) 313–324.

109. Sithole, G. and Vosselman, G., Comparison of filtering algorithms, In Proceedings of the ISPRS working group III/3 workshop, 2003, 71-78.

110. Sithole, G. and Vosselman, G., Filtering of airborne laser scanner data based on segmented point clouds, International Archives of Photogrammetry, Remote Sensing and Spatial Information Sciences, 36 (2005).

111. Montealegre, A., L., Lamelas, M., T. and de la Riva, J., A comparison of open-source LiDAR filtering algorithms in a Mediterranean forest environment, IEEE Journal of Selected Topics in Applied Earth Observations and Remote Sensing, 8 (2015) 4072–4085.

112. Yilmaz, V., Konakoglu, B., Serifoglu, C., Gungor, O. and Gökalp, E. Image classification-based ground filtering of point clouds extracted from UAV-based aerial photos, Geocarto International (2016), 1-11.

113. Haris, K., Efstratiadis, S., N., Maglaveras, N. and Katsaggelos, A., K., Hybrid image segmentation using watersheds and fast region merging, IEEE Transactions on Image Processing, 7, 12 (1998) 1684-1699.

114. Meinel, G. and Neubert, M., A comparison of segmentation programs for high resolution remote sensing data, International Archives of Photogrammetry and Remote Sensing, 35 (2004) 1097-1105.

115. Hay, G., J., Castilla, G., Wulder, M., A. and Ruiz, J., R., An automated object-based approach for the multiscale image segmentation of forest scenes, International Journal of Applied Earth Observation and Geoinformation, 7, 4 (2005) 339-359.

116. Arvor, D., Durieux, L., Andrés, S. and Laporte, M., A., Advances in geographic object-based image analysis with ontologies: A review of main contributions and limitations from a remote sensing perspective, ISPRS Journal of Photogrammetry and Remote Sensing, 82 (2013) 125-137.

117. Belgiu, M. and Drăguţ, L., Comparing supervised and unsupervised multiresolution segmentation approaches for extracting buildings from very high resolution imagery, ISPRS Journal of Photogrammetry and Remote Sensing, 96 (2014) 67-75.

118. Fukunaga, K. and Hostetler, L., The estimation of the gradient of a density function, with applications in pattern recognition, IEEE Transactions on Information Theory, 21, 1 (1975) 32-40.

119. Cheng, Y., Mean shift, mode seeking, and clustering, IEEE Transactions on Pattern Analysis and Machine Intelligence, 17, 8 (1995) 790-799.

120. Zheng, L., Zhang, J. and Wang, Q., Mean-shift-based color segmentation of images containing green vegetation, Computers and Electronics in Agriculture, 65, 1 (2009) 93-98.

121. Comaniciu, D. and Meer, P., Mean shift: A robust approach toward feature space analysis, IEEE Transactions on Pattern Analysis and Machine Intelligence, 24 (5) (2002) 603-619.

122. Lee, I., C., Wu, B. and Li, R., Shoreline extraction from the integration of lidar point cloud data and aerial orthophotos using mean shift segmentation, In Proceedings of 2009 ASPRS Annual Conference, American Society of Photogrammetry and Remote Sensing, 2009, 1-7.

123. Zheng, L., Shi, D. and Zhang, J., Segmentation of green vegetation of crop canopy images based on mean shift and fisher linear discriminant, Pattern Recognition Letters, 31, 9 (2010) 920-925.

124. Ming, D., Ci, T., Cai, H., Li, L., Qiao, C. and Du, J., Semivariogram-based spatial bandwidth selection for remote sensing image segmentation with mean-shift algorithm, IEEE Geoscience and Remote Sensing Letters, 9, 5 (2012) 813-817.

125. Michel, J., Youssefi, D. and Grizonnet, M., Stable mean-shift algorithm and its application to the segmentation of arbitrarily large remote sensing images, IEEE Transactions on Geoscience and Remote Sensing, 53, 2 (2015) 952-964.

126. Pesaresi, M. and Benediktsson, J., A., A new approach for the morphological segmentation of high-resolution satellite imagery, IEEE Transactions on Geoscience and Remote Sensing, 39, 2 (2001) 309-320.

127. Aytekin, Ö. and Ulusoy, İ., Automatic segmentation of VHR images using type information of local structures acquired by mathematical morphology, Pattern Recognition Letters, 32, 13 (2011) 1618-1625.

128. Benediktsson, J., A., Palmason, J., A. and Sveinsson, J., R., Classification of hyperspectral data from urban areas based on extended morphological profiles, IEEE Transactions on Geoscience and Remote Sensing, 43, 3 (2005) 480-491.

129. Akçay, H., G. and Aksoy, S., Automatic detection of geospatial objects using multiple hierarchical segmentations, IEEE Transactions on Geoscience and Remote Sensing, 46, 7 (2008) 2097-2111.

130. Li, P., Hu, H. and Guo, J., Segmentation of high-resolution multispectral image based on extended morphological profiles, IEEE International Geoscience and Remote Sensing Symposium (IGARSS), 2007, 1481-1484.

131. Benz, U., C., Hofmann, P., Willhauck, G., Lingenfelder, I. and Heynen, M., Multi-resolution, object-oriented fuzzy analysis of remote sensing data for GIS-ready information, ISPRS Journal of Photogrammetry and Remote Sensing, 58, 3 (2004) 239-258.

132. eCognition Developer user guide.

133. Kavzoglu, T. and Yildiz, M., Parameter-based performance analysis of object-based image analysis using aerial and QuikBird-2 images, ISPRS Annals of the Photogrammetry, Remote Sensing and Spatial Information Sciences, 2, 7 (2014) 31-37.

134. Lowe, S., H. and Guo, X., Detecting an Optimal Scale Parameter in Object-Oriented Classification, IEEE Journal of Selected Topics in Applied Earth Observations and Remote Sensing, 4, 4 (2011) 890-895.

135. Li, C. and Shao, G., Object-oriented classification of land use/cover using digital aerial orthophotography, International Journal of Remote Sensing, 33, 4 (2012) 922-938.

136. Elmqvist, B., Ardö, J. and Olsson, L., Land use studies in drylands: an evaluation of object-oriented classification of very high resolution panchromatic imagery, International Journal of Remote Sensing, 29, 24 (2008) 7129-7140.

137. Platt, R., V. and Rapoza, L., An Evaluation of an Object-Oriented Paradigm for Land Use/Land Cover Classification, The Professional Geographer, 60, 1 (2008) 87-100.

138. Baatz, M., Benz, U., Dehghani, S., Heynen, M., Höltje, A., Hofmann, P., Lingenfelder, I., Mimler, M., Sohlbach, M., Weber, M. and Willhauck, G., eCognition Professional User Guide, version 4.0, Definiens Imaging GmbH, Munchen, Germany, 2004.

139. Hofmann, P., Strobl, J., Blaschke, T. and Kux, H., Detecting informal settlements from Quickbird data in Rio de Janeiro using an object based approach, Object-Based Image Analysis, Springer Berlin Heidelberg, 2008, 531-553.

140. Adams, R. and Bischof, L., Seeded region growing, IEEE Transactions on Pattern Analysis and Machine Intelligence, 16, 6 (1994) 641–647.

141. Hirschmugl, M., Ofner, M., Raggam, J. and Schardt, M., Single tree detection in very high resolution remote sensing data, Remote Sensing of Environment, 110, 4 (2007) 533-544.

142. Erikson, M., Segmentation and Classification of Individual Tree Crowns in High Spatial Resolution Aerial Images, Doctoral dissertation, Thèse de doctorat, Swedish University of Agricultural Sciences Uppsala, Sweden, 2004.

143. Pitkänen, J., Individual tree detection in digital aerial images by combining locally adaptive binarization and local maxima methods, Canadian Journal of Forest Research, 31, 5 (2001) 832-844.

144. Wulder, M., A., White, J., C., Niemann, K., O. and Nelson, T., Comparison of airborne and satellite high spatial resolution data for the identification of individual trees with local maxima filtering, International Journal of Remote Sensing, 25, 11 (2004) 2225-2232.

145. Dralle, K. and Rudemo, M., Stem number estimation by kernel smoothing of aerial photos, Canadian Journal of Forest Research, 26, 7 (1996) 1228-1236.

146. Lari, Z. and Ebadi, H., Automated building extraction from high-resolution satellite imagery using spectral and structural information based on artificial neural networks, ISPRS Hannover Workshop, 2007.

147. Wang, Z., Jensen, J., R. and Im, J., An automatic region-based image segmentation algorithm for remote sensing applications, Environmental Modelling & Software, 25, 10 (2010) 1149-1165.

148. McGuinness, K. and O'connor, N., E., A comparative evaluation of interactive segmentation algorithms, Pattern Recognition, 43, 2 (2010) 434-444.

149. Bechtel, B., Ringeler, A. and Böhner, J., Segmentation for Object Extraction of Trees using MATLAB and SAGA, SAGA–Seconds Out, Hamburger Beiträge Zur Physischen Geographie Und Landschaftsökologie, Univ. Hamburg, Inst. für Geographie, 2008, 1-12.

150. Böhner, J., Selige, T. and Ringeler, A., Image segmentation using representativeness analysis and region growing, SAGA–Analysis and Modelling Applications; Gottinger Geographischne Abhandlungen; Boehner, J., McCloy, K., R., Strobl, J., (Eds.) 2006, 29-38.

151. Beucher, S. and Lantuéjoul, C., Use of watersheds in contour detection. In International Workshop on Image Processing: Real-time Edge and Motion Detection/Estimation, 1979, Rennes, France.

152. Meyer, F. and Beucher, S., Morphological segmentation, Journal of Visual Communication and Image Representation, 1, 1 (1990) 21-46.

153. Tarabalka, Y., Chanussot, J. and Benediktsson, J., A., Segmentation and classification of hyperspectral images using watershed transformation, Pattern Recognition, 43, 7 (2010) 2367-2379.

154. Saarinen, K., Color image segmentation by a watershed algorithm and region adjacency graph processing, IEEE International Conference on Image Processing (ICIP) 1994, 1994, 3, 1021-1025.

155. Tarabalka, Y., Chanussot, J., Benediktsson, J., A., Angulo, J. and Fauvel, M., Segmentation and classification of hyperspectral data using watershed, IEEE International Geoscience and Remote Sensing Symposium (IGARSS) 2008, 2008, 3.

156. Parvati, K., Rao, P. and Mariya Das, M., Image segmentation using gray-scale morphology and marker-controlled watershed transformation, Discrete Dynamics in Nature and Society, 2008.

157. Shafarenko, L., Petrou, M. and Kittler, J., Automatic watershed segmentation of randomly textured color images, IEEE Transactions on Image Processing, 6, 11 (1997) 1530-1544.

158. Bala, A., An Improved watershed image segmentation technique using MATLAB, International Journal of Scientific & Engineering Research, 3, 6 (2012) 1-4.

159. Gauch, J., M., Image segmentation and analysis via multiscale gradient watershed hierarchies, IEEE Transactions on Image Processing, 8, 1 (1999) 69-79.

160. Rafael Gonzalez, C. and Woods, R., Digital Image Processing, Pearson Education, 2002.

161. Lucieer, A., de Jong, S., M. and Turner, D., Mapping landslide displacements using Structure from Motion (SfM) and image correlation of multi-temporal UAV photography, Progress in Physical Geography, 38, 1 (2014) 97-116.

162. Szeliski, R., Computer vision: algorithms and applications, Springer Science & Business Media, 2010.

163. De Reu, J., Plets, G., Verhoeven, G., De Smedt, P., Bats, M., Cherretté, B., De Maeyer, W., Deconynck, J., Herremans, D., Laloo, P., Meirvenne, M., C. and De Clercq, W., Towards a three-dimensional cost-effective registration of the archaeological heritage, Journal of Archaeological Science, 40, 2 (2013) 1108-1121.

164. Verhoeven, G., Taking computer vision aloft–archaeological three-dimensional reconstructions from aerial photographs with photoscan, Archaeological Prospection, 18, 1 (2011) 67-73.

165. Turner, D., Lucieer, A. Wallace, L., Direct georeferencing of ultrahigh-resolution UAV imagery, IEEE Transactions on Geoscience and Remote Sensing, 52, 5 (2014) 2738-2745.

166. Agisoft Photoscan Professional User Manual 2016.

167. Axelsson, P., Processing of laser scanner data—Algorithms and applications, ISPRS Journal of Photogrammetry and Remote Sensing, 54, 2–3 (1999) 138– 147.

168. Congalton, R., G. and Green, K., Assessing the accuracy of remotely sensed data: principles and practices, Boca Raton, FL: Lewis, 1999.

169. Akar, Ö. and Güngör, O., Integrating multiple texture methods and NDVI to the random forest classification algorithm to detect tea and hazelnut plantation areas in northeast Turkey, International Journal of Remote Sensing, 36 (2015) 442–464.

170. https://www5.djicdn.com/assets/images/products/phantom-3-pro/index/phantom-3-pro-v2@2x-f5e6a62b37e6acd37a375f764ab2b6d9.jpg, 3 October 2017.

171. Chehata, N., Orny, C., Boukir, S., Guyon, D. and Wigneron, J., P., Object-based change detection in wind storm-damaged forest using high-resolution multispectral images, International Journal of Remote Sensing, 35, 13 (2014) 4758-4777.

172. Kim, M. and Madden, M., Determination of optimal scale parameter for alliance-level forest classification of multispectral IKONOS images, In Proceedings of the 1st International Conference on Object-based Image Analysis (OBIA), 2006, Salzburg University, Austria.

173. Tian, J. and Chen, D., M., Optimization in multi-scale segmentation of high-resolution satellite images for artificial feature recognition, International Journal of Remote Sensing, 28, 20 (2007) 4625-4644.

174. https://itk.org/ITK/applications/WatershedSegmentationExample.html, 27 October 2017.

175. Shrestha, R. and Wynne, R., H., Estimating biophysical parameters of individual trees in an urban environment using small footprint discrete-return imaging lidar, Remote Sensing, 4, 2 (2012) 484-508.

176. Lee, J., H., Ko, Y. and McPherson, E., G., The feasibility of remotely sensed data to estimate urban tree dimensions and biomass, Urban Forestry & Urban Greening, 16 (2016) 208-220.

177. Yilmaz, V., Yilmaz, S., C., Tasci, L. and Gungor, O., Determination of Tree Crown Diameters with Segmentation of a UAS-Based Canopy Height Model, IPSI BGD Transactions on Internet Research, 13, 2 (2017).

178. Schreyer, J., Tigges, J., Lakes, T. and Churkina, G., Using airborne LiDAR and QuickBird data for modelling urban tree carbon storage and its distribution—A case study of Berlin, Remote Sensing, 6, 11 (2014) 10636-10655.

179. Alonzo, M., Bookhagen, B., McFadden, J., P., Sun, A. and Roberts, D., A., Mapping urban forest leaf area index with airborne lidar using penetration metrics and allometry, Remote Sensing of Environment, 162 (2015) 141-153.

180. Alonzo, M., McFadden, J., P., Nowak, D., J. and Roberts, D., A., Mapping urban forest structure and function using hyperspectral imagery and lidar data, Urban Forestry & Urban Greening, 17 (2016) 135-147.

181. Zhang, C., Urban Forest Inventory Using Airborne Lidar Data and Hyperspectral Imagery, PhD Thesis, Geospatial Information Sciences, The University of Texas, 2010.

182. Fernández-Sarría, A., Velázquez-Martí, B., Sajdak, M., Martínez, L. and Estornell, J., Residual biomass calculation from individual tree architecture using terrestrial laser scanner and ground-level measurements, Computers and Electronics in Agriculture, 93 (2013) 90-97.

183. Lin, Y., Holopainen, M., Kankare, V. and Hyyppä, J., Validation of mobile laser scanning for understory tree characterization in urban forest, IEEE Journal of Selected Topics in Applied Earth Observations and Remote Sensing, 7, 7 (2014) 3167-3173.

184. Pokharel, H., P., Methods for Estimating Individual Tree Crown Volume Using LIDAR Data, Master Thesis, International Institute for Geo-information Science and earth Observation, Enschede, The Netherlands, 2008.

185. Chen, X., Estimation of Carbon Storage in Urban Trees Using Multispectral Airborne Laser Scanning Data, Master's thesis, University of Waterloo, 2016.

186. Wang, S., Urban Roadside Tree Inventory Using a Mobile Laser Scanning System, Master's thesis, University of Waterloo, 2016.

187. Hyyppä, J., Hyyppä, H., Litkey, P., Yu, X., Haggrén, H., Rönnholm, P., Pyysalo, U., Pitkänen, J. and Maltamo, M., Algorithms and methods of airborne laser scanning for forest measurements, International Archives of Photogrammetry, Remote Sensing and Spatial Information Sciences, 36, 8 (2004) 82-89.

188. Kaartinen, H., Hyyppä, J., Yu, X., Vastaranta, M., Hyyppä, H., Kukko, A., Holopainen, M., Heipke, C., Hirschmugl, M., Morsdorf, F., Næsset, E., Pitkänen, J., Popescu, S., Solberg, S., Wolf, B., M. and Wu, J., C., An international comparison of individual tree detection and extraction using airborne laser scanning, Remote Sensing, 4, 4 (2012) 950-974.

189. Akaike, H., Information theory and an extension of the maximum likelihood principle, in Petrov, B., N. and Caski, F., (Eds.) 2nd International Symposium on Information Theory, 1973, Budapest: Akadémiai Kiadó, 267–281.

190. http://www.biomecardio.com/matlab/polydeg.html, 3 October 2017.

191. Leckie, D., Gougeon, F., Hill, D., Quinn, R., Armstrong, L. and Shreenan, R., Combined high-density lidar and multispectral imagery for individual tree crown analysis, Canadian Journal of Remote Sensing, 29, 5 (2003) 633-649.

192. Wang, L., Gong, P. and Biging, G., S., Individual tree-crown delineation and treetop detection in high-spatial-resolution aerial imagery, Photogrammetric Engineering and Remote Sensing, 70, 3 (2004) 351-357.

193. Leckie, D., G., Gougeon, F., A., Tinis, S., Nelson, T., Burnett, C., N. and Paradine, D., Automated tree recognition in old growth conifer stands with high resolution digital imagery, Remote Sensing of Environment, 94, 3 (2005) 311-326.

194. Chen, Q., Baldocchi, D., Gong, P. and Kelly, M., Isolating individual trees in a savanna woodland using small footprint lidar data, Photogrammetric Engineering and Remote Sensing, 72, 8 (2006) 923-932.

195. Srestasathiern, P. and Rakwatin, P., Oil palm tree detection with high resolution multi-spectral satellite imagery, Remote Sensing, 6, 10 (2014) 9749-9774.

196. Liu, T., Yuan, Z., Sun, J., Wang, J., Zheng, N., Tang, X. and Shum, H., Y., Learning to detect a salient object, IEEE Transactions on Pattern Analysis and Machine Intelligence, 33, 2 (2011) 353-367.

197. Rosin, P., L., A simple method for detecting salient regions, Pattern Recognition, 42, 11 (2009) 2363-2371.

198. Marchesotti, L., Cifarelli, C. and Csurka, G., A framework for visual saliency detection with applications to image thumbnailing, IEEE 12th International Conference on Computer Vision, 2009, 2232-2239.

199. Clinton, N., Holt, A., Scarborough, J., Yan, L., I. and Gong, P., Accuracy assessment measures for object-based image segmentation goodness, Photogrammetric Engineering and Remote Sensing, 76, 3 (2010) 289-299.

200. Johnson, B., A., Tateishi, R. and Hoan, N., T., Satellite image pansharpening using a hybrid approach for object-based image analysis, ISPRS International Journal of Geo-Information, 1, 3 (2012) 228–241.

201. Liu, Y., Bian, L., Meng, Y., H., Wang, H., P., Zhang, S., F., Yang, Y., N., Shao, X., M. and Wang, B., Discrepancy measures for selecting optimal combination of parameter values in object-based image analysis, ISPRS Journal of Photogrammetry and Remote Sensing, 68 (2012) 144–156.

202. Lucieer, A. and Stein, A., Existential uncertainty of spatial objects segmented from satellite sensor imagery, IEEE Transactions on Geoscience and Remote Sensing, 40 (2002) 2518–2521.

203. Neubert, M., Herold, H. and Meinel, G., Assessing image segmentation quality-concepts, methods and applications. In: Blaschke, T., Lang, S., Hay, G., J., (Eds.), Object-Based Image Analysis, Spatial Concepts for Knowledge-Driven Remote Sensing Applications. Springer, Berlin Heidelberg, 2008, 769–784.

204. Bar Massada, A., Kent, R., Blank, L., Perevolotsky, A., Hadar, L. and Carmel, Y., Automated segmentation of vegetation structure units in a Mediterranean landscape, International Journal of Remote Sensing, 33, 2 (2012) 346-364.

205. Whiteside, T., Maier, S. and Boggs, G., Site-specific area-based validation of classified objects. In: Feitosa, R., Costa, G., Almeida, C., Fonseca, L., Klux, H., (Eds.), Proceedings of the 4th GEOBIA, 2012, Rio de Janeiro, Brazil, 153–157.

206. Tonbul, H. ve Kavzoğlu, T., Nesne-Tabanlı Sınıflandırmada Segmentasyon Kalitesinin Sınıflandırma Doğruluğu Üzerine Etkisi, TUFUAB 2017 IX. Teknik Sempozyumu, 27-29 Nisan 2017, 237-241.

207. Bradley, A., P., The use of the area under the ROC curve in the evaluation of machine learning algorithms, Pattern Recognition, 30, 7 (1997) 1145-1159.

208. Galizia, G., Prizio, G., Lieto, E., Castellano, P., Pelosio, L., Imperatore, V., Ferrara, A. and Pignatelli, C., Hemodynamic and pulmonary changes during open, carbon dioxide pneumoperitoneum, and abdominal wall-lifting cholecystectomy, Surgical Endoscopy, 15, 5 (2001) 477-483.

209. Bewick, V., Cheek, L. and Ball, J., Statistics review 9: one-way analysis of variance, Critical Care, 8, 2 (2004) 130.

210. Gorokhovich, Y. and Voustianiouk, A. Accuracy assessment of the processed SRTM-based elevation data by CGIAR using field data from USA and Thailand and its relation to the terrain characteristics, Remote Sensing of Environment, 104, 4 (2006) 409-415.

211. Kim, K., S., Choi, H., H., Moon, C., S. and Mun, C., W., Comparison of k-nearest neighbor, quadratic discriminant and linear discriminant analysis in classification of electromyogram signals based on the wrist-motion directions, Current Applied Physics, 11, 3 (2011) 740-745.

212. Varga, B. and Karacs, K., High-resolution image segmentation using fully parallel mean shift, EURASIP Journal on Advances in Signal Processing, 2011, 1 (2011), 111.

213. Beucher, S. and Meyer, F., The morphological approach to segmentation: the watershed transformation, Optical Engineering - New York - Marcel Dekker Incorporated, 34 (1992) 433-433.

214. Hill, P., R., Canagarajah, C., N. and Bull, D., R., Image segmentation using a texture gradient based watershed transform, IEEE Transactions on Image Processing, 12, 12 (2003) 1618-1633.

CURRICULUM VITAE

Volkan YILMAZ was born in Trabzon, Turkey in 1987. He graduated from Akçaabat Anatolian High School in 2005. He received his B.Sc. and M.Sc. degrees from the Department of Geomatics Engineering, Karadeniz Technical University in 2009 and 2013, respectively. He has been studying in Karadeniz Technical University, Department of Geomatics Engineering as a research assistant since 2010. His main research interests include digital image processing, point cloud processing, unmanned aerial systems, image classification and image fusion. He studied English in the United Kingdom in 2012.